THE ROLE OF CONTACT-DEPENDENT GROWTH INHIBITION TOXIN SYSTEMS IN BACTERIAL COMPETITION AND BIOFILM DEVELOPMENT

Andrew David King

PhD

University of York

Biology

April 2015

Abstract

Contact-dependent growth inhibition (CDI) toxins are a recently identified family of polymorphic toxins, initially found in *Escherichia coli*. CDI toxins are found widely spread in Gram-negative bacterial species, including pathogenic strains, and have been shown to possess a wide range of toxin types which are effective against other bacteria.

This research shows that the *E. coli* EC93 CDI system confers a competitive advantage on bacteria growing in multi strain biofilms with susceptible bacteria. This advantage is due to two factors, firstly the EC93 CDI toxin was shown to be capable of inhibiting the growth of susceptible bacteria in a biofilm and secondly the conserved region of the EC93 CdiA protein was found to increase the rate of biofilm formation.

Analysis of the effects of the EC93 and EC869o11 CDI toxins at the single cell level showed that different classes of CDI toxins can act at different rates and with varying degrees of reversibility. Understanding the variable impact of CDI toxins, in concert with CDI's role in enhancing biofilm formation, aids our understanding of bacterial competition in the natural environment.

Contents

Appendices   139

List of Tables

List of Figures

List of Accompanying Material

One (1) DVD containing two (2) video files of phase contrast video microscopy. Each video file is of the same image series, one provided in .avi format (for Windows PC's) and one in .mov format (for OSX PC's). This video shows *E. coli* bacteria after 9 hours of flow cell growth, illustrating the extent of biofilm growth and the presence of free cells moving with the flow of media (images acquired at 100msec between frames, 100 frames shown). This material is referenced in section 5.2.4.

Acknowledgments

I would like to thank my supervisor Marjan van der Woude for all of her support, encouragement and inspiration throughout the course of my PhD. I would also like to thank the members of the van der Woude lab for their help and camaraderie. Thanks are also due to the staff of the Technology Facility imaging staff for technical advice and troubleshooting discussions around the microscopy based part of my PhD. I would also like to thank my TAP committee members, James Chong and Paul Pryor, for useful discussions and advice throughout the course of my PhD.

Thanks to David Low and Christopher Hayes (University of California) for providing CDI strains and plasmids from their labs. In particular thanks to Stephanie Aoki and Zachary Ruhe for supplying CDI strains and Kiel Nikolakakis for supplying CDI cosmids. Thanks to Zachary Ruhe for sharing of his prepublication results and useful discussions with regards to CDI's role in cellular adhesion.

Most of all I would like to thank my wife Gill for her patience and understanding as her husband became a student again. Finally a thank you to my daughter Rachel for understanding that Dad's bugs sometimes needed him to be in the lab through the night.

Author's Declaration

The work presented in this thesis is entirely my own except for the following items. Sequencing analysis which was performed by the Technology Facility (Department of Biology, University of York). Planktonic assay data on EC93 adhesion which is referred to in the discussion of my results in Chapter 5, which was the work of Zachary Ruhe. Flow cell design was performed in collaboration with Mark Bentley (Workshop Manager, Department of Biology, University of York). This work has not been submitted for examination at this or any other institution for another award.

Chapter 1

Introduction

1.1 Microbial communities

Whilst a tremendous body of knowledge has been obtained using the classic bacteriology techniques of single strain planktonic cultures this situation is vastly different to the environment experienced outside the laboratory. Much as the traditional view of bacteria as a featureless cytoplasmic bag has been revised to capture the intricate structures within cells (Kerfeld et al., 2010; Yao et al., 2014), so the view of bacteria as existing always as individuals responding to only their own needs has given way to at least some aspects of multicellularity (Shapiro, 1988). Part of the reason that social responses were not widely studied is that adaption of strains to the laboratory often leads to loss of social features / behavior's in the 'domesticated' bacteria.

Examples of multi cellular behaviour in bacteria extend across a wide range of species and encompass a variety of degrees of complexity (Claessen et al., 2014). This can be seen in the germination of *Streptomyces* spores where program celled death and differentiation of cell types coordinate to maximise spore production and spreading at times of stress.

Perhaps the most wide spread and medically relevant behaviour is that of bacteria to form biofilms, a community of bacteria adhered to a surface embedded in a self expressed polymeric matrix composed of components such as polysaccharides, proteins and DNA (Kostakioti et al., 2013). This can be thought of as a transient form of multicellularity with the enforced localisation of clonemates leading to a shared fate and shared benefits.

1.2 Bacterial biofilms

The intimate association of bacteria with surfaces has been known of since the first microscopic observations of bacteria growing as plaque reported by Antonie van Leeuwenhoek. Some of the first reports of the importance of the growth on surfaces to environmental bacteria come from Zobell's studies on marine bacteria (Zobell et al., 1935; Zobell et al., 1936) which elegantly demonstrated how marine bacteria's ability to proliferate was directly related to the

surface they had available to grow on rather than the volume available to grow on seemingly poised to multiply once such colonisation was possible. Further work in the field continued for many years focusing on marine and stream ecosystems and the impact that biofilms can have on industrial processes both negative, biofouling, and positive, improved waste processing.

The study of biofilms as a salient behaviour of bacteria related to their pathogenicity was first described by Costerton et al (Costerton JW, Geesey GG, 1978; Costerton, 1999) and is covered in more detail in the following section. The recognition of biofilms role in human disease led to a significant increase in the research interest in biofilms, which coupled with relevant technology becoming available, led to the formation of the following model of biofilm formation, as shown in Figure 1. In this general model surface attachment is initially reversible before expression / upregulation of surface proteins leads to irreversible binding. As the strongly adhered cells grow and divide the start of a true biofilm is formed by the secretion of extracellular polymeric substances (EPS) (Flemming et al., 2007). As this process continues, the biofilm growth on the surface becomes thicker leading to mature biofilm with growth extending tens of micrometers out from the surface and with significant gradients of nutrient levels, oxygen levels and waste products developed across the biofilm due to the combination of metabolic activity and diffusion rate limits (Rani et al., 2007). At some point, dependent on species, growth conditions and flow rates, detachment of cells from the mature biofilm becomes significant allowing seeding to new environmental niches.

Growing in this manner gives bacteria a number of benefits such as the ability to be tethered in a flow environment and hence avoid being flushed away from a site that can have a constant supply of fresh nutrients. Biofilm growth can also provide protection from environmental grazers such as protists (Chavez-Dozal et al., 2013; Matz et al., 2005) as instead of individual bacteria they are faced with a much larger 'slime' covered mass which is harder to engulf.

Elaborations of this general model can occur in which there is more directed differentiation of cells such as is seen in *Pseudomonas aeruginosa* biofilms (Davies et al., 1998). In this case as the mature biofilm forms specific mushroom like structures occur, which then undergo lysis (Ma et al., 2009) of cells in the central cavity, followed by generation of a specific subpopulation of hypermutator cells which are then released for dispersal to new colonisation sites (Conibear et al., 2009). Regulation of biofilm development has been shown to be under the control of multiple factors of which a key one is quorum sensing (QS). Bacteria can produce and secrete small chemical molecules that are stable outside the cell. When detected by those same cells the concentration of these chemicals gives a measure of the population density / rate of diffusion in the environment (Solano et al., 2014). By linking sensing to regulatory pathways modulation of bacterial responses can be made in a density dependent way. A va-
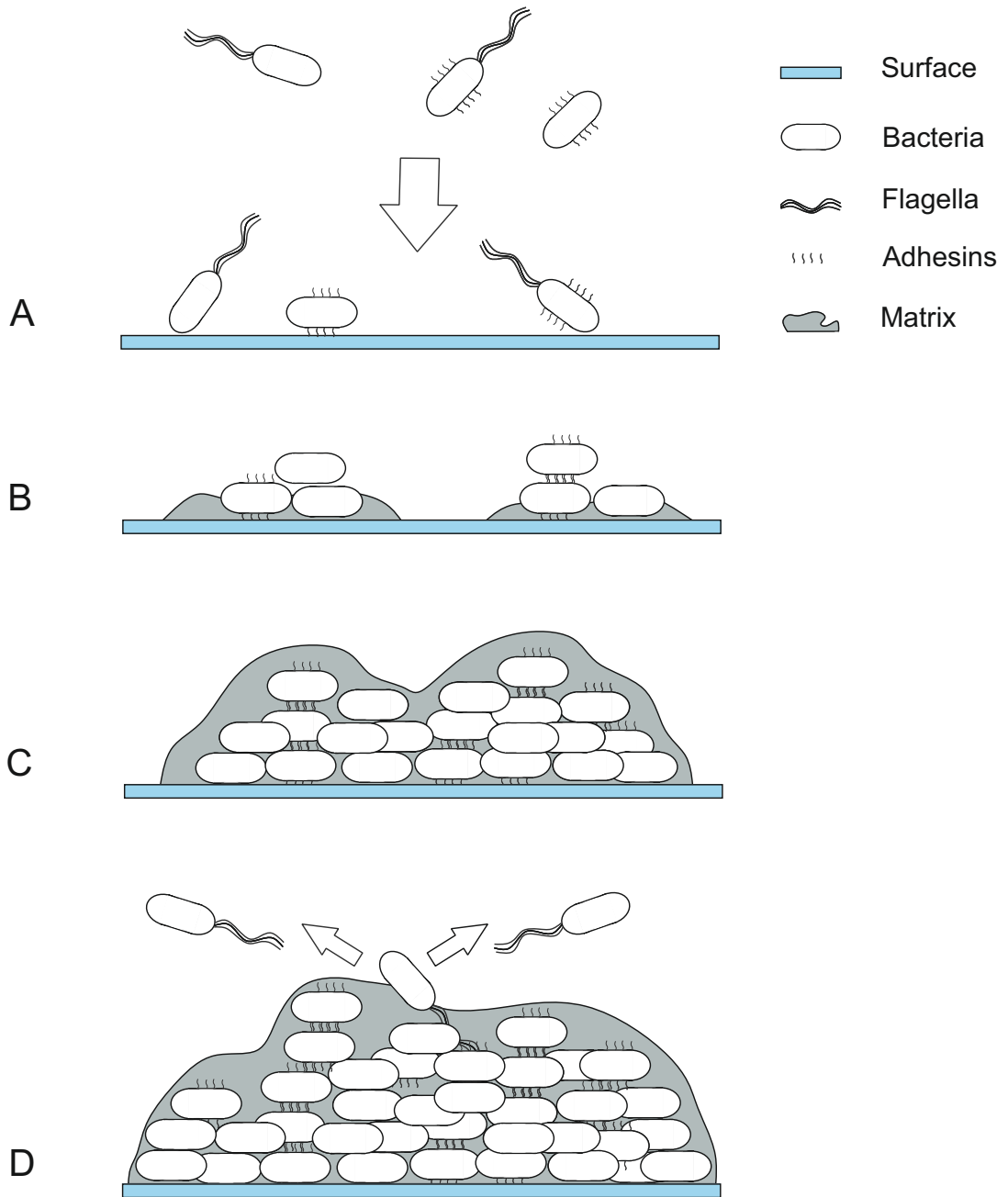
Figure 1: Stages of biofilm growth

Schematic showing a general model for biofilm formation, see top right for component details. Panel A shows initial adhesion of bacteria being driven by factors such as cell mobility (flagella) and expression of adhesins. Panel B shows microcolony growth as surface bound cells start to divide and express matrix, motility factors are downregulated. Panel C shows maturation of the biofilm with further cell growth, combined with sufficent expression of matrix to completly embed the bacteria. Panel D shows release / 'escape' of bacterial cells from confinement within the matrix, enabling dispersion of cells.

riety of different chemical compounds are utilised by different bacterial species in this way including acyl homoserine lactones (AHL) and furanosyl borate diesters (auto inducer 2 (AI2)). Quorum sensing was first shown to be important in the context of biofilms by Davies et al in *Pseudomonas aeruginosa* were disruption of (AHL) production was found to block biofilm development beyond formation of a monolayer (Davies et al., 1998). Further work has shown that AI-2 mediated QS signaling can also affect biofilm formation (Hardie et al., 2008). In both cases the particular strain and conditions seem to have a significant effect on outcomes with quorum sensing having been shown to act at disparate points in biofilm development from initial formation through to dispersion.

1.2.1 Role of biofilms in pathogenesis

Bacteria can colonise a variety of different surfaces within the body both natural, for example teeth (Kolenbrander et al., 2010), lung aveoli epithilium (Ciofu et al., 2012) and wounds(Cowan, 2011), and man made, catheters (Reisner et al., 2014), stents and artificial hip joints (Gbejuade et al., 2014). This has significant implications for management of infections as growth of bacteria as biofilms adds a number of complications to clinical management of such infections. The most well studied example is probably the role that *P. aeruginosa* plays in chronic lung infections of cystic fibrosis patients (Mulcahy et al., 2010). In this case despite patients having a functioning immune system and receiving aggressive treatment regimes, with high doses of both systemic and ventilated antibiotics, there is a failure to clear the bacterial infection. These infections exemplify two of the major factors that make biofilms such a medical issue.

Firstly that biofilms can be extremely resistant to antibiotics, failing to be cleared at concentrations that wipe out bacteria from the same species growing planktonically. Antibiotic resistance is due to three main factors, the bacteria growing in the biofilm are often growing more slowly, or at least the most buried sub population are, due to nutrient limitations, which means that many antibiotics will not be effective due to their mode of action (Rani et al., 2007). In addition a population of persister cells, that is cells which have entered a quiescent state in which they are even more resistant to the action of antibiotics, is generally much higher in biofilms, possibly due to the more nutrient limited state found in their interior. Therefore even if concentrations of antibiotic which are therapeutically effective for the bulk of the population are obtained, a small subpopulation can remain to regrow and maintain infection (Lebeaux et al., 2014). Thirdly the matrix can act to prevent access of the antibiotic to the bacteria by sequestering antibiotics due to electrostatic interactions and limiting diffusion (Walters et al., 2003). Such effects are widely variable between different antibiotics and species and hence can't account entirely for the increased antibiotic resistance (Fux et al., 2005).

Secondly biofilms are resistant to the action of the immune system in two main ways, they cannot be efficiently opsonised as the bacterial surfaces are sequestered withing the biofilm

and in a related effect the absence of the typical signal molecules for phagocytosis and the greater size of the biofilm (much as it is protective against protist grazing) prevents the effective action of macrophages (Hernández-Jiménez et al., 2013; Hirschfeld, 2014).

In the case of mechanical debridement (Leaper et al., 2012), a standard approach taken to clean infected wounds / implants, it is the physical property of the biofilm that can lead to failure to clear infections. The slimy / gelatinous nature of the biofilm means that even after vigorous removal procedures it can quickly reattach to the surface.

As with infections due to planktonic bacteria, different species of biofilm forming bacteria are capable of causing different diseases (Lebeaux et al., 2014; Parsek et al., 2003). In the case of *Escherichia coli* biofilms have been shown to be involved in the pathogenesis of a number of diseases , such as urinary tract infections (UTI), bacterial prostatitis (Costerton, 1999), diabetic foot wounds (Gottrup et al., 2014) and EAEC (Kaper et al., 2004; Croxen et al., 2010).

1.3 *Eschericia coli* biofilms

E. coli biofilms follow the broad pattern of biofilm formation described above and a brief outline of the specifics of the *E. coli* pathway is given below. Initial contact of bacteria with a surface to commence biofilm formation requires them to overcome hydrodynamic and electrostatic forces acting against them. In the case of *E. coli* this is most commonly achieved due to active motility driven by flagella, although over expression of surface adhesion factors can compensate for a lack of motility in certain circumstances (Beloin et al., 2008).

After initial contact cells are held by weak non specific interactions between bacteria and the surface which allow reversible attachment. To convert this to a long term irreversible interaction *E. coli* express surface molecules, specifically fimbriae, with three classes having been shown to have a key role, conjugative pili, type I fimbrae and curli. Conjugative pili, such as those encoded by the F plasmid, have been shown to be sufficient to confer the ability to form thick biofilms to laboratory strains by aiding initial cell adhesion (Ghigo, 2001). It is common for these components to also play a role in later biofilm stages by also promoting cell to cell adhesion.

The regulation of *E. coli* is complex and appears to vary across strains and conditions of growth, however it is possible to pull out some general themes even if they will not apply in all situations. In order for *E. coli* cells to transition from the planktonic mode of growth they need to modulate motility factors, increase for initial adhesion then down regulate, and up regulate matrix and curli expression once adhered to surfaces. *E. coli* strains are capable of quorum sensing via the autoinducer-2 (AI-2) quorum signalling molecule, possessing both the luxS family of genes for AI-2 production and an lsr-like transport system (Beloin et al., 2008; Herzberg et al., 2006). Disruption of this system has been shown to affect biofilm growth

only under some conditions / strains. One such example is the increase in biofilm formation on AI-2 addition via the MqsR (motility quorum-sensing regulator) inducing an increase in cell motility and hence aiding initial biofilm formation as reported by Gonzalez Barrios et al (González Barrios et al., 2006).

CsgD (transcriptional regulator) has been shown to be a key regulator of biofilm formation (Ogasawara et al., 2011). It acts in two ways firstly to repress transcription of the genes for flagellum formation / motility both by directly binding to the promoter region and also increasing expression of AdrA (diguanylate cyclase,) which leads to higher levels of cyclic di-GMP which also represses flagellum formation. Higher levels of c-di-GMP also act to increase cellulose production, a biofilm matrix component (Römling et al., 2013). Secondly CsgD directly acts to activate transcription of genes involved in production of curli which aid attachment to abiotic surfaces and to other bacteria. CsgD levels in the cell are modified by at least five transcriptional factors in response to a variety of external stress factors, such as changes in osmolarity which is sensed by the EnvZ/OmpR two component pathway. As osmolarity is often locally modified at cell surfaces this can act as a marker of initial adhesion having occurred. Other systems of surface sensing include the *cpxRA* two-component regulatory system which is thought to detect adhesion to surfaces due to induced membrane perturbations (Beloin et al., 2008). Phase variation of surface associated structures such as the adhesin Ag43 can significantly impact on the biofilm forming competence of *E. coli* and rates of variation can be modulated by various mechanisms.

Generation of a mature biofilm, defined as the process of significant thickening of the biofilm by cell growth, requires two main factors in order to occur, cell to cell adhesins and matrix production. Adhesins are a class of surface expressed molecules which act to bind adjacent cells to each other (Da Re et al., 2007). The classic example of which is antigen (Ag43) (Woude et al., 2008), which has been shown to mediate cell-cell interactions in *E. coli* biofilms (Danese et al., 2000) and even within mixed species biofilms (Kjaergaard et al., 2000). A wide variety of adhesins have been identified and it appears that they are relatively interchangeable i.e. as long as some adhesins are present to drive cell to cell interactions the specific kind is not of importance

The matrix produced by *E. coli* has been shown to be dominated by polysaccharides (Hung et al., 2013) unlike the biofilms of some other species which are more peptide (Periasamy et al., 2012) protein based *Staphylococcus aureus* (Foulston et al., 2014). Specifically cellulose, Poly-β-1-6-N-acetyl-glucosamine and colanic acid are detectable in *E. coli* biofilms and their removal due to gene deletion or degradation has been shown to correlate with loss of biofilm forming ability. For example treatment of biofilms with cellulase can totally disperse biofilms (Da Re et al., 2006) and gene deletion of *yhjO*(cellulose synthase) leads to seriously weakened biofilms (Hung et al., 2013). It should be noted that the bacteria surface linked polysaccharides

of LPS have also been shown to be important in biofilm formation with UPEC536 cells expressing truncated LPS having a significant decrease in biofilm formation (Beloin et al., 2006). In contrast another class of cell tethered polysaccharides, those that form capsules has been shown (Schembri et al., 2004) to act to block adhesins due to steric interference and also for group II capsules be released into the environment and also interfere with abiotic attachment.

Clear programs of directed differentiation have not been identified for any *E. coli* biofilms (Ghigo, 2003; Lee et al., 2011) to date with responses being generated based on local signals (detection of surface (Beloin et al., 2004), local nutrient concentration (Beloin et al., 2005)) or general community detection (quorum sensing) rather than the specific developmental pathways targeting discrete subpopulations of cells seen in some other species (*Pseudomonas* hypermotile swarmer release).

1.4   Biofilm analysis techniques

As biofilms present such a pressing medical problem a wide variety of techniques have been employed to aid our understanding of their formation. These range from the simplest such as resuspension of biofilms to allow viability quantitation by growth (Ceri et al., 1999) or staining with dyes such as crystal violet (Genevaux et al., 1996) that can bind to carbohydrate / protein components of the biofilm matrix and be read spectrophotometrically. An advantage of these techniques is there suitability for use in 96 well formats allowing higher throughput analysis.

The polysaccharides that compose a significant portion of the matrix of many biofilms can be chemically extracted and analysed using chromatographic techniques such as high-performance anion-exchange - pulsed amphometric detection (HPAE-PAD) to give detailed information on their chemical composition (Denkhaus et al., 2006). Components of biofilm chemical composition can also be studied using a number of different techniques such as spectrometry, Raman spectroscopy gives information on matrix polymers, nuclear magnetic resonance (NMR) (Zhang et al., 2012a) which combined with suitable substrate labeling can allow metabolite concentration determination which is also possible with magnetic resonance imaging (MRI) (Cao et al., 2012). Finally mass spectroscopy can also be used to obtain information on both small molecule and protein composition. With the use of matrix-assisted laser desorption ionisation it is possible to raster across a surface to obtain location information in addition (Lanni et al., 2014).

Direct measurement at locations within biofilms is possible using microsensors capable of measuring a variety of relevant parameters such as pH and oxygen concentration, dependent on configuration, and which can be manipulated to measure transepts throughout the full depth of biofilm growth (Costerton et al., 1995).

Electron microscopy in both scanning or transmission modes can be used to study struc-

tural features of biofilms although particular care in interpretation is required due to the tendency of the biofilm matrix to form artefactual structures due to the harsh preparation techniques / vacumn conditions that are required.

A critical requirement for clinical analysis of biofilms is to understand the particular species composition to aid treatment. In this case polymerase chain reaction (PCR) analysis can be used to type infections (Ren et al., 2013) and recently systems combining PCR and mass spectrometry have been released to make such analysis more feasible in the clinical environment (Ecker et al., 2008).

The analysis of bacteria growing in biofilms presents some unique challenges due to the three dimensional structure and population heterogeneity inherent in this mode of growth. Significant advances in our understanding of biofilm structure came about with the advent of confocal laser scanning microscopy (CLSM) with its ability to provide information in three dimensions by collecting z stacks of images at defined depths within a sample. In combination with the ability to engineer the expression of fluorescent proteins by bacterial strains to be studied, either constitutively or under the control of relevant promoters, information on strain / species interactions and the expression profile of specific promoters can be obtained. Importantly this can be done repeatedly to obtain time courses of responses in live cells with minimal perturbation.

A variety of staining protocols are also suitable in particular the application of fluorescence in-situ hybridisation (FISH) for the study of natural samples in ecological studies. It has also proved possible to apply the full range of genomic and proteomic technologies although in this case it should be borne in mind that spatial patterning will have been lost unless micro sampling techniques have been employed. These approaches have been particularly useful in identifying regulatory networks relevant to biofilms (Ogasawara et al., 2011).

1.5 The role of contact dependent interactions in the action of bacterial toxins

Bacteria growing in the natural environment face a high degree of competition from other microbial strains and species. In order to cope with this situation they have evolved to be capable of expressing a wide range of toxins which act to destroy / damage competing organisms. The most well known of these systems are the soluble toxins secreted / released by cell lysis to the environment classified as bacteriocins and microcins on the basis of the size of the protein toxin. Of these the most widely studied is probably the colicin family of bacteriocins which target *E. coli* strains specifically.

Colicins possess a number of characteristics which in further sections discussing CDI will be seen to have similarities to CDI systems. Colicin molecules are multi domain proteins with

the N terminal region containing domains responsible for receptor binding and membrane translocation and a C terminal toxin domain (Braun et al., 2013). A variety of toxin modes of action have been identified including pore formation, peptidoglycan degradation and nucleases. In order for the producing cell to avoid self intoxication a cognate immunity protein is produced which blocks toxic activity till it is removed at the target cell. The toxin and immunity proteins are expressed from a single operon. It has been shown that colicins are sufficiently modular in nature that chimeric molecules are functional (Braun et al., 2002).

Each colicin is highly strain specific due to binding only to a certain receptor protein on the target cell surface, usually one responsible for nutrient uptake, as these receptor types are diversely distributed the toxin will act only on a small subset of all *E. coli* strains. Transport into target cells occurs by subversion of existing target cell molecular import systems, being either Tol or Ton dependent. The process of translocation or membrane insertion, dependent on toxin type, is dependent on proton motive force (pmf). In the case of colicin proteins which act in the cytoplasm proteolysis to cleave the C-terminal tip is required for the toxin to gain access across the inner membrane.

Despite these similarities there are also a number of significant differences between the systems which are outlined below. Colicins are expressed from a plasmid background rather than a genomic context and do not have additional toxin / inhibitor pairs encoded unlike the polymorphic toxin systems, as defined by Zhang (Zhang et al., 2012b). Export of colicins from the producing cell is not by a directed pathway but most commonly occurs by induced lysis of the cell, although some colicins, such as Colicin M escape by cell wall leakage (Cascales et al., 2007). Colicin toxins, in particular those which form pores in the target cell membrane, are capable of killing sensitive cells in a single hit process. Which can be seen to be a much more dramatic outcome than the growth inhibition induced by the EC93 system.

The diffusible nature of these toxins means that their action can spread over a distance several orders of magnitude larger than the cells that produce the toxin, 5μm length cells vs zones of clearance that are 1-2 mm in radius (Kerr et al., 2002). The diffusible nature of the toxins also means that the flow characteristics of the environment will affect how toxins localise and what concentrations will be acheived. The action of these toxins is typically directly lethal to targeted cells for example the one hit action of colicin toxins (Johnson et al., 2013).

In contrast to this whole area of action approach to toxin delivery there exist a variety of more directed bacterial contact systems which are discussed in the following section.

1.5.1 Contact dependent toxin systems

Bacteria are capable of delivering the cytoplasmically synthesised proteins extracellularly using a wide variety of secretion systems of which four are relevant to contact dependent toxin systems (Hayes et al., 2010). As contact is an absolute requirement for these systems toxin

interactions will be naturally limited to the borders of microcolony interactions and is not dependent on lysis of toxin bearing cells to release toxin as it is already presented / the required structures for toxin delivery are present on the cell surface.

Type III secretion systems (T3SS) use a repurposed flagella based machinery to deliver effector molecules (such as the *E. coli* effector Tir which induces actin polymerisation (Dean, 2011)) to eukaryotic organisms typically in the context of pathogenesis. As they mediate cross kingdom interactions they will not be discussed further in this thesis.

Type IV secretion systems (T4SS) are based on pili like interactions to deliver DNA to bacteria to date the delivery of effector protein molecules has only been reported for eukaryotic systems. Hence they will not be discussed further in this thesis except to note the interaction of the UPEC 536 toxin and F pilus see section 1.5.5.

Type V secretion systems (T5SS) are transfered through the outer membrane through a beta barrel protein that is either part of the same molecule, in the case of autotransporters, or is an accessory protein,in the case of two-partner secretion systems (TPS). Contact Dependent Inhibition of growth (CDI) toxins belong to this class and are described in detail in section 1.5.2. Filamentous haemagglutinin (FHA) is the best known example of the T5SS and by assuming structural homology we would expect CDI toxins to form a β helical fiber (Hayes et al., 2010). FHA does not have a toxic activity it's main known role is to increase intercellular adhesion and this activity has been reported to carry over into cells expressing CDI systems.

CDI is an example of a polymorphic toxin system, that is a system with a diverse range of possible toxin types that can be encoded at the C-terminal most domain with N-terminal domains involved in trafficking across membranes (both host and target). Toxin types identified to date include a range of different nucleases and proton motive force disruption (pmf) (Aoki et al., 2010).

Unlike the other toxin delivery systems described here, which use tubular structures to deliver effector molecules, CDI toxin is delivered from a single large protein tethered to the outer membrane. Delivery of CDI toxins is associated with inhibition of growth of target cells but not cell death. This action is comparable to an induction of a viable but nonculturable (VNBC) state (Oliver, 2005) in intoxicated target cells. Toxin delivery shows a high level of species specificity based on heterogeneity of surface displayed proteins (BamA loops) CDI toxins are commonly found with orphan toxins and inhibitor sequences, these can be expressed leading to a more complex network of immunity and susceptibility than would otherwise be the case.

Type VI secretion systems (T6SS) use a phage-like injection mechanism to deliver toxins to target cells. The tube of this structure is composed of multiple hemolysin-coregulated proteins (Hcp) capped by valine-glycine repeat proteins (VgrG). This system can interact with both bacterial and eukaryotic systems (Schwarz et al., 2010) and is discussed in the context of bacterial

interactions here. Recent work has identified that when cells both possessing T6SS interact a dueling mechanism can be induced increasing the likelihood of formation of a functional T6SS system on the cell membrane adjacent to the other cell(Alteri et al., 2013). T6SS systems have been shown to be a broad specificity toxin system able to target a range of bacterial species in contrast to the more specific species / strain focus of bacteriocins or CDI toxins. Toxin action of T6SS systems is generally lethal to target cells which is in contrast to CDI growth inhibited cells which maintain membrane viability as judged by propidium iodide exclusion (Aoki et al., 2005).

T6SS toxins are also capable of self intoxication and therefore express inhibitor proteins to block this as is also seen with CDI toxins. Orphan inhibitor proteins have been identified in strains not expressing T6SS toxins but the pairing of orphan CT-toxin tips and inhibitor proteins has not been reported. T6SS toxin activity is usually delivered by relatively small effector molecules that can readily traverse the injectisome. As with CDI toxins these cover a wide range of toxin modes of action such as pore formation, peptidoglycan degradation and nucleases (Russell et al., 2014). T6SS toxins are not effective in planktonic culture requiring the presumably more stable conditions of growth on a surface for effective inhibition, this is in contrast to CDI systems which are effective under planktonic growth conditions.

Rhs systems have recently been identified as toxin systems that appear to use the genric T6SS injection system (Koskiniemi et al., 2013). Rhs toxin loci are found linked to *hcp* and *vgrG* genes and, as these are required for effective action of the toxin, they are presumed to form T6SS like injection apparatus. It is not yet clear if such a large toxin molecule, in comparison to the size of T6SS effectors, is capable of traversing the injection apparatus intact. Significant growth inhibition is only seen when competition is monitored by growth on surfaces as would be expected from the similarities with T6SS systems, and again different than the CDI systems.

Rhs toxins were identified, in part, because some Rhs C-terminal toxin tips share significant homology with some CDI C-terminal toxin tips. This suggests that transfer of toxins as modular units is possible even across classes of toxin. As in CDI toxins the C-terminal region is defined by a conserved motif, in this case PxxxxDPxGL. As with CDI systems there are a wide variety of C-terminal tips found spread across different strains which each have cognate immunity proteins to avoid auto inhibition. Orphan toxin and immunity proteins are found in some bacterial strains and Koskiniemi et al have shown that these can recombine to form functional toxins (Koskiniemi et al., 2014). Rhs toxin systems can in some ways be seen as a hybrid of the T6SS and CDI toxin systems (Poole et al., 2011). They will not be covered further in this thesis except where they are illustrative for understanding possible CDI toxin tip recombination, see section 1.5.6.

1.5.2 Contact-dependent growth inhibition toxins

CDI toxins were first reported in 2005 by the Low lab (Aoki et al., 2005) having been identified as an unexpected contaminant in a rat UTI model. In this case the contaminating strain was found to be dominating the urinary tract of the rat, out competing the strains that the experimentalists were trying to use. The responsible strain, *E. coli* EC93 was isolated from the faeces of the rat used in the experiments. Initial work identified the operon responsible for the ability to out compete related bacteria, and on the basis that the growth of cocultured bacteria was stopped in planktonic culture they were assigned as cdi genes, *cdiBAI* operon.

CdiB and CdiA have been assigned as partner proteins in a two partner secretion system (TPS / T5SS), based on sequence similarity, with CdiB delivering CdiA to be displayed tethered on the inhibitor cells surface. The orientation of EC93 CdiA on the cell surface has not been directly determined but its length of 3132 amino acids suggests it could project a significant distance from the cell surface. EC93 CDI toxin was shown by biochemical means to act by a still undefined mechanism to disrupt proton motive force (pmf) and hence disrupt the target cells energy metabolism (Aoki et al., 2009). Expression of the EC93 toxin system is constitutive under the range of laboratory conditions tested with slight changes in expression level being reported on changes in the C source supplied in media (personnel communication, Zachary Ruhe).

Contact dependence has to date been based on two experimental protocols, firstly by showing that separation of CDI+ and target cells by a PET membrane blocked the ability of the CDI toxin when it's pore size was sufficient to block trans migration of bacteria (0.2μm) but still permit exchange of media. Which showed that contact was required and that the toxin was not being dispersed in a soluble form. Secondly, Fluorescence Activated Cell Sorting (FACS) was performed on cocultures of CDI+ and target cells which showed that the colony forming ability of target cells which were cosorted with inhibitor cells was reduced.

1.5.3 CDI species and strain distribution

After being initially identified in *E. coli*, bioinformatic analysis was performed (Aoki et al., 2010) to identify the extent that the CDI system was present in other *E. coli* strains and across to other species. Using the core conserved region of *cdiA* and *cdiB* as search criteria standard bioinformatic search techniques revealed that CDI operons were present across a number of species in the α, β and γ proteobacteria (Hayes et al., 2014), as confirmed by the presence of short ORF's immediately following, corresponding to *cdiI*, that were unannotated/hypothetical protein annotations. Only sequences that contained the DUF638 domain (in which the VENN motif is found) and an N-terminal haemagglutination activity domain with associated hemagglutinin repeats were included in this analysis (Aoki et al., 2010; Ruhe et al., 2013a).

A clear distinction can be drawn between the main group of CDI toxins and those which are found in the *Burkholderia* species (Nikolakakis et al., 2012; Koskiniemi et al., 2015). Firstly the operon gene order is different than all other species being BcpAIOB, with the additional operon component O (Anderson et al., 2012) being hypothesised to be involved in export and maturation of BcpA. Secondly the junction of the conserved region and the variable C-terminal tip is delineated by a different sequence motif, NxxLYN instead of VENN. Finally it should be noted that chimeric CdiA proteins created by swapping of toxin tips between the two CDI systems leads to proteins that are not capable of growth inhibition of target cells.

Control of the expression of CDI systems is poorly understood with the exception of the Burkholderia systems were there is evidence for sporadic induction of expression during biofilm growth (Anderson et al., 2014). Generally CDI systems do not seem to be switched on at detectable levels under laboratory conditions which has lead to much of the work to date being performed on strains in which the expression of the CDI system has been placed under artificial promoters or where a chimeric CdiA molecule is generated with, for example, the conserved region of EC93 CdiA and the CT toxin region of the CdiA molecule from UPEC536. The absence of expression under laboratory conditions is presumably why the CDI systems had remained unreported until 2005. *E. coli* strains which have been identified to contain CDI systems include strains responsible for UPEC and EHEC.

1.5.4 Classes of CDI toxin

The initial toxin activity identified to be present in the EC93 CDI toxin system is currently an anomaly compared to the classes discovered by further bioinformatics analysis both by the Hayes and Low labs , focusing on CDI/Rhs systems, and by the Zhang lab (Zhang et al., 2012b; Zhang et al., 2011) looking at the broadest possible view of toxin families of which CDI is clearly part of the supergroup of polymorphic toxin systems. This work identified 18 families (Beck et al., 2014b) of toxins across the identified *E. coli* CDI loci with a large number of toxins not showing any significant levels of identity with known toxins. This classification is based on pair-wise alignments of *E. coli* CDI sequences aligned the VENN motif (Ruhe et al., 2013a). While there are significantly more toxin sequence classifications than assigned toxin activities it is not clear yet whether each class of toxin sequence represents a unique toxin activity.

Those that have been identified to date, excepting the biochemical approach taken with EC93, are nucleases. In fact the first CDI nuclease activity, ribosomal RNAase (rRNAase), was noted by (Walker et al., 2004) in three different species prior to the first report of CDI as a novel toxin system itself. That these classes have been identified to date may be due to the initial selection bias for nucleic acid degrading folds being readily determined by sequence analysis, as identified as part of wider polymorphic toxin superfamily (Zhang et al., 2012b). The structure of part of only two CDI toxin's has been reported to date with the C-terminal

region of the EC869o11 and ECL CdiA molecules being separately determined cocrystalised with their cognate immunity proteins (Morse et al., 2012; Beck et al., 2014a).

EC93 toxin mode of action was determined using an autoinhibition assay in which cells expressing the EC93 CDI system had CdiI expression under inducible promoter control. This assay looked at the effect of loss of CdiI protection in expressing cells rather than solely delivery of toxin across a membrane. Expression of Pap pili as a control showed that there did seem to be a significant requirement for cell contact for toxin effectiveness (Aoki et al., 2009), supporting the relevance of the assay. However the levels of toxin delivered in such a system may represent a dose of toxin that is not achievable in nature. In addition any statements on recovery from toxin action are definitely not directly relatable to the natural environment as target cells are not likely to suddenly begin expressing the relevant CdiI, either they will lack it or they will have been initially protected. This data however does show that removal of the EC93 CDI toxin does allow recovery and hence the toxin action hasn't set in place an irreversible set of molecular actions.

The UPEC536 is the only example known to date of a CDI toxin which has an additional requirement of the target cell, beyond factors required for its delivery to the cells cytoplasm. Growth inhibition absolutely requires that CysK , a non essential biosynthetic enzyme, be present, a permissive factor, for toxin activity (Diner et al., 2012).

1.5.5   Toxin delivery mechanisms of CDI

The bulk of work looking at the toxin delivery of CDI to target cells has been performed using the EC93 toxin system and it is not clear how applicable it will be to the broad range of CDI systems. Although the conservation of core sequences argues for a universal system one exception / additional route has been identified for the UPEC536 system. The current model of EC93 CDI toxin action is shown in Figure 2 and described below. This model illustrates the dependence of the CDI toxin system on cognate receptor molecules on the cell surface to allow toxin transfer of CdiA. This matches with the requirement of colicin toxins target cells to express appropriate systems. In contrast T6SS effectors are delivered directly to the cell via the virus like injection method. Some form of proteolytic cleavage is then required for toxin activity to be translocated into the periplasm. This is presumably due to the size of a molecule as large as CdiA's are, up to 5,600 amino acids in length (Poole et al., 2011), being significantly more challenging to transport across a membrane than solely the 200 amino acid toxin C-terminal region. Transfer from the periplasm into the cytoplasm also requires specific inner membrane proteins to be present dependent on toxin type as is seen for colicins (ftsH appears to be an example of a shared protein route into the cytoplasm between some CDI systems and some colicins). Again such a requirement is not seen for T6SS toxins. As is seen for though as intracellularly produced CdiA will be the whole molecule and it is not known if such still

tethered toxins would be active, it is more likely to be toxin delivered from clonemates that requires protection, as this would deliver cleaved toxin that is known to be active. The current evidence for this model is discussed below.

Genetic screening for transposon mutagenised target strains resistant to EC93 CDI+ cells (Aoki et al., 2008) identified two genes whose disruption conferred resistance to EC93 CDI toxin. AcrB is part of a multidrug efflux complex in the inner membrane (Tikhonova et al., 2004). Interestingly although this is a multi protein assembly no other components of the complex were picked up in the screen and specific knockouts of the other components had no protective effect against the EC93 CDI toxin.

BamA is an essential protein responsible as part of the Bam for the insertion of β barrel proteins into the outer membrane. As it's absence is lethal it was picked up in the screen by a mutant with decreased levels of BamA on the cell surface. Again though this protein is part of a multi-protein complex disruption of other members of the complex gave only a small protective effect that was determined to be due to increased levels of capsule production. That fragments of Ec93 CDI toxin in conditioned media (Aoki et al., 2005) are incapable of inhibition indicated that the initial interaction of the entire CdiA molecule was a key factor in effective toxin translocation. It has been shown that the EC93 CDI system is only effective against other *E. coli* species (Ruhe et al., 2013b). Further work identified that EC93 CdiA protein recognises specific extracellular loops of BamA and that this requirement for recognition explains the species specificity of the EC93 CDI toxin. It has also been shown for the UPEC536 CDI toxin that the whole of the CdiA molecule can be detected on the surface of target cells, but only the CdiA C-terminal toxin tip could be detected in the cytoplasm of these cells (Webb et al., 2013).

The purified UPEC536 CDI toxin has recently been identified to be capable of using an alternate route by interacting with the F pilus (Beck et al., 2014b). However the lack of any toxic effect of UPEC536 cell supernatants suggests that F pilus binding is not relevant in the natural environment and has been hypothesised to instead reflect an off target effect of an alternate mechanism for target cell membrane translocation.

The Ec93 toxin requires AcrB for toxin delivery, however this requirement has not been found for other CDI toxin systems tested. *E. coli ftsH* (ATP-dependent zinc metalloprotease) mutants are resistant to a small subset of CDI toxins yet susceptible to others(Ruhe et al., 2014), taken together this indicates that their are in fact multiple pathways for different CDI toxin import into the target cell. Recent work has identified that translocation across the inner membrane requires the proton motive force (pmf) for a range of toxins other than EC93 which was not tested for technical reasons (Ruhe et al., 2014).
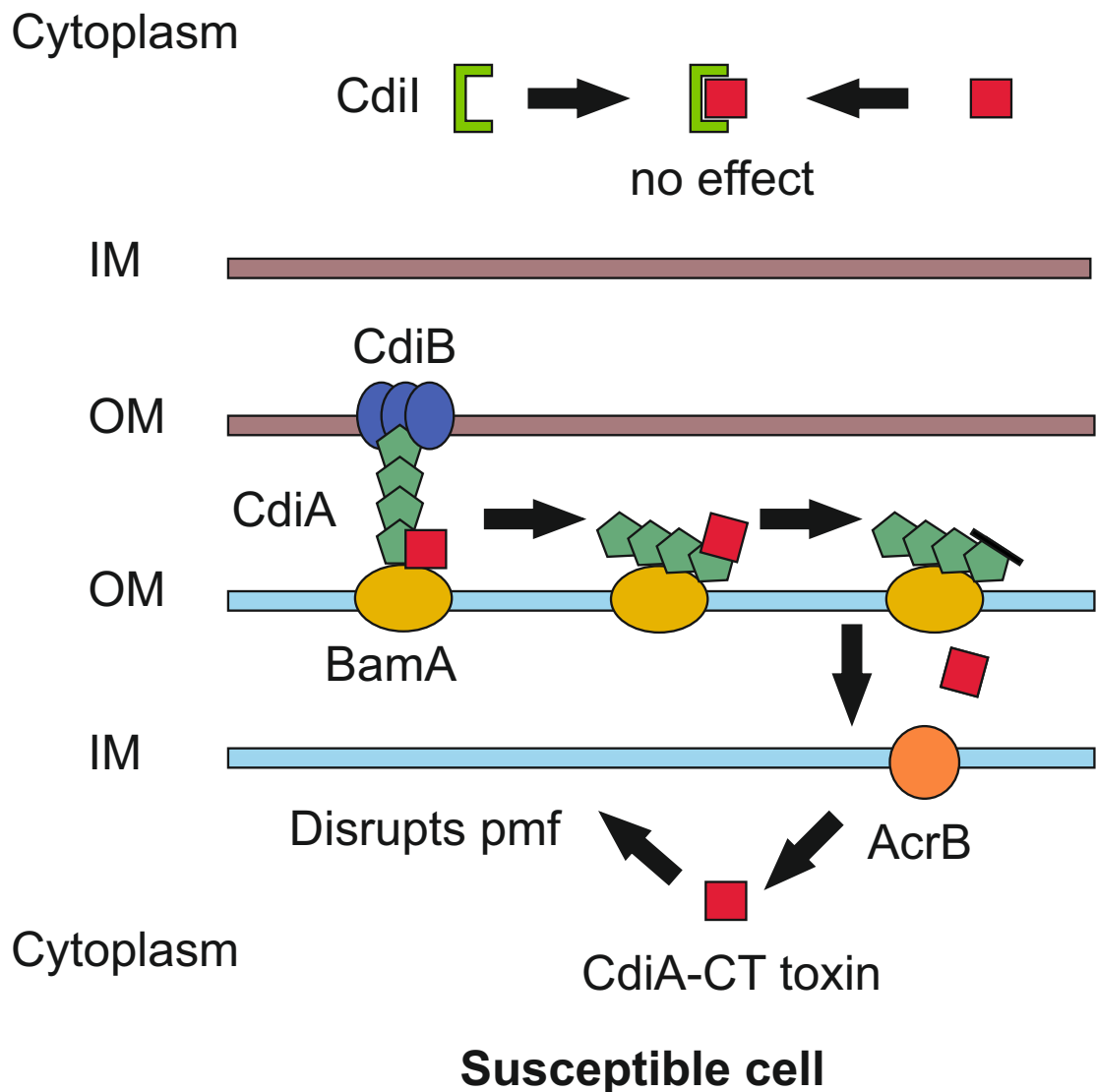
Figure 2: Current model of EC93 CDI toxin action

Schematic showing the current understanding of how the EC93 CDI toxin acts. Stylised representations are shown of two *E. coli* cells, one expressing the EC93 CDI toxin system and one that is susceptible to the action of the toxin. Cell membranes are labeled as IM, inner membrane and OM, outer membrane. CdiA is transfered to the surface of the susceptible cell via an interaction that requires BamA. CdiA is then presumed to undergo proteolytic cleavage, with only the CdiA-CT toxin being transported into the cytoplasm. The toxin then acts to disrupt the pmf of the cell by an unknown mechanism. The EC93 CdiI protein specifically recognises and blocks the action of the EC93 CdiA-CT toxin, which can be delivered to CDI+ inhibitor cells from clonemates. This model assumes that the results of Webb and colleagues (Webb et al., 2013), using the UPEC536 CDI toxin, are applicable to the EC93 toxin.

1.5.6 Orphan CDI toxin tips

During the bioinformatic analysis performed in (Aoki et al., 2010) it became apparent that associated with the main *cdiBAI* operon in many strains were additional immunity proteins and C-terminal (CT) only sections of CdiA molecules truncated so as to encode the toxin region. It is thought on the basis of sequence that expression of the orphan immunity proteins is possible as they can have an appropriate initiation codon and Shine-Dalgarno sequence in a properly spaced position. Natural expression of the EC93 orphan CdiI protein has been demonstrated by RT-PCR detection of mRNA transcripts and protection from the cognate toxin (Poole et al., 2011). It is not thought that the orphan CT CDI toxin is expressed, even if its mRNA is transcribed, as it lacks the features required for translation. This would be expected as it lacks the conserved region of cdiA and hence would not be able to be translocated to the cell surface to play a functional role.

The conservation of orphan toxin function indicates an evolutionary pressure to maintain function and / or a relatively recent transfer. A possible reason for such maintenance of function is that the orphan pairs of toxin tips and immunity proteins represent two different reservoirs of competitive advantage for the cell. As it has been shown for at least some orphan immunity proteins that they are expressed as functional protein (Poole et al., 2011) they can provide protection from the action of toxin from other species / strains present in the environment. This is not the case for orphan toxin tips but they do represent a pool of potential toxins that could be recombined back to fuse with the conserved region of cdiA and hence be expressed at the cell surface and effective. Another possibility is that the presence of these orphan pairs is a record of toxin transfer from other strains and species rather than the reservoir from they can be taken.

1.6 Bacterial competition in biofilms

In order to understand what ecological impact CDI systems could have it is useful to understand how they integrate into the existing body of competition theory. Studies in competition theory have been a fertile field of study fusing the areas of ecology and mathematics since the seminal studies of Hamilton (Hamilton, 1964). Whilst initially confined jr to experimental models based on large animals, the field has moved to embrace microbiological approaches to experimentally addressing competition theory due to the comparative ease with which experiments can be conducted. One of the classic experiments in this field was performed by Kerr and colleagues (Kerr et al., 2002) using a colicin toxin system as a probe of competition in communities expressing varying levels of toxin expression and toxin sensitivity, a system that was also revisited more recently by Nahum et all (Nahum et al., 2011).

Recent work reported by (Nadell et al., 2015) shows that the nature of growth within a

biofilm can provide a competitive advantage against invaders with close cell to cell interactions acting to block the ability of motile *Vibrio cholerae* to invade a preexisting biofilm.

One area of competition theory that is likely to be relevant to CDI systems is that of kin and kind discrimination (Strassmann et al., 2011). The idea of 'green beard' alleles (Hamilton, 1964; West et al., 2010) is particularly relevant when considering bacterial toxin systems. In this concept a 'green beard' trait acts to direct a benefit only to others that carry the same trait. This benefit can be spiteful, that is it can act to harm others that do not carry the trait and hence indirectly benefit the trait carrier. The role of CDI toxins as 'green beard' alleles have been discussed by Ruhe and colleagues (Ruhe et al., 2013b) in the context of cooperativity. In addition to these proposed interactions the presence of expressed orphan cdiI's allows for the possibility of a mosaic population with a complex web of inhibitor, resistant and susceptible cells on a per toxin basis.

Traditional approaches to studying these systems are based on the assumption of a cost to maintenance of systems such as colicins, for example in this case the usual requirement for release of colicins by cell lysis or the maintenance of plasmids encoding for the required factors. In the case of CDI systems the presence of the operon on the genome and the expression of a highly effective immunity protein to avoid self intoxication lead to a situation in which, at least under standard laboratory conditions, maintenance of functional CDI systems does not appear to have an impact on CDI+ strains. This can be seen from the lack of reported differences in growth rate between CDI- strains and both CDI+ strains and strains lacking only the CT-toxin region . It may be that under environmental conditions different selection pressures apply which act to limit the spread of CDI systems across more strains.

1.7   Hypothesis and Aims

This research aims to determine if *E. coli* cells that express CDI toxins have a competitive advantage when growing in a biofilm and if so can the class of the CDI toxin expressed alter the extent of this advantage.

Experiments will be carried out to determine if expression of the EC93 CDI toxin gives a competitive advantage in flow cell biofilms. A quantitative single cell analysis technique suitable for cell-cell interactions will be established. This assay will be used to measure the time course of toxin action, combined with the effects on inhibited cells morphology, and hence define the inhibition phenotype of different classes of CDI toxin.

Chapter 2

Methods

2.1 Chemicals and media

General chemicals used were of ACS or Bioreagent grade and were supplied by Sigma or Fisher. Reagents Stock solutions were stored as autoclaved or 0.2μm filtered solutions at room temperature as appropriate EZ defined rich media was supplied from Teknova and the separate components stored at -20°C until required when 1L of media at x2 concentration would be prepared without carbon source and aliquoted prior to -20°C storage to avoid additional freeze thaws. This stock was found to be stable for 6 months but longer storage periods led to poor culture growth. Water used for solutions was deionised grade (>8MΩcm^{-1}, dH$_2$O)if the solutions were to be autoclaved and ultra high quality grade (>18MΩcm^{-1}, UHQ H$_2$O) if the solutions were to be filtered.

2.2 General culture techniques

2.2.1 Bacterial strains and growth conditions

E. coli strains used in this study are listed in Appendix A. Appendix B shows the plasmids used / generated in the course of this work and all oligonucleotides used are shown in Appendix C.

Three types of liquid growth media were used in this study. LB media contained 20g/L LB Lennox (Fisher). M9 minimal media contained 1x M9 salts (Sigma Aldrich) supplemented with 0.4% glucose , 1mM MgSO$_4$, 0.1mM CaCl$_2$, 0.001% thiamine and 6x10^{-6}% iron citrate. EZ rich defined media (Teknova) is a commercial preparation of the media defined in (Neidhardt et al., 1974). Solid growth media contained the above media components and either an additional 17.5g/L agar or 15g/L of agarose (standard fraction or low molecular weight). Cells were grown at 37°C as a default temperature. Some plasmids used were temperature sensitive so strains maintaining these plasmids were grown at 30°C when plasmid maintenance was required and at 42°C when plasmids needed to be cured.

2.2.2 Strain storage and revival

Strains were laid down for long term storage in LB + 10% glycerol at -80°C in Corning cryogenic vials. Vials were seeded using a sterile cotton bud swabbed over the surface of a confluent LB plate, with appropriate antibiotic selection, which had been grown overnight from a single picked colony spread evenly. Strains were revived from storage by scratching the frozen surface of the preserved strain and streaking on to LB plate with appropriate antibiotics. This plate was then sequentially streaked three times, with intermediate flaming of the loop, so that single colonies grew in the final streak.

2.2.3 Antibiotics

Antibiotics were prepared at stock concentrations at 1000 fold the final concentration to be used in the appropriate solvent. If the solvent was organic antibiotics were stored and used at -20°C without further processing. If the solvent was aqueous the solutions were syringe filtered through a 0.2μm filter into sterile 1.5ml eppendorfs and stored at -20°C, with in use aliquots kept at 4 °C. Final antibiotic concentrations were prepared by dilution into appropriate media immediately prior to use. The following antibiotic concentrations were used ampicillin 100μg/ml, kanamycin 30μg/ml, chloramphenicol 34μg/ml and rifampicin 150μg/ml.

2.2.4 Optical density measurement

Measurement of the optical density of cell suspensions were all made using a Jenway 6505 UV/Vis spectrophotometer spectrophotometer at a wavelength setting of 600nm using 1ml disposable cuvettes. Prior to measurement the spectrophotometer was blanked versus diluent.

2.3 Molecular Biology

2.3.1 Polymerase chain reaction (PCR)

Plasmid and chromosomal sequences were entered into NTI Vector 11 (Invitrogen, Lu et al., 2004) primers designed using the software. Oligonucleotides for use as primers were ordered from Sigma Aldrich and were supplied as a lyophilised powder. Long term stocks were held as 100μM stocks in 1mM at -20°C with working stocks being made by a further 10 fold dilution to 10μM. All dilutions were based on the manufacturers supplied assay data.

Primer annealing temperature was calculated based on the nucleotide composition of the portion of the primer that anneals to the target according to the following formula:

Annealing temperature (°C)= (4(no. of G or C nucleotides)+2(no. of A or T nucleotides) -5

The lowest annealing temperature of the primer pair was used as the basis for initial PCR runs, if it was found to be inappropriate a range of annealing temperatures was trialled in order to determine a suitable temperature empirically. Extension time was varied by product length based on manufacturers recommendation for the particular DNA polymerase used.

PCR was performed with GoTaq flexi DNA polymerase (Promega) for analytical experiments. The manufacturers GoTaq Green buffer was used supplemented with 3µl 25mM $MgCl_2$ per reaction to give a final volume of 50µl. Reactions that were to be used for cloning used KOD polymerase (Novagen) or Pfu (Fermentas) proof reading enzymes capable of high fidelity replication. Again a 50µl was used supplemented with either 1mM $MgSO_4$ or 20mM $MgSO_4$ respectively.

2.3.2   Restriction digests

Restriction endonucleases were sourced exclusively from NEB and the manufacturers instructions followed for their use in the prescribed buffer. Double digestions were conducted under the compromise buffer conditions provided by the manufacturer. Digests were carried out in a volume of 20µl . Diagnostic reactions were performed at the recommended temperature for 1hr 30 minutes. Incubations for cloning were performed at the recommended temperature overnight with a second volume of restriction enzyme added after 1 hour to ensure complete digestion. If required restriction enzyme inactivation was performed by heating the sample to 65°C for 20 minutes.

2.3.3   Agarose gel electrophoresis

Samples were prepared for loading on gels by addition of 5x loading dye (York bioscience) or 6x loading dye (Fermentas) to give a final dye concentration of 1x. DNA electrophoresis was performed in agarose gels ranging in concentration from 0.8 to 2% agarose buffered with TAE buffer (0.04M Tris Acetate, 0.01M EDTA) containing either 0.001% ethidium bromide or 1µg/ml Nancy-520 dye (Sigma Aldrich). At least one lane on the gel was run with a DNA molecular weight marker either Q Step 4 (York bioscience) or Generuler 100-10000 (Fermentas). Electrophoresis was perfomed using voltages in the 22-100V range. Gels were imaged using a G-Box gel imaging system with Genesnap software (Syngene) with dye excitation by UV transillumination (ethidium bromide) or a Dark reader blue light transilluminator (Clare Chemical Research).

2.3.4   Band excision and DNA extraction

Bands to be excised where visualised using the appropriate illumination method for the dye used. If UV illumination was required then only brief illumination with a hand held UV lamp

was performed to minimise UV light induced DNA damage. A fresh sterile disposable scalpel was used for cutting out of each band with care taken to ensure only the band and immediate area were removed. DNA was extracted / purified from the cut band using the QIAEX II gel extraction kit (QIagen) and eluted in 30μl of UHQH$_2$O.

2.3.5 DNA ligation

T4 DNA ligase (Fermantas) was used with supplied buffers according to manufacturers protocol. Ligation ratio was determined using the following formula in order to give a molarity of insert that was three fold greater than that of plasmid:

Ratio of insert to plasmid = 3(insert size x plasmid concentration) / (plasmid size x insert concentration)

Once mixed samples were incubated at 16°C overnight. Samples were then drop dialysed to remove salts prior to electroporation.

2.3.6 Drop dialysis

Removal of salt from samples, typically prior to electroporation, was performed using drop dialysis. 0.2μm filter discs (VSWP filters, Millipore) were floated on top of 20ml of UHQH$_2$O and up to 20μl of sample pipetted on to the center of the disc. Sample was then incubated for at least 1 hour at room temperature. If required completion of salt removal was confirmed by DNA concentration analysis.

2.3.7 Competent cell generation

Competent cells were generated using one of the four protocols detailed below dependent on the level of competence required for the particular application.

2.3.8 Classic electrocompetent cell preparation

Cells to be made competent were grown overnight from a single colony in 5ml LB (with appropriate antibiotics). 2.5ml of this overnight culture was used to inoculate 250ml LB (with appropriate antibiotics) in baffled flasks that were grown at appropriate temperature (typically 30 or 37°C dependent on plasmid stability) to an OD$_{600}$ of 0.5-0.7. The culture was then chilled on wet ice for 20 minutes, all subsequent steps were performed on ice with prechilled containers. Cells were then centrifuged for 7mins at 3000g , 4°C the supernatant discarded and the cells resuspended in 125ml sterile 10% glycerol in UHQ H$_2$O. This process was then repeated with two lots of 5 mins spin / 80ml resuspension before a final 5 mins spin. This final pellet was resuspended in 0.6ml ice cold 10%glycerol and either transformed immediately or flash frozen and stored at -80°C for future use.

2.3.9 Density step electro competent cell preparation

Electrocompetent cells were prepared according to a method based on (Warren, 2011). Overnight culture grown from single colony in 5ml LB and appropriate antibiotics. 2.5ml of overnight culture inoculated into 200ml LB (with antibiotics) in baffled flask and grown at appropriate temperature (typically 30 or 37°C dependent on plasmid stability) to an OD_{600} of 0.4-0.6. Culture was then chilled for 10 mins in an ice water bath and all subsequent steps performed on ice with prechilled containers. Cells were then harvested by centrifugation at 2000g, 4°C in 4 x 50ml sterile disposable centrifuge tubes (Corning). After disposal of the supernatant the pellets obtained were gently resuspended in 1ml UHQ H_2O per tube then aggregated into one tube and made to a final volume of 40ml with UHQ H_2O. 20ml of this suspension was then placed in two fresh tubes and carefully underlayed with 12ml of 20%glycerol / 1.5% mannitol in UHQ H_2O. Centrifuge tubes were then centrifuged immediately at 2000g, 4°C using reduced acceleration / deceleration parameters to avoid disrupting step gradient. Solutions were carefully aspirated to leave cell pellet which was then diluted with 200μ of 20% glycerol / 1.5% mannitol. Competent cells were then transformed immediately or flash frozen and stored at -80°C for future use.

2.3.10 Quick electro competent cell preparation

Quick electrocompetent method was used to generate cells for plasmid transfer in strain backgrounds that were less efficient at transformation (personnel communication, Erica Kintz). Electocompetent cells were prepared by scraping 3 colonies of the required cells from a plate using a sterile pipette tip and resuspending the colonies in 100μl ice cold 10% glycerol. This suspension was centrifuged at 13000 rpm / 16060g for 1 minute at room temperature and the supernatant discarded. The pellet was resuspended in 100μl ice cold 10% glycerol and respun. This final pellet was resuspended in 100μl ice cold 10% glycerol and competent cells transformed immediately.

2.3.11 Electroporation

Electroporation was performed using electrocompetent cells prepared using the methods above with a BioRad Micropulser electroporator. 2mm gap sterile disposable electroporation cuvettes (Molecular Bio Products / Bio Rad) were prechilled on ice before addition of 50μl of competent cells to 1-2μl of DNA solution in the cuvette. This mixture was held for at least 1 minute on ice before proceeding. Electroporation was performed using program Ec2 on the electroporator and 1ml of SOC (2%tryptone, 0.5%yeast extract, 10mM NaCl, 2.5mM KCl, 10mM $MgCl_2$, 10mM $MgSO_4$, 20mM glucose) added immediately afterwords to the cells which were then grown for at least 1 hour prior to plating onto LB agar plates with the relevant antibiotic

selection.

2.3.12 Quick transformation

The quick transformation method was used to move plasmids between readily transformable strains. Competent *E. coli* were generated using the PEG 3350 based protocol described in (Chung et al., 1989).

2.3.13 DNA purification

DNA purification was performed according to the protocols shown below.

2.3.14 Genomic DNA purification

Genomic DNA was isolated using the CTAB/NaCl method described in (Wilson, 2001). Extraction was performed on 1.5ml of overnight culture grown in LB media with appropriate antibiotics. Purified DNA was resuspended in 100µl EB buffer (Qiagen)

2.3.15 Plasmid DNA purification

Plasmid DNA was purified using the QIAprep spin miniprep kit (Qiagen) from 4.5ml of overnight culture grown in LB with appropriate antibiotic. The additional PB wash step recommended by the manufacturer was used. Plasmids were eluted in 50µl of EB for high copy number plasmids or 30µl of EB for medium/ low copy number plasmids.

2.3.16 PCR purification

PCR reactions to be used in cloning were cleaned up using QIAquick PCR purification kit following the manufacturers instructions with the sample eluted in 30µl of EB buffer (Qiagen) or UHQH$_2$O.

2.3.17 Concentration of DNA

DNA concentration was performed in a MiVac DNA concentrator (Genevac) until the desired volume was achieved. Drop dialysis was then performed to remove excess salt.

2.3.18 Determining DNA concentration

DNA concentration was determined on 1.2µl samples using a Nanodrop ND-1000 spectrophotometer blanked with appropriate diluent / eluent. Purity was assessed on the basis of the A$_{260}$ / A$_{280}$ ratio being greater than 1.8. When appropriate examination of the spectra was also performed to determine the level of salt present in the sample.

2.3.19 Genomic integration

Generation of genomic integrants was performed using one of the two protocols detailed below.

2.3.20 CRIM protocol

PCR using oMV429 and omV432 was performed to confirm the presence of the attB site in the EC93 wild type strain. The CRIM protocol defined by Haldimann and colleagues was followed (Haldimann et al., 2001). Strains in which genomic integration was required firstly had the pINT-ts helper plasmid introduced by electroporation. Strains with genomic integration were then obtained by electroporation of plasmid pMV285 or pMV350. Screening for single genomic integrants was performed as described by Haldimann (Haldimann et al., 2001) using oMV429, oMV430, oMV432 and oMV656primers. Successful integration was further confirmed by sequencing the insert. Please see appendices A,B and C for further details of strains, plasmids and oligonucleotides used.

2.3.21 Lambda Red protocol

The lambda red protocol defined by Datsenko (Datsenko et al., 2000) and Sawitzke (Sawitzke et al., 2007) was followed. Strains in which genomic integration was required firstly had the pKD46 helper plasmid introduced by electroporation. Cassettes for insertion where generated by PCR either from chromosomal template, MV1213 (oMV935, oMV936 primers), or from plasmid template pMV370,pMV371,pMV372 and pMV373 (oMV939, oMV940 primers). Prior to use the PCR products were purified by gel extraction. pKD46 containing strains then had λ recombinase genes induced with 0.2% arabinose 1hr prior to harvesting for electrocompetent cell preparation. The purified PCR products were then electroporated into the competent cells. Successful integration was confirmed by PCR and by sequencing. Please see appendices A,B and C for further details of strains, plasmids and oligonucleotides used.

2.4 Single cell analysis

2.4.1 Cell growth conditions

Single colonies were picked from plates and used to inoculate 5ml of EZ defined rich media + 0.4% glucose and grown overnight on wheel in 37°C incubator. After 16 hours of growth overnight cultures were diluted 1:100 in to fresh media and grown for a further 5hrs at 37°C.

2.4.2 CDI Planktonic competition assay

Measurement of the effectiveness of inhibition of CDI systems was performed using a method based on that reported in (Aoki et al., 2010). *E. coli* target strains used were susceptible to CDI (lacking cdiI) but containing a selectable marker present only in the target strain (kanamycin or chloramphenicol resistance in this work). Inhibitor strains tested were those expressing the relevant CDI system or controls in which the CDI system was disrupted, typically by deletion of all or part of the cdiA gene. Inhibitor and target strains were grown overnight from single colonies in 5ml LB + antibiotic if appropriate at 37°C. Inhibitor cultures were then diluted down 100 fold (0.5ml O/N culture to 50ml LB) in baffled flasks and grown at 37°C in a shaking incubator at 200rpm to an $OD_{600} = 0.3$ (1h 45 mins growth time). Overnight target cell culture was then added to give an effective target concentration of $OD_{600} = 0.01$ in the flask and growth continued. Samples of culture were taken at time of addition of target cells and after 3 hours of cell growth. Target cell colony forming units (cfu) were determined by serial dilution of samples, plating out on LB agar plates with suitable antibiotic and counting of colonies on plates in 10-100 colonies/ plate range.

2.4.3 Casting of agarose pads

A variety of different casting methods were trialled with the one described in (Young et al., 2012) being identified as the most suitable to take forward for the bulk of the analysis. Briefly the progression was from:

- Pads excised from normal media plates in standard sized petri dishes mounted on standard lab slides.

- Pads excised from thinner than normal (10ml vs 25ml media/agar volume) placed in cover slip bottomed petri dish.

- Pads cast using low melting point agarose between glass cover slips place in cover slip bottomed petri dish.

Fresh EZ defined rich media + 0.4% glucose was prepared by aseptically mixing 5ml of x2 EZ defined rich media stock solution, 4.8ml autoclaved water and 200µl 20% glucose stock solution. 0.15g of low melt point agarose was added to the 10ml of media in a 50ml sterile disposable plastic centrifuge tube and microwaved in a 800W microwave oven for 20sec medium setting, 10 sec low setting, 10 sec simmer setting. In between each heating the tube was briefly vortexed. The solution was then examined to confirm that all of the agarose had dissolved and an additional 10 sec simmer setting heating performed if required. Once all the agarose was dissolved a final 3 sec simmer heating was performed with no vortexing to aid elimination of

bubbles from the mixture. The solution was then left to cool for 2 minutes at room temperature on the bench. The required number of 22x22mm cover slips were placed onto parafilm on the bench and 1ml of 1.5% agarose solution pipetted per cover slip, ensuring no bubbles were present. This was followed immediately by the careful dropping of a second cover slip from just above the solution surface so as to create a glass, agarose, glass sandwich which due to surface tension is perfectly level and even.

2.4.4   Microscopy

A Zeiss Axiovision 200 microscope was equipped with the equipment detailed in Table 1. Incubation at 37°C was started at least 18 hours prior to the start of the experiment in order to ensure thermal equilibrium had been reached including ensuring the lens oil was in the hotbox. At least two hours prior to acquisition a check of microscope bright field alignment was performed to ensure Köhler illumination was correctly set up, a requirement for high quality phase images to be obtained. This was performed on an empty coverslip bottomed petri dish with a pen mark to aid focus which was sufficiently similar to the pad dishes that only minor adjustment of condensor position was required. Fluorescence source was turned on 30 minutes prior to use to ensure stable emission. Samples were prepared using a lab made hotbox consisting of a 20cm x 10cm x 10cm sealable plastic container with two 30ml sterilins to act as thermal mass. Aliquots of samples and dishes were stored in this container and manipulations performed on the container to minimise thermal shock to the cells. 1µl of each strain to be studied were pipetted onto the glass cover slip portion of a prewarmed cover slip glass bottomed petri dish (MatTek P35G-1.5-14-C 35mm petri dish 14mm Microwell, no. 1.5 cover slip (0.16-0.19mm)) so that their surface tension kept them apart. A 5mm x 5mm pad was freshly cut from a prewarmed pad using a sterile scalpel and carefully placed over the two droplets so that they spread and mixed as a thin layer between the pad and the cover slip. This process was then repeated for up to five different pads per dish.

2.4.5   Image analysis

Images stacks acquired in Axiovision zvi format were imported into OMERO and converted to OME-TIFF format as part of this process. As time lapses were acquired as a series of separate image stacks the stacks corresponding to the field of view to be analysed were concatenated in Image J (Schneider et al., 2012). The concatenated image stack containing solely sequential phase contrast images was then taken forward for processing by two routes. Firstly the assignment of cell outlines was performed using MicrobeTracker version 0.935 (Sliusarenko et al., 2011) software running in Matlab R2010b (7.11.0) with the corresponding version of the Matlab Image Processing Toolbox. Full software processing instructions are available from the website but in brief the image stack to be processed was imported and aligned using the

Table 1: Single cell microscopy equipment

Role	Equipment name	Advantage
CCD camera	Zeiss Axiocam Hrm	Monochrome camera for maximum sensitivity
Stage heater	Large incubation chamber	Enclosing a large part of microscope leads to greater thermal stability
Microscope stage	Motorised stage (in x,y,z) with μm accuracy	Multiple fields of view can be returned to with high precision, allows autofocusing and automation of runs
Objective	Plan-Apochromat 100x/1.4 NA oil	Enables high resolution image capture
Shutter	Fast action motorised shutter	Minimises unwanted light exposure and allows automatic aquisition
Filter carousel	Motorised filter holder	Allows rapid changes and automatic aquisition
Filters	Fluorophore specific filter sets	Optimised filters for fluorescence aquisition let lower light levels be used minimising phototoxicity
Autofocus system	Axiovision software, Zeiss	Allows automated aquisition without focal drift

built in automatic tool. In some cases purely automatic alignment was not successful and so an additional MicrobeTracker alignment tool was used which allows for manual marking of a constant position which is then used as an anchor for image correlation between frames to generate an aligned image set. As the pads imaged always contain some slight imperfections from the casting process which are visible in the phase contrast images one of these which remained outside of the areas of microcolony growth for the time period to be analysed was chosen as a marker site. Once aligned the alignment was saved as a Matlab file so that it could be reconstituted at a later date if required, the images were then shifted so that the final outline assignment would be available as an aligned data set.

Images were processed using the independent frames setting as the time lapse outline assignment was found not to be robust after the initial period of micro colony growth. Segmentation was assessed using the preview mode so as to ensure clear cell outlines were obtained and appropriate parameters adjusted if required, see Table 2. Based on the initial fluorescence images target cell and inhibitor/deletion mutants were identified and regions were interaction occurred were taken forward for analysis. Automatic assignment of outline was performed and then reviewed to identify any cells which had incorrect outline assignment for example due to inappropriate splitting of a cell outline for a cell that had yet to divide. As only the growth of target cells needed to be followed outline assignment was performed for all target cells in the region analysed but only for inhibitor / deletion mutant cells were it aided interpretation as to the contact point of the differing microcolonies.

Cells which had thus been identified were then corrected using the manual options included in MicrobeTracker (e.g. Split, Join etc.). This process was repeated for all frames up until buckling and overriding of the cells was visible in the images as at this point it is no longer possible to assign areas to the cells lying out of the horizontal plane of view. After correction the data set was exported to Excel as a matrix of cell numbers per frame with measured area and length, in addition an image stack of the phase contrast image overlayed with the cell outline and cell number plus frame reference was exported in preparation for the next stage of analysis.

Building on the individual cell parameters the next stage performed was to assign this data to the appropriate cell lineages. Annotation of the overlay image stack was performed by importing the stack into ImageJ and manually annotating each lineage using differently coloured dots to represent each unique cell. On cell division the mother cell, cell with old pole (assigned randomly for cells in first frame of experiment) retains the same coloured dot and the daughter cell is assigned a new coloured dot. By iterating through all possible lineage branches of the target cells in the initial frame a complete annotation of lineage is obtained. Comparison of this annotated image stack is then made to the snapshot fluorescent images taken for strain assignment to both confirm that target strain lineage has been assigned appropriately and to

Table 2: MicrobeTracker processing parameters

Variable name	Range of Values	Property affected
areaMin	120-200	Minimum area of the region or the cell that is kept
areaMax	2000-2200	Maximum area of the region or the cell that is kept
thresFactorM	0.95-1.125	Image intensity threhold factor
movelall	0.1-0.2	Whole cell motion coefficient
fitStepM	0.5-0.6	Norm of the step size of the whole cell motion (in pixels)
splitThreshold	0.15-0.35	Relative threshold determining when the cell has to be split into two
attrCoeff	0.3-0.5	The force attracting the contour to the dark areas outside of the cell
repCoeff	0.25-0.3	The force repulsing the contour from light areas inside the cell,

allow marking of inhibitor / deletion mutant cells when they have come into contact with target cells. This final annotated image is then used as the basis of manual transcription into an Excel file of the cell numbers for a given cell lineage through the time course of the experiment with additional annotation of cell division points, links to daughter cells and contact with inhibitor cells being recorded. These cell number lists were then correlated with the cell parameters exported from MicrobeTracker using a custom spreadsheet to automatically transpose the appropriate data using built in Excel array search functions.

This data was then transposed to a single column format in Excel and further manually annotated with cell cycle and cell lineage numbers and the resulting data exported as a CSV file. R (R Core Team, 2013) (ver 2.14,2.15 and 3.02) using Rstudio (RStudio, 2014) with R packages ggplot2(Wickham, 2009), plyr(Wickham, 2011), lme4(Bates et al., 2013), reshape(Wickham, 2007), scales(Wickham, 2012), devtools(Wickham et al., 2013) was then used to perform a linear regression fit to the data on a per cell cycle basis with the slope of this graph being taken as a measure of the growth rate in arbitrary units. This data was also graphed using per cell cycle and per lineage binning in order to assess the quality of a linear fit to growth rate and to look for general trends in interactions.

2.5 Initial biofilm flow cell protocol

2.5.1 Cell growth conditions

Single colonies were picked from plates and used to inoculate 5ml of LB broth and grown overnight on wheel in 37°C incubator. After 20 hours of growth overnight cultures were either used directly for inoculation or diluted down using fresh LB broth to give final OD_{600} of 0.8 or 0.016 dependent on co seeding conditions required.

2.5.2 Flow cell assembly

All parts were autoclaved prior to use. Assembly was performed in a laminar air flow (LAF) cabinet as no additional sterilisation procedures were used prior to running the experiment. To allow co seeding to be performed the flow cell (Model FC 281; Biosurface Technologies, Bozeman, MT, U.S.A.) was half assembled and initial cell seeding performed, this culture was then aspirated and the final assembly of the flow cell performed followed by tube and bubble trap attachment. Media transfer from filtration apparatus was made in the LAF cabinet into conical flask with bung and appropriate tube vents. The completed apparatus was then transfered to the incubation chamber and peristaltic tubing installed into 205S Watson Marlow peristaltic pump with the media container being placed in a 37°C water bath. Media in its sealed filtration container was equilibrated to 37°C for several hours prior to transfer to the final media vessel to ensure it was already at a suitable temperature for media flushes.

2.5.3 Initial flow cell growth and imaging

Co seeding protocols used a variety of different start inoculation concentrations dependent on the requirement for how heavy an initial seed cell concentration was required. Heavier initial inoculums lead to faster cell mass accrual within the time course of experiments. Cells were inoculated in two stages using different approaches as the flow cell was assembled. Firstly 1ml of 1st cell inoculum dilution was pipetted onto each channel of the half assembled flow cell in the LAF cabinet. This solution was spread out by pipette to ensure it contacted all of the cover slip surface then covered with the top half of a sterile plastic petri dish to ensure the solution was not dried out by the airflow of the LAF cabinet. An incubation of 1 hour at room temperature was then performed with the inoculum then being aspirated by pipette to waste with care being taken not to touch the glass surface to which the cells had adhered. Final assembly and transfer as detailed above was then performed as rapidly as possible to avoid the cells drying out.

The first media flush was then performed for 5 minutes at 5ml/min/channel after which the inlet tubing was clamped to avoid any possibility of back flushing on injection. The second inoculation was then performed via the injection ports built into the flow cell inlets with 1ml of cell solution being injected using a sterile syringe. Post injection the inlet port was wiped with 70% ethanol. Incubation of the 2nd seeding was performed for 1hr at room temperature before the inlet clamp was released and the second media flush performed for 5minutes at 5ml/min/channel. The flow cell was then incubated for the required time at 37°C at a flow rate of 1ml/min.

After an appropriate incubation time (typically 14 hours) the flow was stopped and the tubing on either side of the flow cell clamped so as to leave 20cm of tubing from the flow cell to the clamps in order that the weight of the camps would rest on the stage edges and not catch when the flow cell was maneuvered. The tubing was then cut and sprayed / wiped with 70% ethanol. The separated flow cell was carefully placed on a bed of tissues within a metal tray with care being taken not to dislodge any bubbles that may have formed during the time course of the experiment. The flow cell was then taken immediately to the microscope for imaging with all subsequent steps being performed at room temperature.

Confocal microscopy was performed on a Zeiss LSM 710 / Axio Observer.Z1 invert confocal microscope using filters and laser lines suitable for the fluorescent proteins used as detailed by Lakins and colleagues (Lakins et al., 2009). Due to the dimensions of the flow cell used the microscope set up required some modifications in order to be able to access the optical surfaces without fouling the surrounding metal frame. All objectives apart from the one used for imaging (x40 DIC or x63 Ph oil,). The remaining objective was then mounted on a brass extension collar. Finally the normal stage holder fitting was removed and a custom made stage insert fitted. This set up along with warming up of lasers and software parameter configuration

was performed prior to terminating the flow cell flow so as to minimise hold time post flow stop. The flow cell was carefully balanced on top of the stage insert with the cover slip side pointing downwards and taped into place if required. If required oil was applied onto the objective and applied across the cover slip surface by manipulating the stage. A second application of oil was then made to the objective to ensure sufficient oil would be present as the objective tracked over relatively large distances. Care was taken to ensure the objectives were not crashed into the frame as there was very little clearance. A mid channel position was used for image acquisition as the objective could not fit in the cell edges. Images were acquired sequentially from the two channels as movement between the two channels required the objective to be fully wound away from the surface and then carefully brought back to the next channel due to the presence of the metal holding frame between the channels.

After image acquisition was completed the flow cell was reattached to the original tubing and the whole system flushed with water. On completion of the water flush the system was dismantled with the flow cell being cleaned of glass and sprayed / wiped with 70% ethanol prior to autoclaving of all used parts and fresh tubing cut to size as required.

2.6   Second biofilm flow cell protocol

2.6.1   Cell growth conditions

Single colonies were picked from plates and used to inoculate 5mls of LB and grown overnight on wheel in 37°C incubator. After 16 hours of growth overnight cultures were diluted 1:100 in to fresh media and grown for a further 9hrs at 37°C. At this time point OD_{600} readings were taken of diluted samples (dilution performed in M9 salts) and assuming samples had an undiluted OD_{600} of 3.2 they were diluted in 2mls of fresh media to as to give a final OD_{600} of 0.016.

2.6.2   Flow cell assembly

All parts were autoclaved prior to use except the polycarbonate flow cell, see Appendix D for design based on previous work by Pamp, Wolfaardt and colleagues (Pamp et al., 2009; Wolfaardt et al., 1994), which is not suitable for autoclaving. Then a glass cover slip (22 x 22 mm, no. 1.5, SLS) required to complete the flow cell was glued over the channels using silicone glue (RS code no. 692-542) and left to adhere at room temperature for at least 24 hours to ensure curing of the glue was complete. Tubing and flow cell were assembled on the bench and transfered to 37°C incubator. Sanitisation in place (SIP) was performed in place using 0.5% Sodium hypochlorite in water with a minimum contact time of 2 hours with 0.175ml/min flow rate. System was filled and drained at least twice during this procedure to ensure full contact on all areas (no areas shielded by bubbles of air). After completion of SIP the system was flushed with 0.2μm filtered water for two hours with multiple flushes of the system and swapping to fresh water containers

to ensure complete removal of hypochlorite from system. While this SIP protocol was being performed a filtered media vessel was fitted with autoclaved piping and prewarmed in a 37°C water bath to give chance for degassing to occur prior to flow commencing. Immediately after SIP rinse was completed connection was made between media vessel and flow system to complete the system.

2.6.3   Flow cell growth and imaging

Inoculation of media equilibrated flow cell was performed using needle and syringe. The tubing area to be injected was first wiped with 70% ethanol solution , the inlet to the flow cell clamped and the peristaltic tubing/frame released from the pump to allow free flow of inoculum. The needle was then gently inserted into the tube ensuring that only one wall of the tube was penetrated and the culture pushed in as gently as possible (1ml in 1min 40 secs). The peristaltic tubing/frame was then replaced into the pump. The area was then sealed with a small blob of silicone glue. This process was repeated for each channel with the incubation time starting once all channels had been inoculated. At the end of the incubation period the clamps were released and the pump run at 0.875ml/min for 5 minutes in order to flush non adhered from the flow cell. Once the flush was completed the procedure was repeated for a second set of inoculation injections. The coseeded flow cell was then incubated for the required time at 37°C with a flow rate of 0.175ml/min.

After an appropriate incubation time (typically 9 hours) the flow was stopped and the tubing on either side of the flow cell clamped so as to leave 15cm of tubing from the flow cell to the clamps in order that the weight of the clamps would rest on the stage and not act to lift the flow cell up. The tubing was then cut and the ends sprayed / wiped with 70% alcohol so as not to contaminate the microscope with bacteria. The now separated flow cell was carefully placed on a bed of tissues within a metal tray to protect it and kept at room temperature from this point forward. The flow cell was immediately transfered to the confocal microscope which had been previously initialised for use, to ensure there was the minimum delay in observation time from stopping the flow of media. The flow cell was gently transfered to the stage holder (standard sized slide adjustable length holder used) and clamped into place, with care being taken to ensure the cover slip glass bottom was not crushed. The short distance of the remaining lines were placed so as not to interfere with stage movement and taped into place if required. Secondary adjustment of flow cell position was performed if initial observation of confocal stacks indicated that a planar arrangement had not been achieved.

Confocal microscopy was performed using a Zeiss LSM 510 meta / Axiovert 200M confocal microscope. No exchange of objectives was required with this flow cell design, but the imaging protocol followed was otherwise as described in Section 2.5.3. As images were acquired across a large area of the cover slip surface care had to be taken to ensure a sufficient level of lens oil

was applied to maintain sufficient contact as the oil immersion lens traversed long distances. This was achieved by adding oil to the lens and using the stage to move this across the surface of all the areas to be observed. A second lot of oil was then added to the lens and observations commenced. As confocal z stacks take a non trivial amount of time to collect and the flow of media was no longer occurring care was taken with the order of image stack acquisition so as not to possibly bias results. Images were acquired at the same relative x position in each channel before moving on to the next x position and so on iterating down the channel. In this way images from each channel were acquired at similar times so that any effects of hold time would not skew results between channels. Suitability of confocal acquisition parameters were checked at the start of each experiment to ensure a signal utilising the full range of the confocal detector was obtained and that the ramping of laser power and detector sensitivity with increasing z depth was sufficient to allow cell detection.

After image acquisition was completed the flow cell was reattached to the original tubing and the whole system SIP'd using the protocol described in the previous section. On completion of the water flush the system was dismantled with tubing / small parts being immediately autoclaved with fresh tubing being cut to length and autoclaved as required. The flow cell was prepared for subsequent work by carefully removing the coverslip and associated glue using a scalpel to carefully scrape clean the flow cell surface. The surface and built in tubes were cleaned with 70% ethanol and air dried ready for the next experiment.

2.6.4   Flow cell growth and time-lapse imaging

In order to perform time-lapse imaging analysis a change to the above protocol was required to allow mounting of the flow cell on the microscope stage with flow of media. . Time-lapse imaging analysis was performed with amendments to take advantage of the availability of a confocal microscope with a full stage incubator. The media was preheated to 37°C and using a smaller reservoir vessel, capable of fitting in the incubator itself, a temperature controlled supply of media could be provided at the microscope. This was then connected to the flow cell with tubing being carefully secured to the stage by tape at positions which would not interfere with its operation. The tubing then exited the incubator for the remainder of the flow path allowing the pump to be situated away from the microscope on a separate part of the table from the vibration platform to ensure its operation did not affect the stability of the microscope. In order to avoid the potential leakage of aggressive chemicals onto expensive equipment the SIP and rinses, which were performed as detailed above, were performed in the main lab and the assembled apparatus then transfered to the microscope with out any need for connections to be broken and remade, hence there was no increase in contamination potential.

The experiment was then conducted in a similar manner to that detailed in section 2.6.3.

Sufficient tubing length was used so that the flow cell could be removed from the incubator enclosure for inoculation both for practically of access and to avoid any chance of getting glue on the optic path / other parts. Unlike the issues with pulsation reported in (Lakins et al., 2009) when imaging with the flow on the inversion of pump placement to suck media through the flow cell resulted in a smooth flow that did not give any artefact's within the z stack. Images were acquired at one to three hour intervals dependent on the rate of biofilm growth to minimise the effects of over exposure to fluorescent light by observing only at points when significant change will have occurred.

Chapter 3

Single cell analysis method development

3.1   Introduction

In order to perform image based analysis of bacterial cells at the single cell level three different stages of the protocol must be operating effectively. Firstly software capable of measuring the size parameters of individual bacterial cells automatically is required. Secondly the preparation of the bacteria for microscopy must allow growth over several hours while maintaining a planar field of view that is compatible with phase focus microscopy. Finally the microscope used must be capable of acquiring high quality images of multiple fields of view during time lapse experiments. The method development performed to optimise each of these stages is detailed in the sections below.

3.2   Single cell image analysis

With advances in computational power and software techniques it has become possible to quantify images rather than simply make qualitative statements on the phenomena they represent. Commonly available computer hardware is now sufficiently powerful so as to allow image processing without dedicated high end workstations. Image analysis of bacteria presents a number of unique challenges due to the small size, rapid movement and the frequency of cell division under growth under common experimental conditions. A successful option for analysis must be able to cope with all these different constraints.

3.2.1   Survey of software options for analysis single cell level bacterial images

Three main classes of imaging analysis software can be identified that are relevant to research:

1. Commercial packages which are general in scope, being capable of analysing a wide

range of types of images in a variety of ways but also tending to be biased to match the work flow required for the most popular work flows, for example eukaryotic cell analysis using confocal microscopy. Examples of these programs would include Imaris and Volocity (Perkin Elmer). This kind of software while expensive is often provided as a service by Imaging facilities and has a significant of support available from both vendors and public forums and colleagues.

2. General academic projects which are multi year funded from technical grants with the aim of providing free customisable software to aid research groups work. The classic example of this is ImageJ (Schneider et al., 2012) which contains a core set of imaging tools useful in almost any image processing situation. In addition due to its ubiquity and extensible nature, it has a plethora of plugins to allow more specialised analysis which are widely shared / packaged (e.g. LOCI) within the community. Support is available via public forums and colleagues.

3. Specific lab software which has been generated in support of work done in a scientific grant. In this case the software has been written to fill a specific analytical need in the authors lab e.g. Schnitzcell (Locke et al., 2009) , MicrobeTracker. (Sliusarenko et al., 2011). As the software was not written for general use it may lack significant documentation, it will have no ongoing support as the developers have moved onto other projects and significant bugs / inabilities to run in other computing environments may exist. However it is likely to be an extremely focused solution to a specific analytical problem that may not be tractable using the tools available from routes outlined in a) or b).

The image analysis work flows used in this thesis were developed using a blend of all three kinds of software identified as offering the best solution after trial of the most relevant options used in the literature.

In order to follow bacterial growth in mono layers the class of image to be followed needs to be determined with the options being light microscopy or fluorescence microscopy both of which have their own unique advantages and disadvantages. In order to visualise bacteria by light microscopy a method to increase the contrast of the bacteria from their background is required as due to their small size and transparent nature they are otherwise only barely distinguishable. The historic methods of staining bacteria while capable of revealing even fine details (e.g flagella staining (Mayfield et al., 1977)) are not compatible with live cell imaging. Instead physical methods of manipulating the light field can be used of which the most relevant to bacteria is the use of phase contrast microscopy. This technique uses the difference in refractive index as a way to introduce contrast with the more commonly used positive phase contrast giving dark cells on a light grey background. However as the contrast generating mechanism is dependent on the density differences around samples dense dark cells are only

obtained when bacteria are spread singly or in small groups (< 4 cells). As microcolonies grow in a mono layer rod like cells naturally grow in a raft like manner with adjacent cells closely opposed (Shapiro et al., 1989). This leads to a marked change in the density surrounding the cells, from the low density of agarose/media to the high density of a packed bacterial cell body. During assay development it became apparent that an additional complication was that interior cells, particularly those growing rapidly, exhibited a mottled appearance, see section 3.3. This lack of uniformity in the cell interiors greyscale image further complicates cell assignment.

Furthermore as a time lapse image of cells needs to be analysed there needs to be a method (either manual or automatic) to follow the growth and splitting of cells into mother and daughter cells and to link the measured areas to this lineage. Finally as CDI is a contact dependent phenomenon a method to track when interaction between cells of differing microcolonies occurs. In order for any of these approaches to be viable excellent quality images must be available for analysis, that is high resolution with even illumination, minimum of phase artefact's due to imperfections in mounting medium. Details of how this was achieved are given in the appropriate method development section.

In combination these factors present a complicated problem for computational analysis which requires dedicated software in at least part of the pipeline. The common approach taken is too generate an outline of each bacterial cell. This cell outline can hence be used to calculate the length, width and area of the bacterial cell it was derived from. By examining the same cell in a series of time lapse images a measure of its growth rate can be made by plotting cell area over time, as the cell grows the area increases up until the point of cell division at which point the cell area will be assigned to the mother and daughter cells. An additional level of information can be determined if a grid is superimposed across the cell shape to allow determination of positioning of secondary imaging data, commonly focal fluorescent signals originating from labeled or tagged proteins.

The first step that is taken by all the laboratory software that has been reported in the literature is to perform a watershed transformation of the image from greyscale to black/white with transition parameters defined so as to pick a greyscale cut off that leaves filled cell blocks. This simplified image is then amenable to outlining by computational analysis. Programs such as Schnitzcell (Young et al., 2012) leave the refinement of cell outlines at this point. Some groups have however focused on questions which required more precise localisation within a cell framework and/or application to cells with an elongated phenotype. In these cases as simple thresholding will not lead to an assignment of cell shape with sufficient accuracy. MicrobeTracker software (Sliusarenko et al., 2011) takes a more sophisticated approach to allow refining of cell outlines based on the initial water shedding analysis. In this case for each individual cell an iterative force based refinement is performed see Figure 3 with a wide

variety of parameters being used to model attraction to areas of an image that represent the cell and repulsion from areas of the image that represent areas outside the cell. Once this refinement is confirmed cell areas are compared and overlapping cell areas assessed for joining and elongated cells checked for splitting, based on areas within outline that represent 'pinch points' in cell outline. Once completed on the whole of area of an analysed image this approach can cope with cells that are elongated and with cells that do not exhibit a uniform interior level of contrast. Whichever approach is taken it is common for a manual method of cell outline assignment to be included as perfect assignment rarely occurs for all cells in a crowded field.

To assign lineage a comparison between images in a time lapse must be made, as the lineage is of the cells being observed this is in fact done on the processed image. In order for this approach to be practical it is essential that the images to be worked on are correctly aligned. That is any shift in the field of view is taken into account. Ways to minimise shift are discussed in the relevant section but even with those approaches some degree of shift will always have occurred when working at the high magnifications required to study bacteria. Correct alignment can be recovered in three possible ways.

- Manually : shifting of image alignment using minor defects in the agar the cells are embedded in is possible for small numbers of images but quickly becomes impracticable

- Semi automatically : Time lapse series of images are marked with a cardinal point which represents a known same point. This can be added deliberately for example by including a low level of beads in cell mix (Young et al., 2012). But practically there is always a minor defect that can be picked out on the agarose surface. Once this known good position has been marked in all frames or at least those before and after any significant shifts it is a simple matter for a computer program to use this data to correct alignment.

- Fully automatically : Algorithms exist to automatically calculate alignment and are generally effective however due to the nature of the images where significant changes across the field are occurring with a large number of similarly shaped objects it is possible for them to become 'confused' and miss assign frames in which case the semi automatic method can be used as a fall back.

These options are all based on shifts of the whole image frame (i.e. same manipulations for each x,y position) rather than the approach taken for example in correcting lens defects were the transform applies across the image would vary by position.

For lineage assignment two different approaches have been taken in the literature, firstly the simplest approach is to take each image as an independent frame generate cell assignments for all these frames then use comparative algorithms to assign the most probable cell location in the following frame based on previous location and extent of shift. When the predicted position of a cell now contains two cells a cell division event can be assigned. The
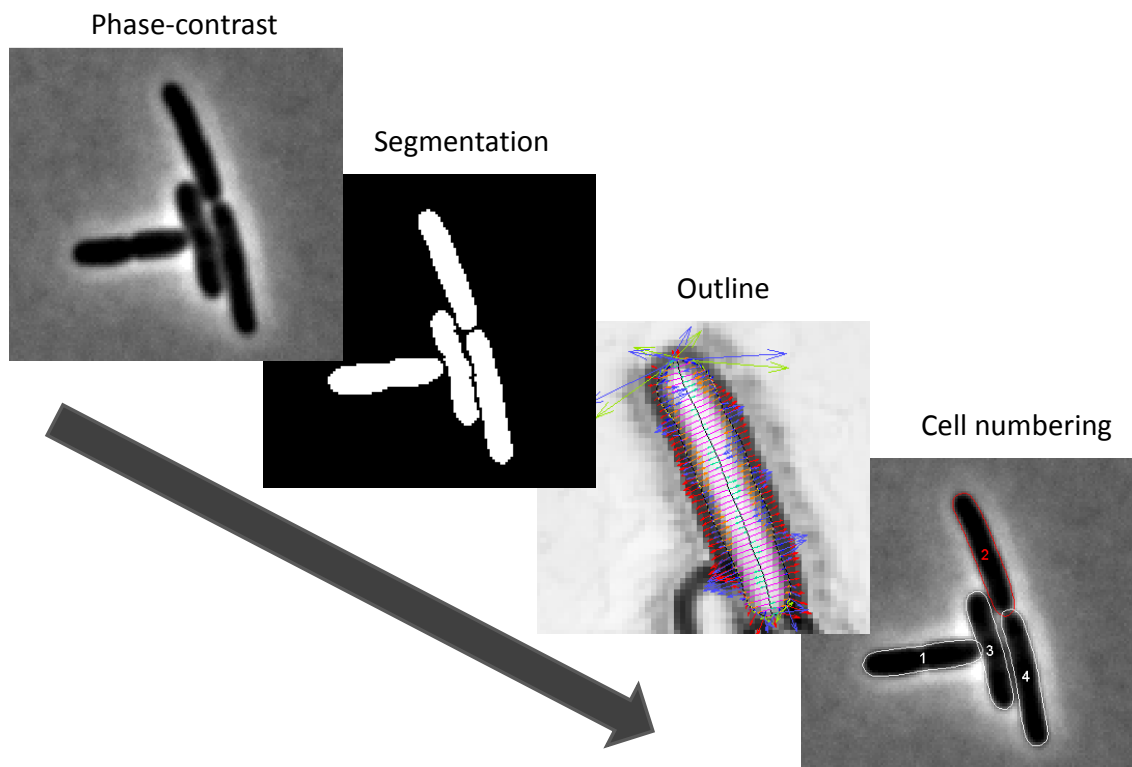
Figure 3: Stages of computerised cell outline assignment using MicrobeTracker software
Phase contrast image (x63 objective) of bacterial cells is first segmented using a watershed algorithm. An initial cell outline is fitted to this segmented image and the fit iteratively optimised using a force based model. Once cell outlining is complete a unique number is assigned to that cell outline and properties of cell dimensions (area, length) can be obtained.

second approach is to use the information that the individual images are related in time to systematically work through from the start of image acquisition using the previous images cell assignments as the basis for analysing the watershed image of the next frame. This approach is potentially more robust as it should be able to generate cell assignments ready for lineage assignment that are more likely to reflect the actual biological lineage that is being measured.

Both of these approaches rely on there being sufficient information in the images to un-ambiguously assign cell lineage. In terms of growth of bacteria in mono layers this equates to having sufficiently frequent observations (~3mins for log phase growth *E. coli* based on the literature, (Campos et al., 2014)) that the movement of cells between frames is not too large. Even with a short time frame of observation the cumulative effects of cell growth can lead to relatively large shifts in cells position within a micro colony so often the ability to manually intervene in assignment of cell lineage is included.

Once analysed data is then available as an array of cells per frame with relevant parameters and if lineage has been assigned information on unique arbitrary cell identifying number and number of divisions plus which cells that cell is related too as mother / daughter.

3.2.2   Identification of software solutions for lineage tracking and analysis

Initial work looked at the commercially available software packages but it quickly became apparent that the generic approaches were more suitable to analysis of eukaryotic cell move-ments which tend to be better separated and of a different character to the bacterial images. Attempts to use with bacterial images failed to extract biologically relevant assignments.

ImageJ was then used and the variety of plugins examined to determine if a suitable option existed. It was found that some parts of a complete work flow were possible but critical capa-bilities were lacking as detailed below. A number of water shedding solutions are available to enable initial segmentation of the images to a suitable level. Tools also exist to allow image alignment of time lapse images. However ways of assigning outlines to the water shedded images that were robust in rejecting any stray pixels that have been assigned from the back-ground were not available, with outlines tending to follow the contours of the water shedding cutoff. In addition while a variety of particle tracking plugins are available they are focused on dealing with tracking point sources within images from frame to frame (e.g. chemotaxing bacteria, beads in solution) and are not appropriate for use with mono layer bacterial images. Hence there is no appropriate automated tool for lineage assignment in ImageJ.

As the generalist tools I had previous experience of were not capable of analysing the images I was generating I reviewed the literature on bacterial image analysis and identified two pieces of academic laboratory software that were stated to be publicly available with some level of documentation and had been used in multiple laboratories in the field. These were Schnitcell from the Elowitz laboratory and MicrobeTracker from the Jacobs-Wagner laboratory.

Firstly I trialled the Schnitzcells software as it comes from the laboratory of one of the key exponents of bacterial imaging quantification and has been widely cited in studies in other labs (Adiciptaningrum et al., 2009; Locke et al., 2009). The code is publicly available and is partly open source but comes with no support and is not maintained. The software runs analysis in a modular manner and I was able to successfully use the first part of the analysis pipeline. Unfortunately I was unable to get the later stages of the analysis software to run at all despite testing on a wide variety of software platforms / versions. The error traced to the closed source portion of the program and hence I wasn't able to proceed further with troubleshooting and had to move onto another option.

Secondly I trialled the MicrobeTracker software which is actively maintained and fully open sourced. MicrobeTracker is built on top of MatLab and its add on package Imaging Toolbox and consists of a main Graphical User Interface (GUI) interface for cell outline and lineage assignment a secondary GUI for image frame alignment. Its standard output is a Matlab array of cell dimensions and lineage if analysed. This can however be converted to a Excel (.xls) file format if that is more convenient for work flow. In my hands MicrobeTracker has been a stable and useful piece of software.

Initial trials were performed using the supplied example data and with reference to the supplied documentation could be readily completed. Moving onto the data that I was generating there was initially less success in obtaining reasonable cell outline assignments. Extensive iteration through the analysis algorithm options was made, guided by a clear understanding of what each parameter was affecting. Initially this had limited success but as technical improvements were made in image quality (see section 3.3) reproducible cell outline assignment with only minimal manual intervention was achieved using the parameters detailed in Table 2. One area that did require manual intervention was the selection of the micro colony area per frame due to the water shedding algorithm being very dependent on the extent of background (i.e. cell free) included in the image. It would appear this occurs due to the mottling in micro colony interiors discussed elsewhere. Despite success in assigning cell outlines it proved impossible to get correct lineage assignment beyond about 20 frames into the time lapse (equating to 60 mins of growth). It is unclear why assignment fails to work further into micro colony growth images in this study. A comparison of my data sets with those published as examples or included in paper data sets does not yield any obvious difference beyond a slightly stronger mottling effect in my data. Images are captured at equivalent μm / pixel pitches and post software calibration are very well spatially calibrated. While there are no lineage specific parameters exposed in the program, trials of different image processing parameters were undertaken to determine if an alteration in these would improve lineage assignment, no such combination was found.

While MicrobeTracker provided a solution that could robustly assign cell outlines and cal-

culate cell parameters on a per frame basis a solution was still required to assign lineage. As no other automated options could be identified it was decided to implement a manual lineage tracking work flow. While this does reduce the number of cells which can be practicably measured it at least has the benefit of linking with the annotation of contact which would probably require manual assignment in any case. ImageJ was chosen as the software to perform the tracking in as it has a flexible range of tools for working with image stacks allowing cutting, cropping and image annotation. Cell lineage tracking could be performed by stepping through the images marking each cell and iterating through to include daughter cells in later frames. The cell numbers could then be manually transcribed and linked within excel to the corresponding cell data using macros. As part of this process annotation of when cell contact occurred between target and inhibitor cells was performed. Once completed this spread sheet contained a full record of micro colony growth and interactions ready for statistical analysis.

3.3 Bacterial sample preparation for single cell image acquisition

An ideal acquisition protocol would be able to follow the growth of bacteria over several hours at a rapid growth rate, due to CDI being effective only at log phase growth in planktonic assays, with cells constrained to grow only in two dimensions (x,y) in order to allow unambiguous observation of cellular positions. In addition multiple fields must be observable with high clarity and excellent spatial accuracy and reproducibility. Phase contrast imaging quality must be high and there should be a low background fluorescence level and no impediment to fluorescence illumination.

Following on from work performed in my masters (King, 2010) I started with the most basic methods available to observe bacteria, spreading on glass (free / immobilised) or sandwiching of cells between glass cover slip and thick agar pads. Following bacteria on glass has a number of significant limitations. If plain glass is used cells will show minimal levels of interaction with the glass, unless significant pretreatment times are used. Those cells which are adherent will tend to attach, at least initially, by flagella and hence the cells are in motion. In order to follow interactions growth of the cells is required so a nutrient media must be supplied if this is solely in the liquid phase only a thin layer is held by the cells limiting nutrient availability. In addition the act of observing the bacteria using a microscope leads to a reasonable degree of heating of the glass and solutions due to the high levels of illumination required when observing with high power objectives (x63, x100). This heating induces convection flows which are significant when working on the scale of bacteria leading to removal of the bacteria from the glass surface, flowing freely in solution. Finally while the opposition of two high quality glass surfaces (cover slip and glass slide in this case) is very close it is insufficient to hold bacteria in place or even aligned to the plane of observation. Presumably this is because the hard surfaces are held

apart by any slight imperfections / environmental contaminations as they lack any give and at the micron scale of bacteria the size of any such defects needs to be only very minor to have an effect. It was however possible to use this approach to verify that bacteria were motile and that fluorescent proteins introduced into strains were functional.

The next protocol trialled was to use slabs of agar cut from normally cast LB agar plates. 25ml of LB agar in a standard sized petri dish gives a depth of 7.5mm which was cut to approximately the size of a glass slide using a sterile scalpel. 5µl of overnight culture was then pipetted onto the surface and spread by applying a cover slip. This approach gave a significant improvement in images obtained as the soft surface of the agar adapts closely to the opposing glass cover slip surface effectively surrounding the bacteria and pressing them against the cover slip. As a uniform pressure is applied across the surface rod like bacteria will automatically orient so that they lie flat against the glass, that is the length of the bacteria is parallel to the plane of the cover slip. As the depth of the agar retains the LB it was cast with there are significant levels of nutrients which can be maintained by diffusion through the pad available to the cells, just as is the case during colony growth under the normal conditions agar plates are used.

By experimenting with a range of dilutions a suitable concentration of bacteria was identified which contained a significant number of cells but not so many that clumps of bacteria were observed. If the concentration of bacteria was too high then a mono layer of cells was not obtained and individual cells could not be observed. Observations were initially made across multiple time points by transferring the bacterial slides between an incubator and the microscope. As the sides of the slide were not covered this left a significant area open to evaporation. In order to mitigate this slides were incubated in slide holders initially just as is but when this proved to be inadequate to prevent dehydration with the addition of moist tissue to maintain humidity. This combination provided a limited ability to observe growth as shown in Figure 4.

Problems encountered using this technique were:

1. The adherence between the cover slip and the top of the agar pad was limited which combined with the use of high powered oil objectives which have to come extremely close to the surface led to skewing of the cover slip across the surface dragging bacteria from where they had been embedded.

2. LB has a significant level of fluorescence associated with it leading to high background levels of fluorescence. In addition the depth of LB agar lends a significant colour cast to light images but more significantly contains imperfections that are amplified under observation using phase contrast objectives.

3. Evaporation could not be completely countered leading to eventual dehydration of the cells (as shown by rounding up of cells) and prior to this distortion of the agar due to the dehydration.
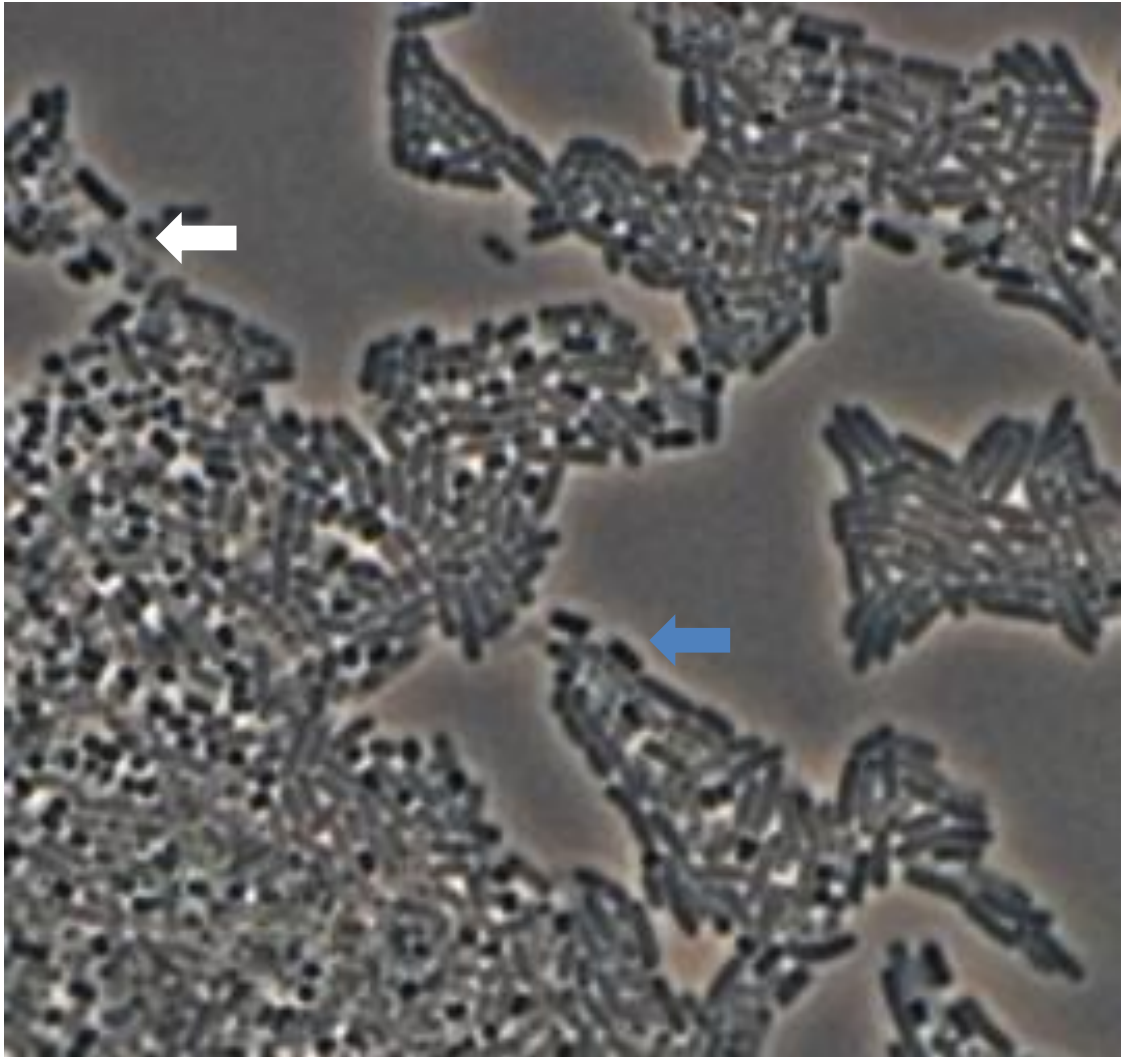
Figure 4: Effect of agar pad desiccation on *E. coli*

Phase contrast microscopy image (x63 objective) of K12 F+ *E. coli* grown on an agar pad which has dried out during the course of cell growth. Round black dots are desiccated *E. coli* prior to lysis (blue arrow). Lighter grey cell shapes are lysed *E. coli* (white arrow).

4. As the microscope was at room temperature significant growth of cells required incubation and hence removal from the scope which as it was a purely manual scope and with high powered objectives the field of view is very small made returning to the same previous field of view essentially impossible.

In response to the issues with microscopy in particular but also with the aim of dealing with the evaporation issue, a move to a higher specification microscope with a more controllable manual stage was made also giving the ability to use a stage mounted incubator with built in humidification system. The first challenge this lead to was the change from an upright to an invert microscope as this then meant the entire assembly was then dependent on resting on the coverslip. This was partially alleviated by reducing the volume of agar used from whole slabs across the full thickness of the slide to individual strips of agar. This reduction in weight allowed the slide apparatus to be successfully mounted without excessive bending and had the advantage that different mixes of bacteria could be visualised with no possibility of cross contamination between the now distinct pads. With the ability to incubate the pads on the microscope the need for removal of the slide was negated and initial time lapse data could be acquired. However even with the humidified system the flow of air used to maintain temperature control in this system lead to significant rapid dehydration of the agar in the pads resulting in movement of the cells out of the frame of view and optical distortion. Furthermore, the previous issues of fluorescence background and phase contrast artifacts remained.

Examination of the literature identified a wide variety of different approaches to these issues focusing on maintaining optical quality (low background, parallel surfaces) and minimising evaporation. Considering only those protocols dedicated to static bacterial incubation not those were media replacement is possible there are two main approaches taken to achieve these aims. Firstly a standard microscope slide set up can be modified in order to generate a chamber either by stacking a normal and a slide with a whole cut out or by using a premade slide with an indentation ground out. An attempt was made to fabricate a stacked slide chamber but in my hands it proved difficult to get surfaces adhered with sufficient precision that a cover slip placed on top was not distorted. The second option was not readily available commercially or able to be sourced by the dedicated imaging support facility at the department. In addition these techniques are best suited to use in upright microscopes were the fragile cover slip is facing upward and the weight of the assembly is held in place by the strong base glass slide. The suitable microscopes, discussed in section 3.4, identified within the department were invert scopes where the cover slip glass would be face down and liable to breaking.

Secondly it is possible to purchase prefabricated plastic ware in microscope compatible formats (i.e. slide, small petri dish) that have high grade optical cover slip adhered on the bottom. These are commonly used for eukaryotic cell culture where the cells can be grown adhered to the glass surface whilst covered in liquid media with gas exchange possible due to

loose fitting lids. Both formats of plastic ware were trialled but the difficult of maneuvering agar pads into the tight confines of the slide based format led to that being abandoned in favour of the small petri dish style format. This has the advantage of much greater accessibility for working with the small liquid volumes / mm pad sizes this technique requires. Initial work used a large pad agar pad size cut directly from a normal petri dish cast to a lower than usual level to give thinner pads. This work was also done with no seal on the pad lid. This approach showed that even with the lid on the chamber there was still sufficient moisture exchange to dehydrate the agar. In addition the image quality was not yet at the quality of the best examples in the literature.

In order to improve image quality a trial of using low molecular weight agarose with a rich defined media was performed as this was used by several labs in the field. This change lead to a marked improvement in phase contrast image quality, see Figure 5 presumably due to the combination of several factors:

1. The different plasticity of the low molecular weight agarose which may be better able to envelop the bacteria

2. The loss of impurities from the cruder LB preparation which can be significantly magnified in appearance due to the nature of phase contrast imaging

3. The loss of colour cast to the image moving from the yellow-brown cast of LB to the visually clear defined media.

The move to a defined media also reduced the level of background fluorescence as the contribution from autofluorescence of the complex mix of components in LB is absent.

In coordination with this change pad size used was reduced to 3mm x 3mm so as to be able to fit several separate pads in one petri dish which were sufficiently separated so as to avoid cross contamination of different strains, see Figure 6. To avoid the agarose drying out the petri dish was sealed with a thin strip of Parafilm. The included air volume represents a significant reservoir of oxygen for the quantity of bacteria being cultured over the experimental time of observation and hence should not be limiting.

Experiments with this set up showed a consistent improvement in image quality but it was still not quite at the level of previously published images. Also on occasion it was found that the Parafilm seal would fail leading to desiccation of pads. The final changes to the protocol to address these issues were to move to a new casting protocol, based on the work of Young and colleagues (Young et al., 2012), in which the media/agarose mix was cast between two cover slips relying on surface tension to give a very smooth parallel pad finish which contributed to getting the image quality to a level which matches the best published images in the literature. At the same time the sealing procedure was changed to use a thick bead of vacuum grease
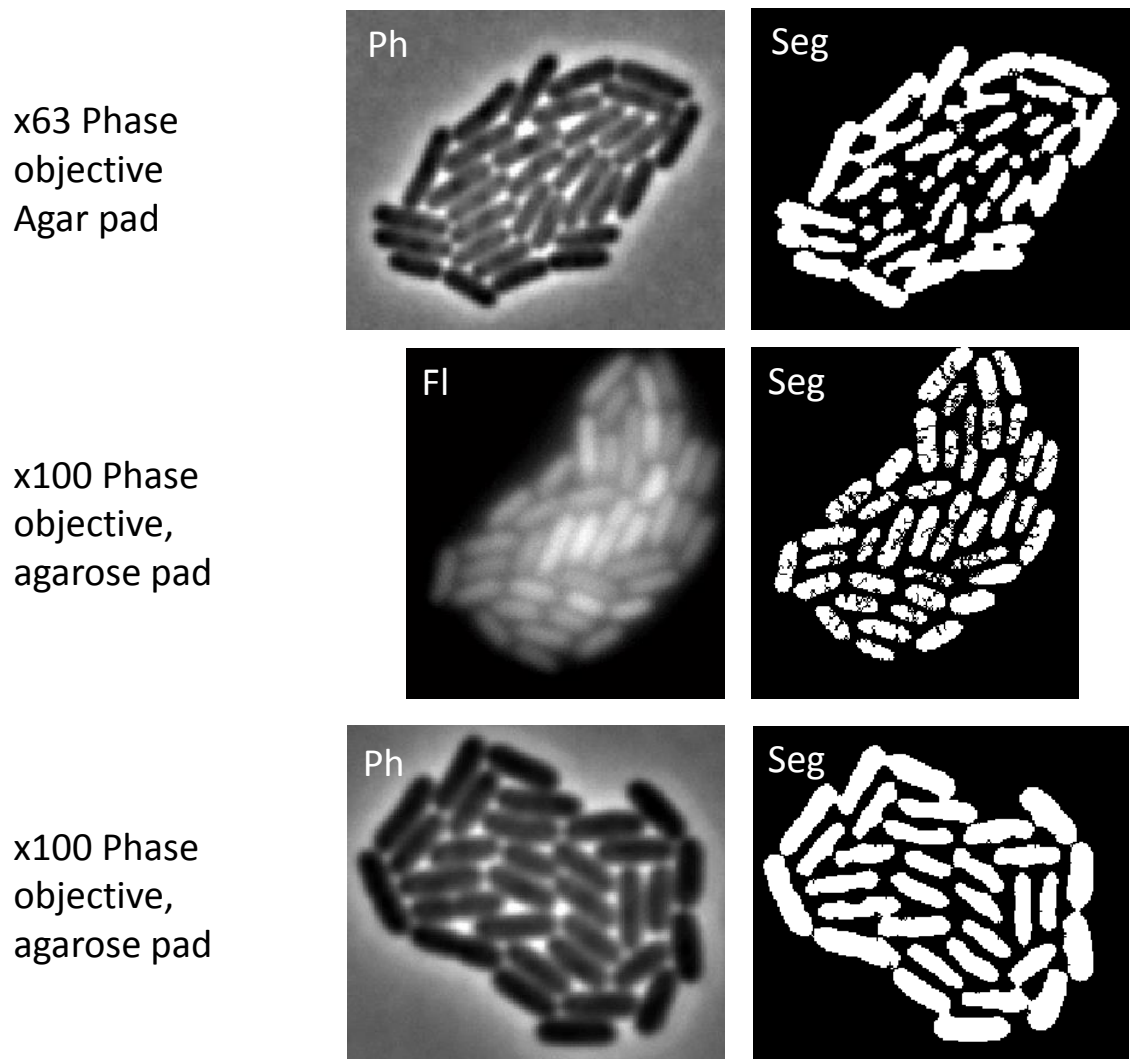
Figure 5: Comparison of the effects of different experimental conditions on image segmentation by MicrobeTracker software

Images of bacterial microcolonies collected under conditions as noted, with channels indicated by letter code: Ph = phase microscopy, Fl = GFP fluorescence channel and Seg = Relevant image segmented by MicrobeTracker. Initial analysis using a x63 phase objective with an agar pad gave phase contrast images that could not be segmented in a way that preserved the detail of all of the cells in a microcolony. Analysis of fluorescent images (GFP fluorescence channel shown) with a x100 objective gave segmentation with a 'fractured' appearance which led to errors in processing. Using a x100 phase objective with an agarose pad gave images which were amenable to robust computational processing.

A

B

Agarose pad

Coverslip
bottomed petri
dish

Side view

x100
Ph 3

Heated objective
collar

Stage incubator

Objective
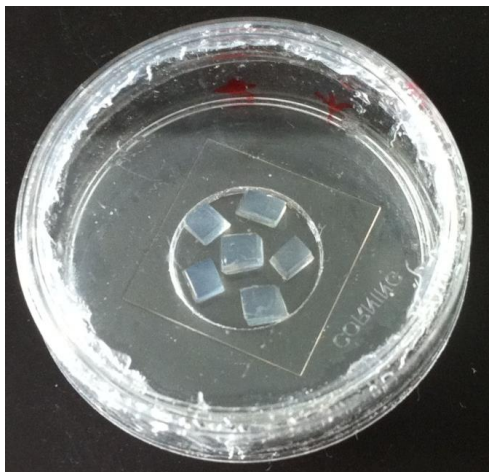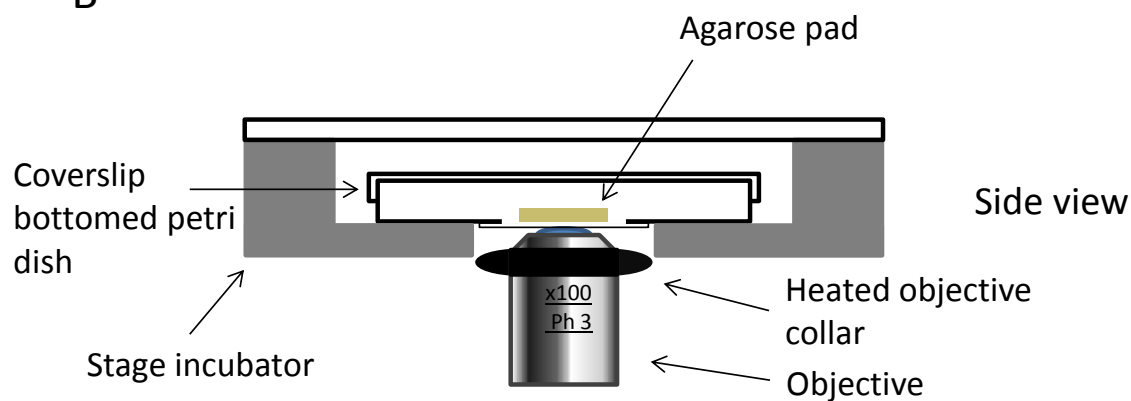
Figure 6: Microscopy set up for time-lapse imaging acquisition

A : Agarose pads shown placed on glass of coverslip bottomed petri dish, with bacterial cells held in place between the coverslip glass and agarose pad. Vacuum grease is used to seal the lid and prevent evaporation. B : Schematic showing the arrangement of equipment and sample used for time-lapse image acquisition. Note that later experiments used microscope box incubators, rather than stage incubators.

around the rim of the petri dish which was found to give a robust seal much less prone to leaking.

3.4 Identification and implementation of microscopy platform for single cell analysis

Initial work was performed on a Zeiss Axioplan microscope and Optronics camera which is a manually controlled microscope with a low resolution / low sensitivity camera. While this was sufficient to obtain images of bacteria they were not of a suitable quality for computational analysis and the stage set up lacked fine control of xyz positioning or any way to temperature control the set up which are critical for live cell time lapse microscopy of *E. coli.*

3.4.1 Development of microscopy setup

The next microscope, Zeiss Axiovision 200M, to be trialled again had a manual stage but this time one with a high quality mechanism making fine manipulations of field xy position / focus possible. Control of temperature was possible using a stage mounted incubation chamber and objective heating collar.The technical aspects of the microscope and the improvements they enabled are detailed below.

The key part of any microscope is the quality of the microscope light path which is largely determined by the quality of the objective lenses. The new system had planar corrected optics with additional adaptations to make them suitable for fluorescent imaging . In addition the illumination system was capable of being adjusted to give correct Köhler illumination at high magnification (x63 Ph objective used). Adjustments to such illumination particularly using high magnification require a light system that can be finely adjusted and is not in turn warped by the adjustments made and holds the changed position, these characteristics had not been found in the previous microscope. During initial experiments it was found that in order to obtain the best quality phase images not only must the Köhler illumination be perfectly aligned but the level of illumination controlled by the aperture stop must be adjusted to avoid over illumination of the image, too much light washes out the contrast in the image, leading to greying out of areas of the image that should be black. It was found that this adjustment needed to be performed, or at least rechecked, on the pad to be imaged itself as stand in surfaces or pads of even slightly different thickness could require different adjustments. Theses changes gave planar images with high contrast phase images and fluorescent images with crisp delineation of fluorescence area (as no smearing due to changes in how lens focuses different wavelengths of light were occurring)

Another key part of the microscope system is the image capture system which in modern normal mode microscopes is a digital Charge Coupled Device (CCD) system. The key parame-

ters of a camera system are the sensitivity to the light being detected in the wavelengths being observed (as sensitivity can vary markedly across wavelength ranges), the resolution of the camera image both in terms of the pixels acquired in a field of view and how the original optical image is mapped to those pixels which is a function of sensor size and the microscopes optical magnification/light path and the acquisition time. A Zeiss Axiocam Hrc camera which is a peltier cooled CCD capable of colour image acquisition using a Bayer sensor mask. The presence of this mask does lead to some light loss and hence a reduction in camera sensitivity.

Acquisition time is a factor when imaging live cells for two reasons. Firstly while bacteria trapped by the pad are not motile in the sense of swimming they do undergo significant movement due to the rapidity of their growth both at the level of the single cell but more significantly due to the sum effect of all those growing movements leading to bulk movement within a micro colony. If the camera acquisition time is of the same order as the movement rate of the cells being observed significant blurring will occur and acceptable images will not be obtained. With a reasonable level of normal light illumination acquisition times of 25msec where obtained, which meant that crisp phase images could readily be obtained. Secondly there is a need to ensure that the live cells are not affected by the illumination either by excess sample heating (normal light) or by direct photo toxicity (fluorescent light). For fluorescence images the signal level in this experimental system is as expected much lower which means that a trade off must be made between acquiring enough light for a decent image, with the three factors involved being illumination intensity, camera sensitivity and time set for acquisition. These factors can be traded off in various ways but for live cell imaging it is best to use a longer acquisition time, which does not lead to blurring, with a lower level of illumination in order to reduce the photo toxic effects of the intense illumination. In the context of a standard CCD camera the sensitivity is a fixed value dependent on that particular unit but different cameras can have significant differences in sensitivity.

Manual operation of the camera xyz alignment meant that observation of only a single field was possible due to the lack of any register for a given position and the very small field of view of a uniform looking sample making tracking back to other fields very challenging and hence not a practical option for 10's of observations of each field. Manual operation of the filter shutter wheel and light filter was also required which both further made multi field observation impossible due to the time to effect the required changes in microscope configuration and also meant that light exposure of the sample was greater than required solely for exposure. This is a particular issue for fluorescent light illumination which is far more toxic.

Finally the use of a stage mounted incubation has limitations in the accuracy of temperature control. In particular the entrance of the objective to the chamber is prone to condensation even with an objective heater in place. Even when this was successful there are still temperature gradients across the stage area from the unheated to heated areas which cause

issues for stability when working at high magnification with bacteria where the slightest drift causes a loss of focus from the 1μm plane containing the bacteria. These drifts meant that minor manual corrections in focus were regularly required (every other frame) in combination with accidental movement / knocks due to all the manual operations of filters / lights which affected xy position and also required extremely careful manipulation to restore correct position meant that operation of a time lapse was an extremely intensive and skillful operation in order to obtain useful results for a single field.

The outcome of this work was that a time lapse of phase images with a few snapshot fluorescence frames could be acquired for one field of view of bacterial microcolonies growing and interacting. This was sufficient to provide proof of principle for this analysis mode, but it was clear that changes to the microscope would be required in order to obtain a robust experimental system. During operation of this protocol it was noticed that there was a significant lag in growth of bacteria transfered from log planktonic growth at 37°C to pad growth on the microscope. Manipulations to assemble bacterial pads were performed as quickly as possible but at room temperature so it was assumed that some degree of heat shock on temperature downshift was responsible for this growth lag. Therefore to minimise temperature changes a 'hot box' was constructed from a plastic container containing water filled sterilins to provide thermal mass. This was held at 37°C when not being used and all containers and pads prewarmed prior to dilutions being performed. With these changes any temperature change induced lag was greatly reduced to only 10 minutes.

3.4.2 Final microscopy set up

With a proof of principle demonstrated a list of additional equipment required to upgrade the available microscopes was made and checked against the results of a literature review of equipment used in labs specialising in this area of imaging. After a successful funding application experimental work was continued on a microscope using this upgraded equipment, see Table 1. Again each specific improvement in the microscope will be described and the improvements they enable identified.

The upgraded microscope was fully automated so that no manual intervention was required for changes of the filter wheel or control of the light shutters. In particular a high speed filter shutter was fitted to enable light exposure only when required eliminating excess illumination which could have photo toxic effects. The automation also extended to the stage which had full xyz control and which was capable of μm positional accuracy. This allowed for both multi position acquisition as stage positions could be identified manually (e.g. to ensure appropriate initial cell distribution to increase chances of useful observations being made) and then returned to with high accuracy during the time course of time lapse acquisition. Initially the slight changes in z axis position during the experiment meant that manual focusing

was still intermittently required to ensure fields didn't drift out of focus. But as z axis control was available the chance to use the Zeiss Axiovision software auto focus module was possible, this normally uses fluorescent images as an input (which represent a much clearer signal for computational analysis), but it was found that it was also suitable for use with phase contrast images as an input. Therefore by specifying that before each frame auto focusing should be performed using the phase input, and this identified position also used for any appropriate fluorescent images, fully automated acquisition could occur eliminating the possibility of any manual errors prematurely ending the experiment.

In order to achieve greater thermal stability (which aids the stage accuracy mentioned above) a full microscope light tight incubation chamber with full temperature control was used. Including more of the microscope, such as the objectives and the whole stage area, gives a more stable temperature environment preventing minor changes in dimensions due to fluctuations in temperature. This change also lead to less lag in cell growth on transfer presumably due to more rapid equilibration of temperature as the larger unit has greater thermal mass and also to the ability to hold the sample hotbox withing the microscope incubation chamber during final set up.

A change to the camera was made to improve image sensitivity, with a switch made to the Hrm camera, the mono version of the Hrc previously used, which lacks the colour sensor and hence avoids the light loss mentioned previously. In combination an increased magnification objective, x100 Ph, was used so as to increase the pixels per μm in order to allow oversampling of the bacteria in the final image which can aid computational analysis of an image.

This final protocol was capable of acquiring high quality phase images of multiple fields of view during several hours of time lapse microscopy. These images were then analysed using MicrobeTracker to obtain measurements of single cells and this data then linked manually using ImageJ to generate lineages, see Figure 7. This data was then processed in excel to generate single cell growth curves for further analysis, see Chapter 4.
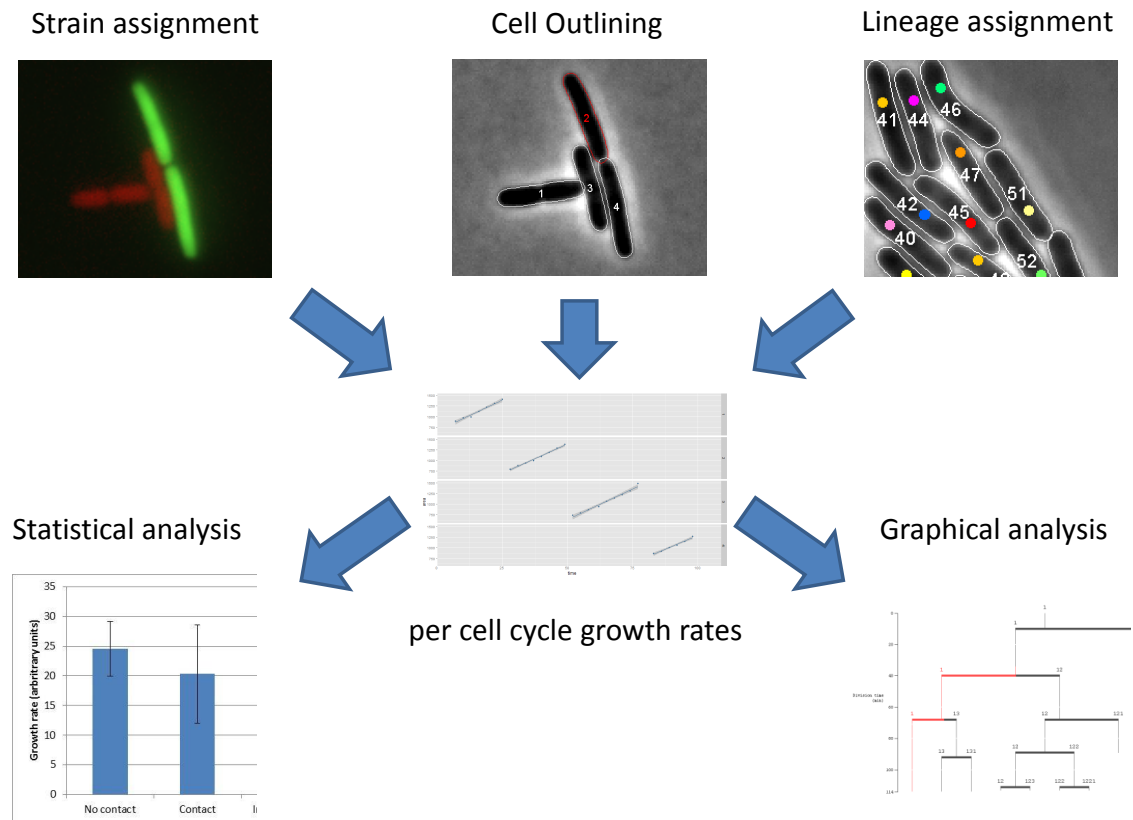
Figure 7: Schematic showing the analysis workflow for quantifying the effect of CDI toxins at the single cell level

Phase contrast time-lapse images were analysed using MicrobeTracker to assign cell outlines which were manually linked to generate lineages. Strain assignment was performed using snapshot fluorescent images of the K12 F+ and EC93 strains, which expressed different fluorescent proteins. This data was processed to generate per cell cycle growth rates of individual cells which can then be analysed graphically to aid interpretation of the complex data set and statistically to determine the significance of comparisons.

Chapter 4

Effect of EC93 toxin on target cells at the single cell level

4.1 Introduction

Assays of CDI toxins looking at the mechanism of toxin action have to date only been performed on planktonic cultures. Analysis of bulk suspensions of cells does not allow for the number and timing of CDI interactions with susceptible cells to be determined, and can only give averaged measures of cell response using indirect outputs such as reductions in cfu/ml. Important parameters relevant to understanding how CDI toxins act in nature, and in particular what the impact of the different classes of toxin may be, can only be measured by performing analysis at the single cell level.

4.2 Strain generation

In order to best understand the natural role of the EC93 toxin system the wild type strain was used, and hence has the CDI *cdiBAI* system in its native genomic context under natural promoter control rather than a cosmid based system / one under artificial promoter control. Strain MV1394 (Aoki et al., 2005) which is the wild type strain apart from experimentally selected rifampicin resistance was used in all experiments as the CDI+ / inhibitor strain. As a control strain an EC93 Δ cdiA deletion strain MV1395 completely lacking the CDI toxin was used. As it is not possible to differentiate between strains on the basis of phase contrast images expression of different fluorescent proteins in each strain was required. Cells from Ec93 Inhibitor / control strains were transformed with plasmid pMV371, which codes for constitutive expression of mCherry fluorescent protein using the chemical competence protocol.

Strain MV1257 (Lakins et al., 2009; Da Re et al., 2007) was used as the target strain having a K12 F+ background and hence being susceptible to CDI. The presence of the F' plasmid means that this strain is capable of robust biofilm growth and was therefore able to be used

in biofilm work, see Chapter 5, allowing direct comparison of results on the same strain in the two different experimental set ups. Strain MV1257 has the pZE21-gfp plasmid coding for constitutive expression of GFPmut3.1 (Cormack et al., 1996), which is suitable for use in the same imaging experiments as mCherry (Shaner et al., 2004) with minimal unwanted spectral overlap.

Transformed strains were tested for robust fluorescent protein expression / plasmid maintenance by microscopy of overnight cultures and log phase cultures. No cells lacking fluorescent protein expression, compared to the phase contrast image, could be seen and there was a significant level of fluorescent protein expression as judged by ability to clearly detect fluorescence in cell cytoplasm with minimal levels of excitation illumination (data not shown). Strains with multi copy plasmids grow at the same rate as cells lacking these components and have identical sizes and morphology (data not shown). This indicates that there are no significant impacts on cell physiology in maintaining fluorescent protein expression.

4.3 Ec93 strain background does not itself affect growth of target strain

The Ec93 *E. coli* strain used is a wild type strain isolated from mouse faeces and therefore has the potential to harbor additional factors that would enable it to affect other strains growth. Examples of such systems include colicins (Cascales et al., 2007) and Type VI secretion systems (Kapitein et al., 2013). In order to determine if this was occurring experiments in both planktonic and micro colony culture were performed using the EC93 ΔcdiA strain. If no additional growth inhibitory factors are present in the strain background then cogrowth of this strain and target strain should show no difference to that of target strain with itself.

Planktonic assays were performed using the method defined in (Aoki et al., 2005; Aoki et al., 2010). The expected 10^6 fold reduction in cfu/ml was seen when target cells (both F+ and F-, data not shown) were competed with wild type Ec93 cells whilst there was no significant difference between K12 F+ / K12 F+ cogrowth and that of ΔcdiA / target cell strains. In all reported data to date on the EC93 toxins effect on planktonic systems a small proportion of cells appear to be unaffected by growth inhibition even when incubated with a large excess of CDI+ cells over a significant period of time.

As the situation in growth at the monolayer microcolony level is markedly different (fewer, longer contacts) compared to liquid culture lack of growth inhibition also needed to be demonstrated using the K12 F+ / ΔcdiA strains co cultured on agarose pads, as for example T6SS systems have been reported to be effective in growth on surfaces but not in planktonic culture (Hood et al., 2010; Lossi et al., 2012; Russell et al., 2014).

In order to give the maximum chance for any growth effects to be detected micro colonies

of ΔcdiA and K12 F+ cells which were adjacent from the beginning of the experiment were selected . This way any potential toxins had the maximum possible time to affect growth. As the point of this analysis was to detect if any possible effects were occurring only the K12 F+ cells in contact with ΔcdiA cells were analysed (As noted in section 4.4 growth rate using this protocol was found to be highly reproducible). As shown in Figure 8 (two bars on the right) there is no significant difference between growth of target cells interacting with clone mates or with cells of the EC93 strain which lack a functional CDI system. Taken together this data shows that there is no detectable effect of the EC93 strain background on K12 target cell growth in the absence of a functional CDI system.

4.4   Uniform microcolony growth

It was not clear at the start of this work what the level of growth heterogeneity between individual bacterial cells in micro colonies would be in our experimental system. Variability could arise within microcolonies due to self generated gradients in nutrient density, due to diffusion rate limits from the agarose pad, or excretion of waste products from colony mates.

In order to test this, growth of individual cells representative of the whole colony was followed, including cells which had not made contact with inhibitor cells. Cells from strain MV1257 (K12 F+) and strain MV1586 (EC93 wild type) were grown together but for this analysis only the subset of MV1257 cells which did not make contact with inhibitor cells were considered. As shown in Figure 9 a plot of cell area over time leads to a characteristic sawtooth profile as cells grow then divide. With the mother cells area being reduced after the daughter cell 'birth' as the undivided mother cell's area is now assigned to the daughter cell. It can be seen from the plot that the gradients of growth are parallel and the volume at which cell division occurs are very similar in mother and daughter cells. Any changes over time, note the subtle decrease in volume at division occurring over time, happens to all cells within the microcolony to a similar extent. The level of variation in cell division times is small enough that the microcolony as a whole is dividing in synchronicity when not under any other influences. This demonstrates that the experimental conditions obtained using this protocol give steady state cell growth and hence provide a suitable background for picking out potentially subtle toxin effects.

4.5   Inhibition prior to cell monolayer growth is not detectable

The protocol used for seeding the agarose pads for monolayer growth relies on rapid spreading of separate dilute cultures by physical application of the pad. While this is performed as rapidly as practicable with liquid spreading occurring in under a second it is still theoretically possible that there could be some contact of inhibitor and target cells in the liquid phase prior
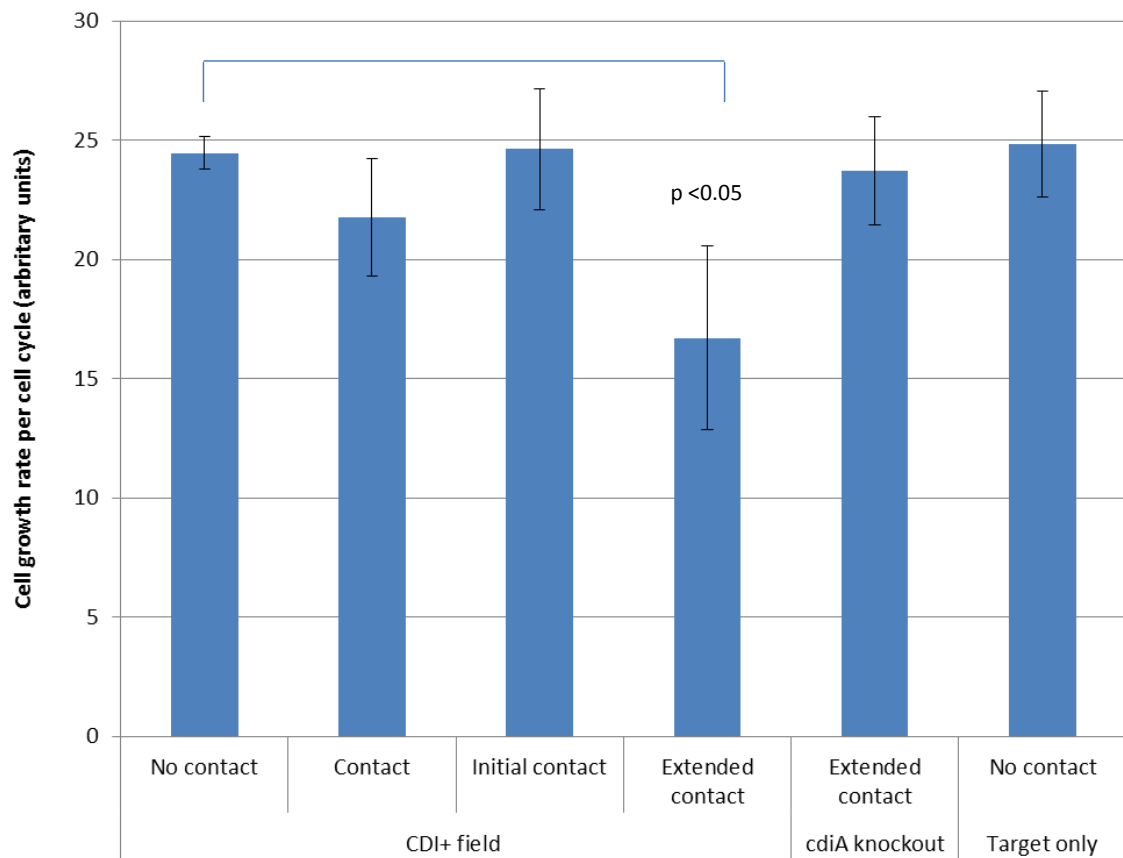
Figure 8: Single cell level measurement of EC93 CDI toxin effect on K12 F+ *E. coli* growth rate

Growth rate per cell cycle of K12 F+ cells either in / out of contact with EC93 cells with cell types as indicated on bottom axis, CDI+ field (EC93 wild type), CdiA knockout EC93 (ΔcdiA) and target only (no EC93 cells only K12 F+ cells present on pad).

Growth rate is defined as the gradient of a linear regression fit to the plot of cell area / time, measured from cell birth till the point of cell division. This was was determined by MicrobeTracker analysis of phase contrast time-lapse images followed by curve fitting per cell.

Initial contact period was defined as occurring in the first two cell cycles of contact, extended contact period defined as all subsequent cell cycles in which contact is maintained.

There is a significant decrease in the growth rate of cells undergoing extended contact with CDI+ cells compared to target cells (CDI+ field), as is shown in figure annotation. No significant difference in growth rate was seen for other conditions.

Cell cycle numbers measured, contact, n=36, no contact n= 188, cdiA knockout n=23, target only = 31 , +/- 2 s.e., two biological replicates.
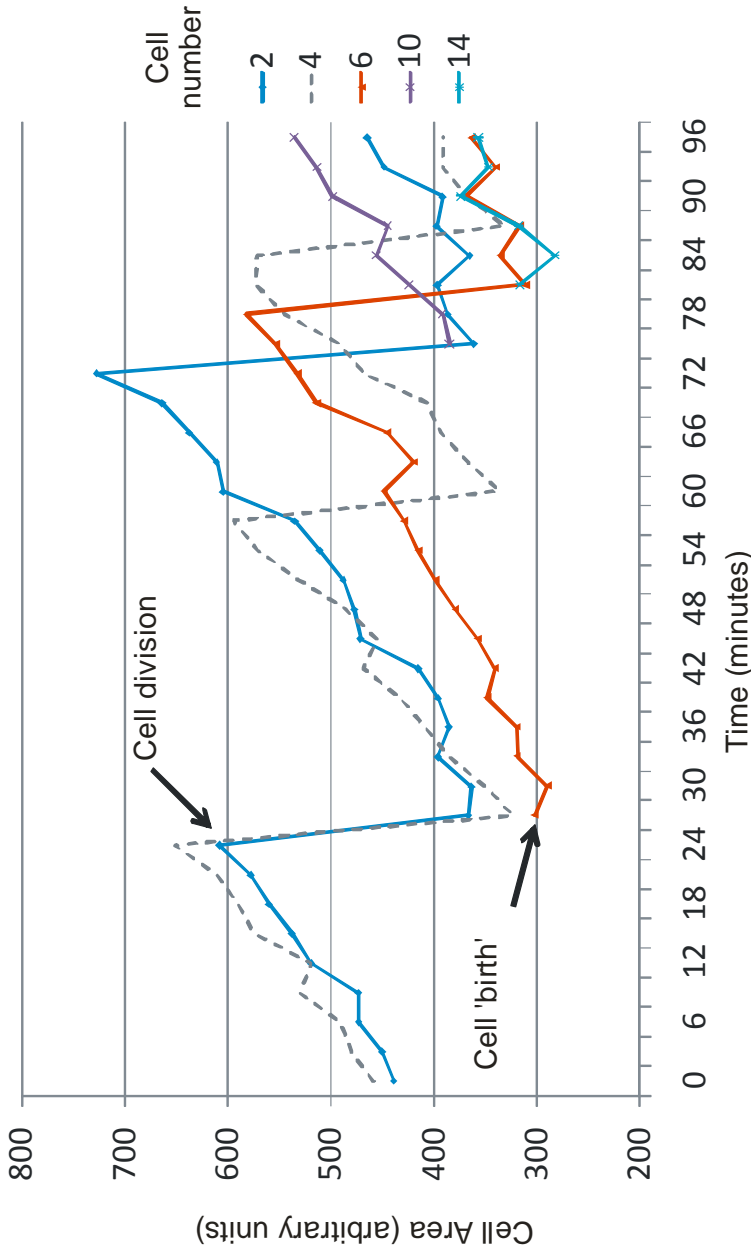
Figure 9: Single cell growth, division and 'birth' plots shows a characteristic sawtooth profile

K12 F+ cell area is plotted against time for each cell to give growth curves of individual cells. Cell area was determined by MicrobeTracker analysis of phase contrast time-lapse images for a subset of tracked cells from the same microcolony. At the point of cell division, as judged from phase contrast images, the area measured is split between the resultant mother and daughter cells. An example of this is annotated on the timeline of cell 2 growth at 27 minutes, division of cell 2 leads to the 'birth' of daughter cell 6. All cells for which growth data is shown were in contact with CDI+ cells at the start of the experiment and this contact continued for the duration of the experiment, with the exception of cell 4. Cell 4 broke contact with CDI+ cells at 27 minutes and goes on to show the rhythm of normal cell growth, comparable to that seen for cells which have not come into contact with CDI+ cells.

to immobilisation between the cover slip glass and the pad. As the basis of the experiment assumes that CDI exposure will only occur as cells come into contact due to microcolony growth it is important to be able to rule an effect of prior exposure out.

This was done by comparing the growth rate of target cells growing on a pad without any inhibitor cells being seeded on the same pad, and hence there being no possibility of contact with inhibitor cells giving the natural uninhibited growth rate, with the growth rate of target cells that were classified as having no contact with inhibitor cells, post pad application, on a mixed strain pad. If prior contact of toxin cells was able to skew the experimental results we would predict that the target cells on the mixed pad that had never come into contact with an inhibitor cell during the period of observation would have a lower growth rate than those on the single strain pad.

This data is shown in Figure 8 where the no contact target only cells represent the result of the single strain pad and the no contact CDI+ column results show the results for the mixed pad. There is no significant difference in per cell cycle growth rate between the two populations of cells and hence there is no measurable effect of prior contact on the relevant experimental parameter.

4.6   Assessment of EC93 toxin effect

4.6.1   Rationale for choice of fields to be collected and assessed

In order to determine the effect of the EC93 CDI toxin, K12 F+ and EC93 wild type cells were observed growing and interacting in monolayers of cells by phase contrast and epi fluorescence microscopy. Full method details are shown in Chapters 2 and 3 but the key parameters controlled in order to obtain biologically meaningful data are discussed below.

K12 target cells and EC93 inhibitor cells were coseeded under agaraose pads 37°C at a low seeding density so that approximately 4 cells of each strain type would be in a field of view. Fields for timelapse acquisition were assigned on the following basis:

1. Examination of the phase contrast image to ensure that only a few, relatively closely placed microcolonies were present in the field of view (and that a heavier than average seeding density was not present immediately out of frame as this would lead to rapid overgrowth mid experiment)

2. A field of view that contained microcolonies from target and inhibitor/control strains that were not in contact but were in close proximity (approximately 10μm). A single exposure at each excitation wavelength was performed, in order to determine the strain type of each microcolony present in the frame. In order to avoid multiple exposures,

due to out of frame illumination by excitation light, a significant translation between assessed frames.

This procedure was repeated so that a suitable field of view was found on each pad to be observed in the experiment. Time-lapse acquisition was then performed with phase contrast images being acquired at three minute intervals, fluorescent images were acquired at every approximately sixty minutes to minimise phototoxic effects of excitation light illumination. Images at each position were captured using the Axiovision software multiacquistion tool and hence were always acquired in the same order with the same spacing of timing. With the rapid growth rate of *E. coli*, observations for 4-5 hours were sufficient to follow growth through to the point of confluence and/or the stage when bacteria would start to overgrow each other and hence no longer be uniquely identifiable.

The acquired phase contrast timelapse images were converted to contiguous TIFF image stacks per pad and examined to determine if they were suitable for further analysis on the basis of the following criteria, using the snapshot fluorescent images as a guide to assign strain type to cells:

1. Was the drift between frames within a correctable range?

2. Had the predicted interaction of microcolonies occurred? If so had the interaction occurred early within the observation period so as to present a significant set of interaction observations?

3. Had growth continued as a continuous monolayer up until the end of the experiment?

Note that these objective criteria make no prejudgment as to the presence or absence of any toxin effect. For each combination of strains studied an image stack which matched the above criteria, was quantitatively analysed from each of two biological replicate experiments performed on different days.

4.6.2   Toxin effect occurs in two stages

An overview of an example data set from K12 F+ and EC93 wild type CDI+ cells interacting is shown in Figure 10. By splitting the data set on the basis of lineage, the initial target cells present at the start of the time lapse, and cell cycle number, which growth cycle the cell is in as measured from the start of the experiment. Starting from the single cells in the top panels division and subsequent growth for mother and daughter cells is then shown in the panel beneath and so on. It can be seen that lineage does not have any obvious effect on cell growth patterns, as would be predicted for pads seeded from a clonal population.

Contact with EC93 wild type cells, indicated by blue colour, can be seen to not immediately lead to growth arrest as the cells continue growing at the same rate hence giving a similar

gradient in this plot. However within the time range of the quantitative experiment it can be seen that intoxicated cells go on to either halt growth or exhibit a reduced level of growth (shallower gradient). Presenting the data in this way clearly shows the disruption of intoxicated cell growth against the background of the regular pattern of normal cellular growth.

Further analysis of the time course of K12 F+ cells growing in contact with CDI+ cells, see Figure 11 which shows a small representative portion of a microcolony lineage, highlights the biphasic nature of inhibition. It can be seen that cells growing without contact with EC93 wild type cells divide regularly (black, right). The intoxicated K12 F+ cell (red, left) comes into contact at 36mins and continues growing with a normal cell cycle length in that cell cycle and the next, as judged by comparison with its clone mates. Only after two 'normal' cell cycles have been completed does the third cell cycle show significant changes being significantly longer due to slowed growth rate.

Quantitation of this effect was performed by fitting a linear regression curve to each individual cell cycle of growth independently. The gradient of each of these linear fits was then taken as the measure of cell growth rate for that cell cycle with the measure being reported in arbitrary units as it was to be used for comparative purposes only, although it would be possible to convert to an area increase/second value. Each cell cycle was categorised on the basis of what contact the target cell had had with inhibitor/control cells either just in that cell cycle or within a defined number of cell cycles as appropriate.

As shown in Figure 8 there was no significant difference between the averaged growth rate of all cells in contact and those not in contact with inhibitors. However from the previous observation we know that the time course of inhibition is biphasic and that this averaging therefore obscures the biological reality that there is a time delay before the EC93 CDI toxin has its effect.

Whilst there is some variability in the time before growth inhibition occurs, examination of the data, such as Figure 11, supports a definition of the delay as occurring after contact with an inhibitor cell over two cell cycles. When the growth data is analysed using this way of splitting the data then there is no significant difference between target cells growing on their own and those growing in the initial stages of contact, see Figure 8. In contrast a statistically significant reduction in growth rate is seen for cells which have been in contact for over two cell cycles. That the fate of these cells is complete growth arrest has been confirmed qualitatively by manually following the growth of inhibited cells at later time points. In these later images, that weren't amenable to computational image analysis, it can be seen that the quantified slowed growth was a prelude to complete growth arrest (data not shown).
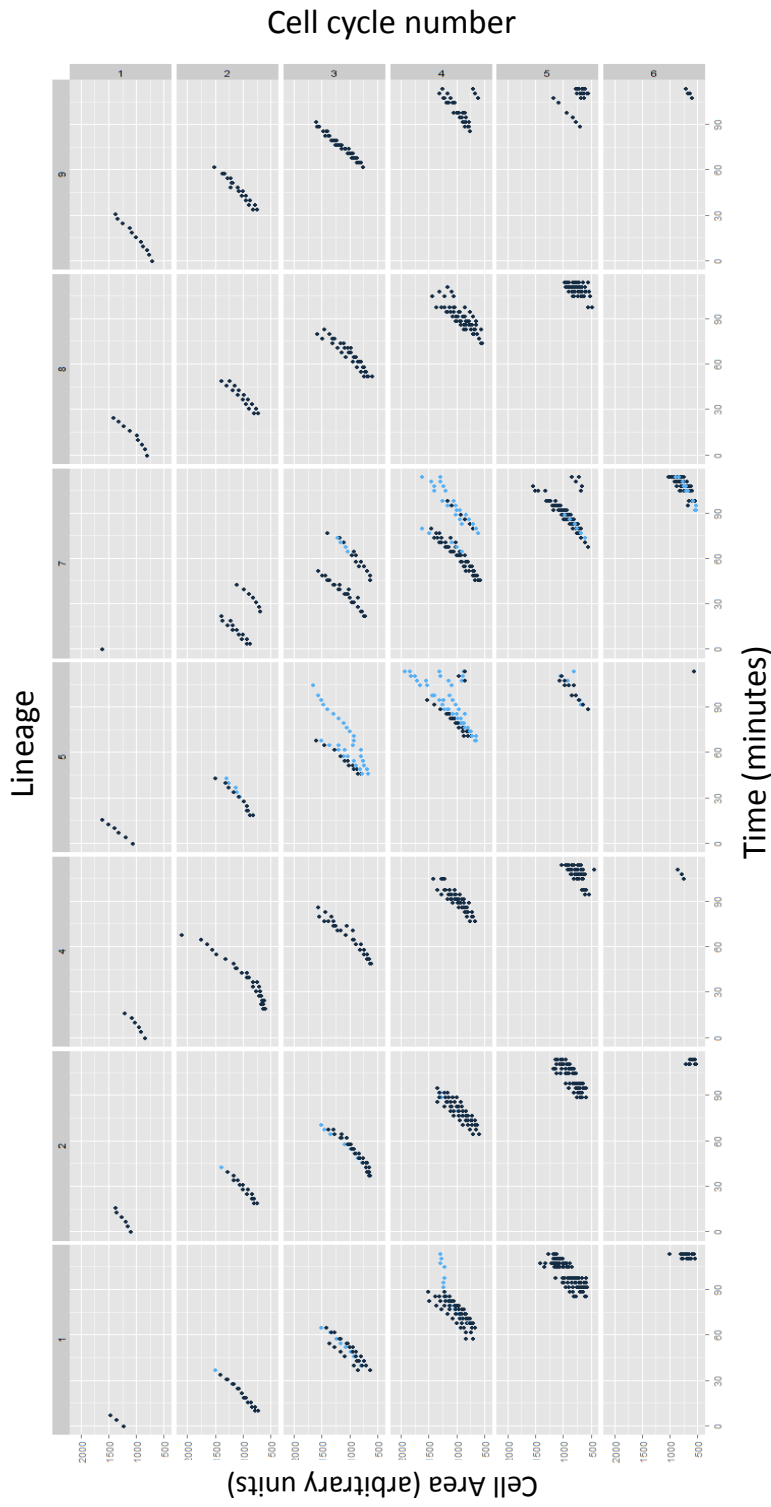
Figure 10: Comparison of K12 F+ single cell growth curves with and without contact with EC93 wild type cells

Growth data for all K12 F+ cells of a microcolony which came into contact with CDI+ cells over the course of the experiment. Growth data is presented in a matrix format, each column of graphs representing a lineage, the cells grown from a single mother cell at the start of the experiment, and each row showing which cell cycle cells are in within the experiment. The first cycle of growth observed in the experiment is defined as cell cycle 1 and the count is increased by one on each subsequent division with daughter cells inheriting the count of the mother cell. Each data plot of cell area over time within this matrix is an overlay of all cell measurements that satisfy the relevant criteria, for example for the bottom left plot is cells descended from cell 1 in the intial frame and that are in their sixth cell cycle. Blue data points indicate K12 F+ cells which are in contact with CDI+ cells (expressing EC93 CDI toxin). Black data points indicate K12 F+ cells not in contact with any EC93 cells.
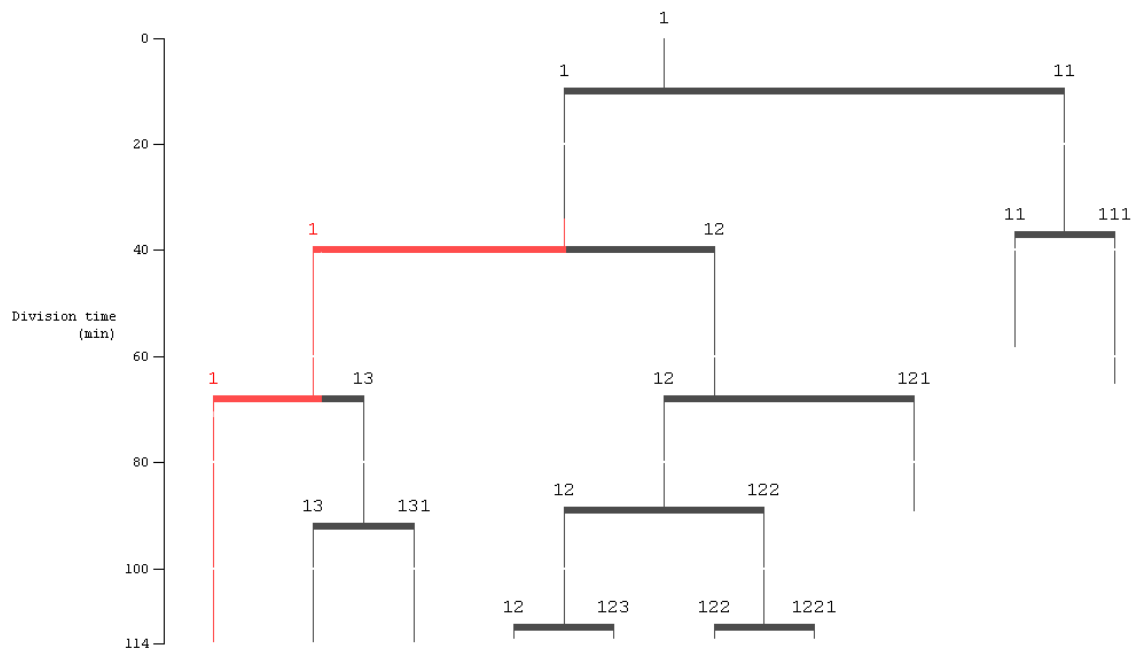
Figure 11: Growth inhibitory effect of EC93 CDI toxin does not occur immediately

Lineage tree showing time to division of single original K12 F+ *E. coli* mother cell and subsequent offspring, each number represents a single cell. K12 F+ cell in contact with EC93 wild type cells is shown in red. Note the loss of contact with EC93 cell at division point of cell 1 to cells 1 and 13.

4.7 EC93 CDI growth inhibition effect is entirely contact dependent

CDI toxin systems are so named on the basis of the work of Aoki et al (Aoki et al., 2005) with the contact dependence having been demonstrated using a filter based approach at the population level. Briefly cells were separated by membranes that had pores wide enough to allow cells through, 8μm, or block cells, 0.4μm. On this basis contact dependence can be assigned if a growth inhibition effect is seen only when physical passage of CDI+ cells is possible through the membrane. However the membranes themselves are 10μm thick so a short range effect from an unstable diffusible toxin would not be detectable using this system. However using a single cell approach we have the data to definitively address this question as cell growth can be followed for cells both at a range of distances from inhibitor cells and also in contact with cells that are being directly inhibited. This allows both the possibility of short range effects to be observed but also to see if transport of toxin on the outer membrane to other cells could occur.

As the whole of target cell microcolonies growth is quantified on a cell by cell basis it would be predicted that any effect of toxin at a distance, and/or mediated by membrane contact, would lead to a significant heterogeneity in the growth rate of cell cycles assigned as no contact in CDI+ fields (see Figure 8). This is because the no contact classification includes cells which are at a wide range of distances from inhibitor cells. If toxin was active at a distance from inhibitor cells the populations growth would be differentially affected leading to a wide range of growth rates.

In fact the data in Figure 8 shows that the 188 no contact cell cycles measured show a tight distribution of values. Hence we can see that there is no diffusible toxin induced variability in target cells growth rates. Using this single cell approach we can conclude that direct cell to cell contact is absolutely required for CDI toxin action.

4.8 Effect of EC93 toxin on bacterial morphology

Growth rate is not the sole measure of cell state that can be derived from these observations, length and width are also recorded for each data point and allow statements to be made as to the changes in bacterial morphology. A constant cell width is robustly maintained by *E. coli* across a variety of growth conditions/ situations in contrast to the significant variations in average cell length which occur under such conditions (Volkmer et al., 2011). Significant perturbations such as antibiotics which target cell wall synthesis leading to degradation / abnormal synthesis of the cell wall are generally required to alter cell width although it has also been reported that extreme spatial confinement can reversibly alter morphology (Männik et al., 2012).

E. coli target cell width was found to be constant across target cells under all conditions

studied. This is consistent with the current understanding of the EC93 toxins mode of action being to disrupt the cellular proton motive force (Aoki et al., 2009) which would not be predicted to impact on cell wall rigidity / induce abnormal cell wall synthesis. In contrast length of target cells prior to septation was found to be increased in a significant proportion of intoxicated cells prior to complete growth arrest. Affected target cells either undergo a gradual halt in growth after the initial delay in toxin effect or they proceed into a period of unusually elongated growth and then cease to grow further. The filamented growth phenomena was captured during the quantitative portion of the experiment, see Figure 10, and the growth arrest confirmed by manually following the growth of these cells through the remainder of the experiment. It should be noted that even cultures of *E. coli* K12 will show a low frequency of elongated cells (Wang et al., 2010), that is even in the presence of no other factors such as plasmid maintenance, fluorescent protein expression or toxin action some cells will elongate. These are then seen to be able to bud off new 'normal' cells capable of further division, a behaviour which is not seen for EC93 CDI toxin affected cells: recovery and normal septation was not seen on any occasion.

4.9   Escape from growth inhibition possible if contact broken

In addition to the quantitative analysis presented above, extensive qualitative checks of the data by visually tracking target / inhibitor interactions were made during processing. As bacterial cells grow in a monolayer they naturally form 'rafts' of cells which push and jostle against each other in unpredictable ways. This means that when microcolonies merge together, in these experiments target and inhibitor cells come into contact, target cells which have been in contact and exposed to toxin can be pushed by the movement of the microcolony such that this contact is broken. In addition as *E. coli* grows by division it is possible for one of the resultant cells to no longer be in contact with an inhibitor cell as the continuous cytoplasmic link between cells is broken by septation.

It was identified that in the few observed cases where movement of the microcolony broke contact between target and CDI+ cells the target cell was capable of continued growth. This is illustrated in Figure 12 where the fate of two cells derived from the same intoxicated mother cell is shown. The outlined cell has initially not had any contact with inhibitor cells and goes onto divide at which point one of the resultant cells comes into contact with inhibitor cells (Panels A,B). As reported in section 4.6.2 growth is not immediately inhibited and the intoxicated cell goes on to divide. At this division point one cell is left in contact with inhibitor cells whilst contact is broken for the other one, see Panels C,D, as completion of cell division interrupts the contiguous cytoplasm / membranes of mother / daughter cells.

The cell which broke contact can be seen to divide normally and carries on growing whilst

the cell which continues to receive toxin fails to septate, see Figure 12, Panels E,F. Following the cells growth in further frames (data not shown) showed that this pattern continued with the intoxicated cell going into full growth arrest. This result illustrates that a cell which has been exposed to toxin, one which has had shared cytoplasm with a cell which goes on to be inhibited, is capable of continued growth and division.

4.10 Conclusion and Discussion

This work has applied quantitative single cell techniques to the analysis of the EC93 toxin for the first time. Using time lapse microscopy to study toxin activity expressed from the EC93 wild type strain gives the most ecologically relevant insight into the dynamics of toxin action on an individual rather than a population basis. It was shown that the EC93 strain background, lacking a functional EC93 CDI system, contains no other detectable systems which modulate target cell growth and that therefore the wild type strain was suitable for studying solely the action of the CDI toxin.

As the experimental system used was new to our laboratory it was particularly important to characterise that growth was uniform enough to be sensitive enough to pick up toxin effects and that the coseeding approach taken did not lead to prior growth inhibition. The system was effective in both these ways as demonstrated by the synchronicity of individual cell growth cycles and the normal growth rates of K12 F+ cells coseeded with, but not in contact with, EC93 wild type cells.

Analysis of single cell growth curves showed that K12 F+ cells continued growing normally after contact with EC93 wild type cells over two cell cycles. Only after this point did the cells growth rate reduce and during this time there was an increase in the rate of filamented cells. It is interesting to note that the increase in cell length without septation prior to complete growth arrest could be related to the role of pmf in bacterial cell division noted by (Strahl et al., 2010). Complete growth rate arrest occurred only after the time range of quantative data acquisition (120mins). This is in marked contrast to the more rapid and drastic effect seen with other bacterial contact toxins such as the Tse1 effector, delivered by T6SS (Leroux et al., 2012).

Intoxication of cells does not inevitably lead to progression to growth arrest if contact with inhibitor cells is broken in the early stages of intoxication. Due to the nature of microcolony growth, the occurrences of this escape from inhibition were due to division of cells during the delay period prior to growth arrest as illustrated in Figure 13. Statements about the reversibility of the EC93 toxin have to date been based on the work of (Aoki et al., 2009) which used an artificially arranged system of inducible CdiI expression to monitor the effect of removing CdiI from a population of CDI+ cells. This is a very different situation to that seen in nature

81
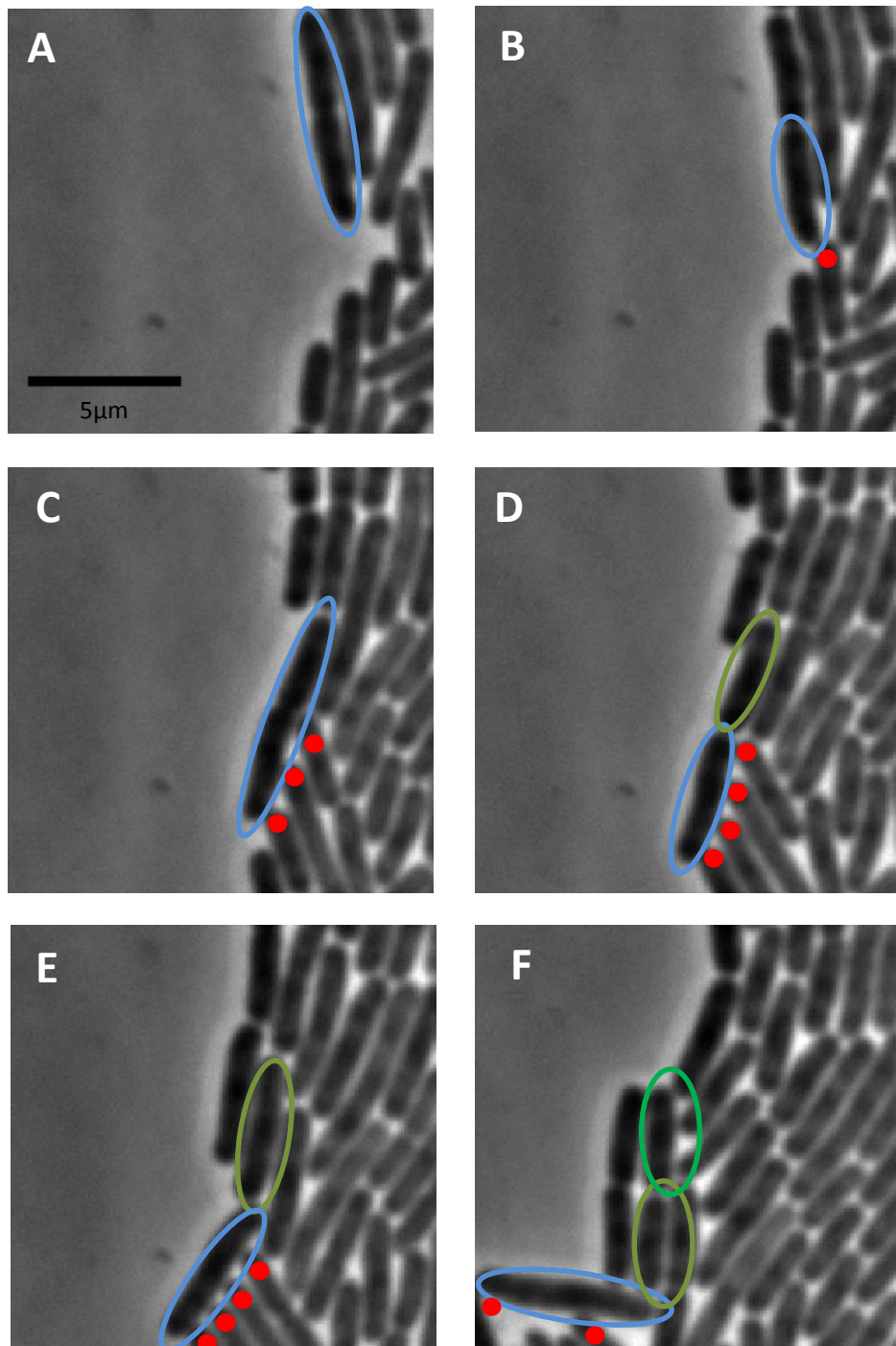
Figure 12: K12 F+ cells which break contact with EC93 wild type cells due to cell division can escape growth inhibition

Time-lapse phase contrast images of K12 F+ and EC93 wild type *E. coli* cogrowth. K12 F+ cell (blue), divides and comes into contact with EC93 wild type cell (A,B). As the K12 F+ (blue) cell divides again the daughter cell (green) is no longer in contact with EC93 wild type cells (C,D). The daughter cell (green) goes onto grow and divide (light green) while the mother cells (blue) growth is inhibited and no cell division occurs (E,F). Outlined cells are the same K12 F+ cells, coded by colour, followed through time-lapse. EC93 wild type cells in contact with outlined K12 F+ cells are highlighted with red dots.
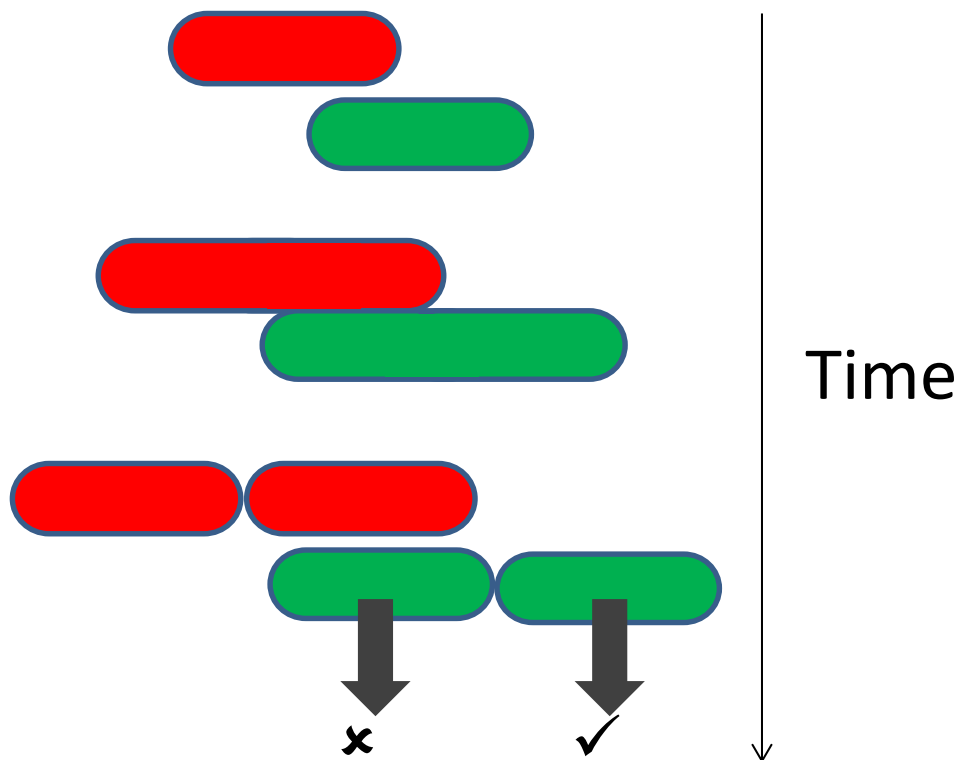
Figure 13: Schematic showing idealised outcome of K12 F+ cell growth breaking contact with EC93 CDI toxin expressing cells

Cell growth of EC93 wild type (red) inhibitor cells and K12 F+ (green) target cells shown over time. Cross indicates no further growth, tick indicates growth continues normally.

where susceptible target cells will be receiving toxin trans-located across their membranes from adjacent CDI+ cells. In this case two key factors are different:

1. Under natural conditions the cells susceptible to the EC93 CDI toxin will never have CdiI present in their cytoplasm. So recovery under the conditions tested in this thesis show that even in the absence of a cognate antitoxin molecule the cell can clear/tolerate the level of toxin already delivered.

2. It is not clear if EC93 CdiA toxin produced intracellularly in a cell lacking CdiI is capable of inhibition. Levels and the nature of inhibition could potentially be different in this artificial situation. This could be tested by performing similar experiments but in a strain background which was immune to self intoxication by virtue of having a BamA molecule which would not interact with CdiA for example expressing chimeric salmonella extracellular loops. In this case interaction between clonemates to deliver toxin would not be possible only and potential intracellular effects would be seen.

It should be emphasised that one of the benefits of this single cell analysis approach is that the toxin effect can be monitored in a system where the normal growth state of the cell prior to toxin analysis is known and that comparison of an intoxicated cell with a clone mate of identical growth history, that had until very recently contiguous cytoplasm is possible.

Previous approaches taken to assign the CDI toxins as contact dependent left open the possibility that a very short range effect could still be occurring ($<10\mu$m). Quantification of the effect of the EC93 CDI toxin at the single cell level has demonstrated that the presence of EC93 wild type cells near, but not in contact with, K12 F+ cells had no detectable effect on the growth of those K12 F+ cells. If a short range effect was occurring then K12 F+ cells 'behind' the line of clone mates in direct contact with EC93 CDI toxin or growing near to a separate EC93 microcolony would be expected to have reduced growth rates. In neither case is any such effect seen hence these results support EC93 CDI toxin has no short range effects and is completely contact dependent.

These results represent the first detailed description of the action of the EC93 CDI toxin at the single cell level, under natural conditions of expression. They show that the reversibility of the EC93 CDI toxin action, seen under artificial conditions, can apply under more native conditions to allow escape of intoxicated cells from growth inhibition. In addition they demonstrate that direct contact between EC93 wild type and K12 F+ cells is absolutely required for the EC93 CDI toxin to act.

Chapter 5

Effect of EC93 toxin on competition and adhesion during biofilm growth

5.1 Introduction

Specific detail on the small scale action of toxins is important in determining mechanisms of action (Sochacki et al., 2011; Leroux et al., 2012; Choi et al., 2015), but will not present the whole picture of the role of CDI's ecological relevance. In order to assess this population level studies are required in a state that is relevant to growth in the natural / medical environment, that is growing as a biofilm expressing significant levels of matrix. This is most readily achieved in the laboratory using flow cells in which bacteria are grown on surfaces amenable to further study, glass in the case of microscopy, with a constant flow of nutrients to allow cell growth and which acts to remove non adhered cells. This work looks at the contribution of the different regions of the EC93 CdiA toxin molecule when *E. coli* are growing in a biofilm.

In order to isolate the effect of different regions strains capable of expressing either the wild type CdiA molecule, only the conserved CdiA (no toxin activity) or no CdiA at all were used to separate out the effects of the two main functional regions of the protein, see Figure 14.

5.2 Development of flow cell protocol

5.2.1 Generation of strains expressing fluorescent proteins for confocal analysis

Initial experimental work indicated that one of the strains previously used in the laboratory (King, 2010; Lakins et al., 2009) had issues with variable expression levels of GFP / tdTomato (Shaner et al., 2005) under the flow cell conditions to be used for biofilm analysis. In addition it was considered desirable to try to obtain a strain with genomic integration of fluorescent protein expression as this would be predicted to avoid loss of fluorescent protein expression due to failure of plasmid maintenance and would allow more freedom to use other constructs for
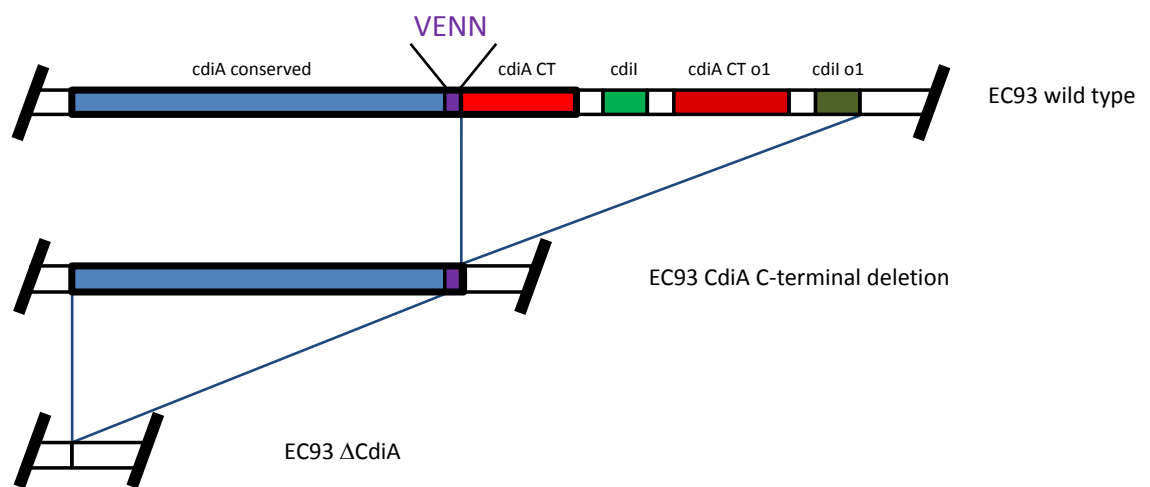
Figure 14: Schematic showing the organisation of the wild type cdiA region and downstream sequence

Components shown are conserved cdiA region (blue), VENN motif (purple), cdiA C terminal region (red) and cdiI inhibitor (green). Orphan regions are shown in a darker shade. Black slashes indicate transition to the EC93 genome.

example cosmid system for expression of alternative CDI toxins in the same strain background. These points were addressed in two ways.

Firstly the pool of fluorescent proteins used in the laboratory was expanded from the initial two, GFP and tdTomato to include YFP, CFP and mCherry. These proteins were examined for suitability based on factors such as significant expression levels, maintenance of significant expression during rapid cell growth and robustness to multiple rounds of exposure to excitation light during imaging. Based on these assessments mCherry was taken forward as a suitable replacement for tdTomato and one which was spectrally compatible with the already used GFP.

Secondly significant efforts were made to establish a system for achieving fluorescent protein expression from a genomic location in the EC93 strain background. In the first instance the CRIM system (Haldimann et al., 2001) was used to obtain integration of a fluorescent protein expression cassette into the attB site present within K12 and EC93 bacteria (confirmed by PCR). This was successful at the sequence level with integration confirmed by sequencing in both strain backgrounds. However there was no detectable fluorescence present above background autofluorescence levels despite significant production from the plasmid used as template. While a higher level of production would be predicted from the multi copy plasmid the single copy under the control of a highly effective promoter should have been sufficient to achieve detectable levels of fluorescent protein based on reports in the literature (Batchelor et al., 2006) the ready detection of fluorescence in single copy genomic integrants that had been provided to the lab for other projects. It may be that gene silencing is occurring, as has been reported by Lucchini and colleagues (Lucchini et al., 2006), due to the histone-like nucleoid-structuring protein (H-NS) acting to neutralise 'foreign' DNA inserted into the bacterial genome. H-NS molecules have been shown to bind preferentially to regions of DNA which are AT-rich in comparison to the rest of the bacterial genome in which they reside, a trait characteristic of xenogenic DNA. The increased levels of H-NS binding can lead to interference with the action of RNA polymerases, either by exclusion of RNA polymerase from binding sites due to steric hinderance (Navarre et al., 2007; Ali et al., 2012) or by trapping of RNA polymerase at promoters by blocking the formation of initiation competent open promoter complexes (Shin et al., 2012).

The next step taken was to switch integration system to the lambda red system (Murphy, 1998) (Datsenko et al., 2000), and even though it was targeted to integrate into the same attB site used with the CRIM approach, using the same promoter driving fluorescent protein expression, significant levels of fluorescent protein expression were observed. This could be due to differences in the inserted sequence, linear DNA with only required sequence for the lambda red system compared to the additional vector sequence incorporated when using the

CRIM system. Unfortunately whilst this system was successful in obtaining integrants in K12 and EC93 ΔcdiA strain backgrounds it proved impossible to obtain integrants in the wild type EC93 strain despite multiple attempts. This is presumably due to the known recalcitrance to transformation of some wild type strains of *E. coli* (Murphy et al., 2003). As no system capable of achieving genomic integration in all of the required strains was successfully implemented it was decided to proceed using plasmid based systems with the EC93 strain.

5.2.2 Flowcell seeding and growth conditions

Initial experimental work was performed using a set up essentially as detailed in (Lakins et al., 2009), but while this was capable of growing a very thick biofilm, required for that particular set of work it had a number of drawbacks for use in the particular experiments required for later work.

In order to obtain uniform expression of fluorescent protein with the amended pairing changes were made to both the seeding density and growth time prior to image acquisition. The initial protocol called for 14hour incubations with a high seed density of 1.0 OD_{600}. In my hands this lead to a very thick biofilm ill suited to studying the nature of strain interaction and also more importantly showing a very variable level of functional fluorescent protein in cells particularly those expressing proteins other than GFP. In order to overcome this the seed density was reduced to 0.016 OD_{600} so that excessive growth had not occurred at the 14 hour time point used. This gave acceptably uniform levels of fluorescent protein expression for GFP but not other fluorescent proteins.

On the basis that likely factors to be affecting levels of functional fluorescent protein would be the growth stage of cells and the presence of sufficient oxygen to ensure fluorescent protein maturation, a shorter growth time before imaging was trialled. Growing cells for nine hours prior to imaging still lead to significant levels of biofilm formation but with uniform levels of fluorescent signal from both proteins used to mark cells.

A final modification to seeding densities was required when the CDI toxin negative strain was altered from ΔcdiA to the C terminal cdiA mutant for reasons detailed in section 5.4. The significant difference in inherent biofilm formation ability meant that an equal level of coseeding lead to overgrowth of target cells even in the absence of toxin. Increasing the seeding level of the target strain by 20 fold (from OD_{600} 0.016 to 0.32) resulted in significant levels of target cell growth when coseeded with cells with an EC93 strain background but only in the absence of toxin, see Figure 15.

Confirmation that all cells were accounted for and that there had been no loss of fluorescence expression due to plasmid loss or other factors was obtained using confocal reflection microscopy (Yawata et al., 2010) which shows cell positions independent of any markers, see Figure 16.

EC 93 strain

EC93 wild type

EC93 cdiA C-terminal deletion

Low seed density

High seed density

A

B

C

D

xz

xy

yz

40μm
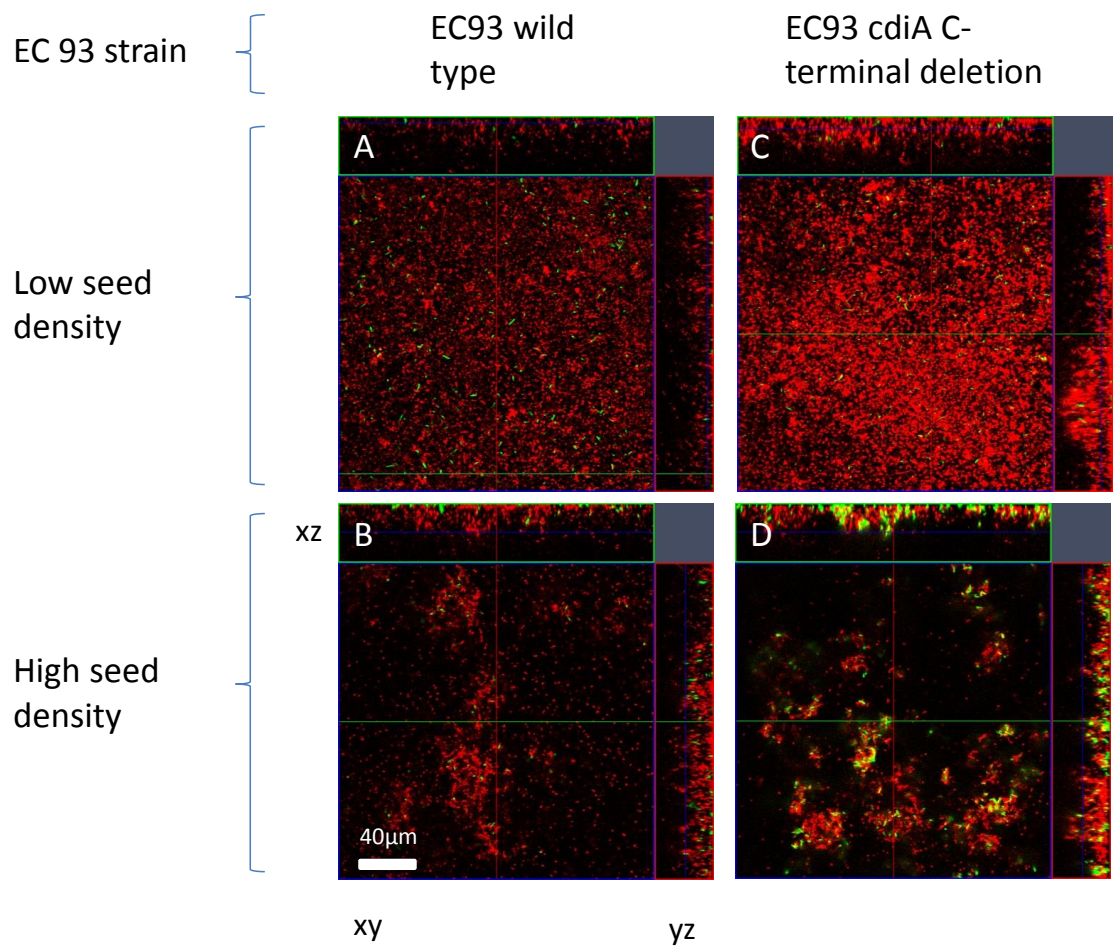
Figure 15: Inoculation density effects on competition outcomes in flow-cell biofilms

Representative confocal z stacks after 9 hours of growth post coseeding of K12 F+ cells (green) with either A,C ,low seed density ($OD_{600} = 0.016$) or B,D, high seed density ($OD_{600} = 0.32$) of EC93 strains (red)
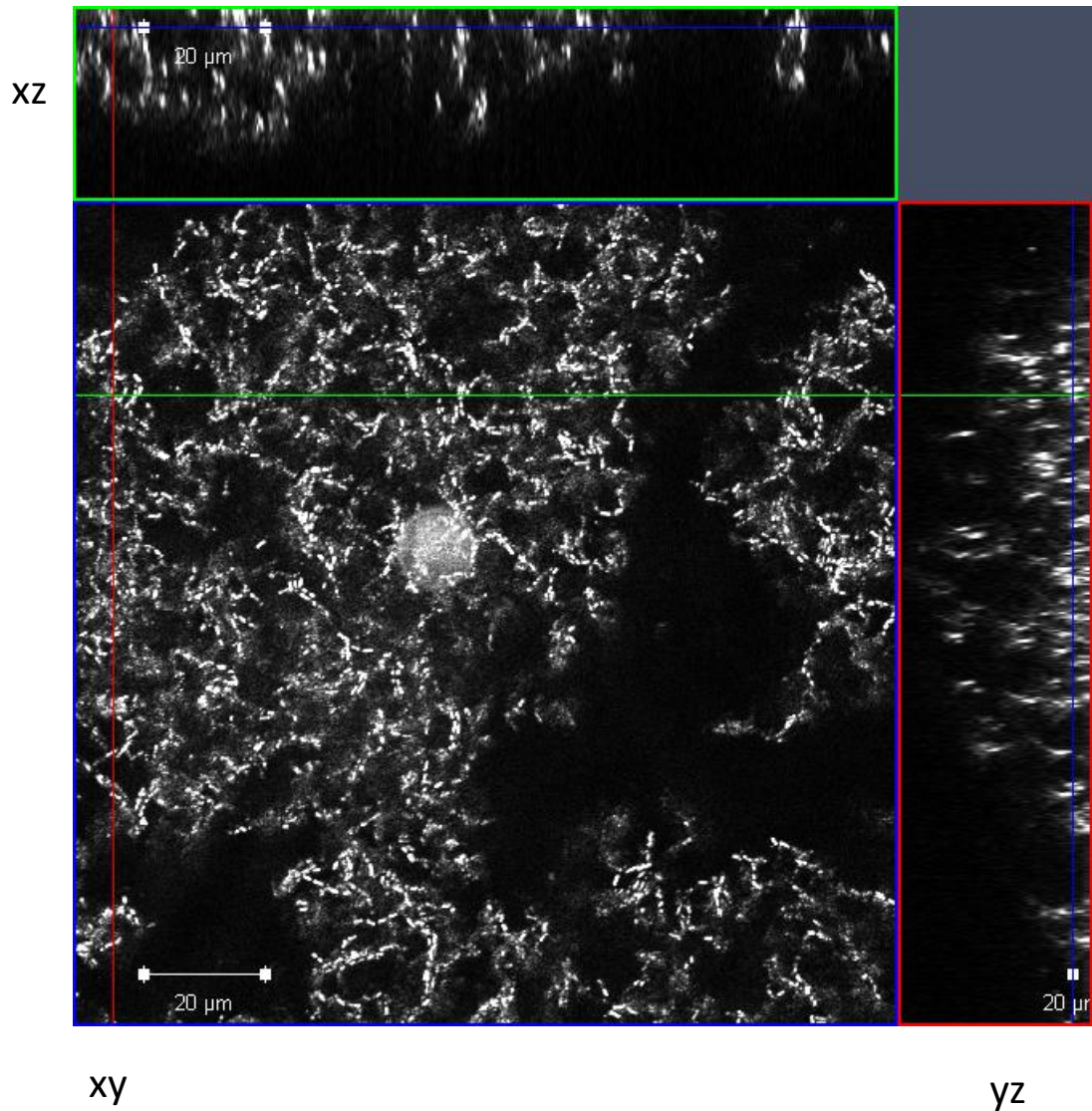
Figure 16: Label free imaging using confocal reflection microscopy

Z stack of confocal reflection images, acquired using 633nm laser light, of a flow cell biofilm, individual bacteria can clearly be distinguished. Note that the white circle is an artifact of reflection within the confocal microscope.

5.2.3 Flow cell design and set up

In addition to the protocol changes detailed in the previous section the flow cell and pumping apparatus setup initially used (also based on the work of Lakins and colleagues (Lakins et al., 2009)) were altered for the purposes of this work. In brief the flow cell used was changed from a commercially available model (Model FC281, Biosurface Technologies, Bozeman, MT, U.S.A.) to a custom fabricated flow cell. This flow cell was a redesign by Mark Bentley and myself of the design reported in (Pamp et al., 2009) which itself was based on the work of (Wolfaardt et al., 1994). The main design changes made were taken so as to make the design of the flow cell suitable for use in an invert microscope, with precise position control and without catching media tubing on the microscope apparatus during operation. The final design obtained after three iterations is shown in Appendix D.

The set up of the media and pump were also inverted similar to the method of (Crusz et al., 2012) but without inversion of the media container which was found not to be necessary in my hands to reduce bubble formation. Moving to pulling media through the apparatus avoids bubble formation due to the action of the pump and avoids positive pressure in the system which can cause leaks / glass cracking. Instead negative pressure is applied which ensures that leaks from the system cannot occur, instead in the event of a leak air is sucked into the system. When the system is installed on a microscope for time-lapse acquisition this is a much safer failure mode to avoid equipment damage as media cannot be pumped onto the microscope itself. Additionally it was noted that the flow obtained in this configuration was smoother than that with a push configuration. This allowed for confocal z stack acquisition without stopping the media flow during time-lapse acquisition something which had not been possible using the (Lakins et al., 2009) protocol.

5.2.4 Confocal z stack data analysis

When assigning fluorescent signal as being a component of the biofilm a number of different approaches can be taken. Comstat / Comstat2 (Heydorn et al., 2000) (Vorregaard, 2008) use a conservative approach to assignment of fluorescent signal as cellular biovolume by assigning any volume that cannot be connected back to the substratum as not part of the biofilm. This approach has the draw back of being likely to underestimate the true level of biofilm. This is due to the fact that the confocal z stack will almost always be a small part of the total biofilm, hence any biofilm which is part of the field of view but connected to the substratum outside of the imaged volume will be falsely assigned as not part of the biofilm. Given the often complex and varied nature of biofilm formation this is potentially quite a common occurrence.

In order to appropriately analyse and assign the confocal z stacks obtained from flow cell experiments assessment of the actual biovolume of cells embedded in matrix, and hence part

of the 'true' biofilm, was performed with and without media flow.

Firstly with media flow stopped the mobility of cells was assessed in three ways using confocal microscopy:

1. Repeat observation of the same position within the flow cell at widely spaced time points, in this way any free floating cells will most likely have moved in the interim time period as there will be no restraining matrix to maintain there position

2. Monitoring for 'tracking' of cells across adjacent z planes. Confocal microscopy has a significant acquisition time compared to rates of cell drifting / motility driven movement. As bacterial cells will typically be detected in multiple frames any cells which are moving will not be seen in the predicted position in adjacent z stacks. Instead they will be displaced to the position they had moved to when the next frame has been acquired.

3. Monitoring for cell movement after perturbing the flow cell system by administering a rapid move and return 'knock', by rapidly moving the stage. This induces sufficient movement in the media to make non adhered / matrix embedded cells move.

Secondly with flow maintained during image acquisition it is possible to observe which cells are being moved by the force applied by the flow across the biofilm as visualised using phase contrast video microscopy (see List of Accompanying Material, pg 11). This shows that there are four classes of cells observed:

1. Firmly embedded biofilm

2. Loosely attached biofilm which can be seen 'fluttering' as pushed by flow of media

3. Cells free in solution but undergoing 'tumbling' transient interactions with cell surface

4. Cells completely in solution following bulk liquid flow with no additional interactions

In summary these approaches both showed that the vast majority of biovolume signal imaged is from cells which are completely immobile. As bacteria in free solution even when not actively swimming will still move this is sufficient evidence to assign this fluorescent signal as biovolume due to bacteria embedded in matrix and hence part of a biofilm. These observations also demonstrated that the hold time during acquisition did not lead to any significant dissolution of the biofilm, unlike the situation seen with other bacterial species (McDougald et al., 2011; Thormann et al., 2005).

As very few cells were not assignable to the biofilm the decision was made to assign the total fluorescence measured as biofilm. An attempt was made to use the erode function of Volocity's quantitaion analysis software with the aim of reducing small level signals most likely to be due to the few free cells but this was found to also reduce signal from cells embedded in

the matrix. The data presented in this work will therefore be a slight overestimate of biofilm biovolumes but will not have falsely rejected actual biofilm signal.

5.3 Effect of CDI on competition between coseeded target and inhibitor cells

In order to study the effect of CDI within biofilm growth cells of target and inhibitor / control cells were grown in flow cells so as to obtain biofilms with significant levels of matrix production. The outcome of competition between cells growing from this initially well mixed seeding position was assayed by measuring the biovolume of each strain after 9 hours using CLSM, once the media flow had been stopped . As individual randomly chosen fields within the flow cell will be variable in the extent of biofilm formation the ratio of target cell biovolume to inhibitor cell biovolume was calculated for each field and this ratio value used for comparison between fields.

5.3.1 Cogrowth of target and inhibitor cells occurs initially

As the coseeding protocol was a novel one it needed to be confirmed that the initially seeded target cells were viable for biofilm formation and had not been preinhibited. Previous work by Aoki et al (Aoki et al., 2005) showed that for planktonic inhibition to occur inhibitor cells needed to be in log growth phase. Also assays used a large excess of inhibitor cells over target cells with significant incubation times, typically 3 hours to achieve the significant levels of growth arrest reported. There was also evidence for reversibility of the action of the EC93 CDI toxin (Aoki et al., 2009) albeit in an artificial situation. Taken together these factors would predict minimal opportunities for the CDI expressing inhibitor cells to act on target cells using a protocol where the CDI+ cells are seeded first. As the majority of inhibitor cells will have been washed off prior to target cell addition, the cells present are not in log phase growth as there is significant growth lag as they adapt to changes in nutrient availability in media (LB to M9) and growth mode (planktonic to biofilm). If any effective intoxication has occurred then it will only have been transient as cells post coseeding flushing are seen to be separate so further intoxication will not be occurring and any growth inhibition would be reversible.

Viability of coseeded target cells was checked by two methods - evidence of motility and evidence of growth in the initial stages of biofilm formation, prior to microcolony contact.

1) This could be seen by a visual check of seeded cells where motility was still present in spinning target cells at the end of the coseeding protocol. These cells are being rotated by there flagella which are interacting with the glass coverslip surface and acting to tether the bacteria in position. The motor action is still however driving rotation as the flagella are fixed this leads to movement of the cell, much as is seen in some experimental set ups (Berg et al., 1993). As a

cell with a significant proton motive force is required for motor movement this demonstrates that at least a proportion of the cells had not been affected

2) In addition while only individual cells were observed on initial seeding it could be seen that even when CDI toxin activity was inhibiting significant growth there was some expansion of the population of target cells which existed at the start of the flow cell incubation period. See also Section 5.3.4 for microscopy showing growth of initially seeded target cells over time.

5.3.2 Ec93 CDI toxin increases strains competitive effectiveness in a biofilm

Competitive effectiveness of the EC93 toxin was judged by comparing the biovolume ratio of target to Ec93 strain cells grown in the presence or either CDI+ wild type cells or CDI- ΔcdiA cells. It can be seen in Figure 17 panel A that expression of a functional EC93 CDI system leads to growth inhibition of the target cells and hence to overgrowth by the wild type EC93 strain. This is a novel demonstration of the effectiveness of the EC93 CDI toxin when cells are growing in a biofilm. Isolated target cells up to small microcolonies of ~10 cells can be identified in the larger body of inhibitor cells. The presence of target cells spread through the biofilm is most likely due to the pushing action of cell growth/matrix production. This effect was quantified by calculating the ratio of K12 F+ cells (target cells, that is susceptible to CDI toxin) to EC93 strain cells using biovolume, calculated from appropriate fluorescent signal. The greater the ability of the EC93 strain to grow relative to the target strain the lower the value of this competitive index.

As shown in Figure 17 panel A target cells are able to grow in the presence of the EC93 ΔcdiA strain showing that, as found in Chapter 4, the EC93 strain background did not stop target cell growth, this time in the context of biofilm growth. The result is that starting from a random arrangement of cells a well mixed two strain biofilm is formed in the absence of CDI toxin.

Expression of different fluorescent proteins could theoretically alter the growth rates of strains, even though no such effect was seen in planktonic growth, or beii detected to different extents, although confocal settings were adjusted to give comparable responses. This was tested for by analysing flow cells with both options for expression of GFP or mCherry. There was no significant difference in the response of target cells to CDI+ cells when they were expressing either of the fluorescent proteins used as a complementary pair in experiments see Figure 17.

It was noted that there seemed to be a more variable, and overall lower, absolute level of biofilm formation in flow cells in which Δ cdiA cells were grown. This lead to the work shown in section 5.3 looking solely at biofilm formation of single strain biofilms.
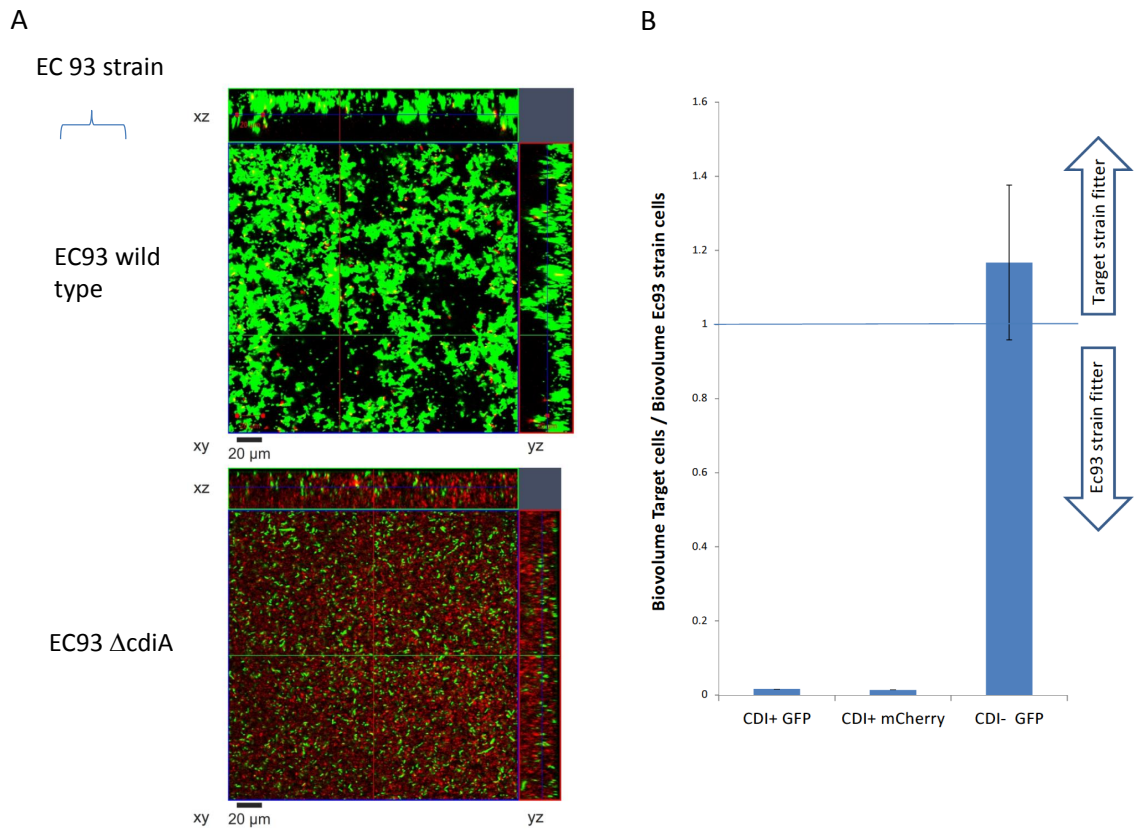
Figure 17: EC93 CDI effect on competition within a biofilm

A : Representative confocal microscopy z stacks showing the outcome of competition after 9 hours of growth post coseeding with cell suspensions of $OD_{600} = 0.016$. K12 F+ cells are shown in red, EC93 strain cells shown in green. B : Comparison of the competitive index (determined by biovolume) of K12 F+ cells versus EC93 strains expressing either mCherry or GFP proteins, to act as a control for any effects of fluorescent protein expression, and a CDI- strain expressing GFP, n=5 fields, +/- 1 standard deviation.

5.3.3   Ec93 toxin action alone impacts on biofilm competitive effectiveness

To demonstrate the effectiveness of only the toxin portion of CdiA, coseeding experiments with the C-terminal cdiA deletion strain were performed. As covered in Section 5.4 the core conserved region of CdiA has a role in biofilm formation so in order to isolate the increased rate of biofilm formation effects from the toxin growth inhibition of target effects an EC93 CdiA C-terminal deletion strain, which has only the toxin portion missing, was used. As this lacks the toxin there will be no growth inhibition but it should retain comparable levels of biofilm formation ability. As shown in panels B and D of Figure 15 and quantified in Figure 18 the change in strain leads to biofilm formation which shows comparable levels and characteristics, degree of 'clumping', between each strain indicating that there was indeed a significant difference being seen when the ΔcdiA control had been used previously, see Section 5.3.2.

As is common with biofilm analysis there is variation in absolute values of biofilm reported between replicates but the same conclusion can be drawn, that there is a statistically significant reduction in competitive fitness within a biofilm on loss of the C terminal toxin portion only. Therefore it can be concluded that the change to strains with comparable levels of biofilm production has not removed the effect of CDI toxin on biofilm competitive ability. It can however be seen that the magnitude of the effect has decreased, compare Figure 17 panel B with Figure 18, indicating that there was previously a significant contribution of growth differences to the measured levels of competition.

5.3.4   Time lapse analysis of competition

In order to obtain an insight on the dynamics of competition between target and inhibitor cells in a biofilm, and also to confirm that no inhibition prior to biofilm growth was occuring with the coseeding protocol used, timelapse analysis of biofilm growth was performed. In this case the protocol was modified so that rather than taking a single set of measurements at 9 hours multiple observations across the period up until 13 hours of growth were obtained.

As shown in Figure19 the initially widely spaced and randomly positioned single cells seen at t=0 hour show growth of both inhibitor cells and target cells after three hours of growth. Correlating the two z slices of the same field of view shows that the bulk of cells present in the 0hr image are still present at the 3 hour time point, the others have presumably been lost to the bulk media flow due to insufficient adhesion. Of the cells which remained the majority of them appear to have undergone growth / division. This demonstrates that the target cells are capable of growth after the coseeding protocol and hence that prior inhibition by CDI cells has not occurred.

Comparison of later time points (10 through to 13 hours) shows no change in the levels of target cells present but a change in position of the non growing target cells as they appear
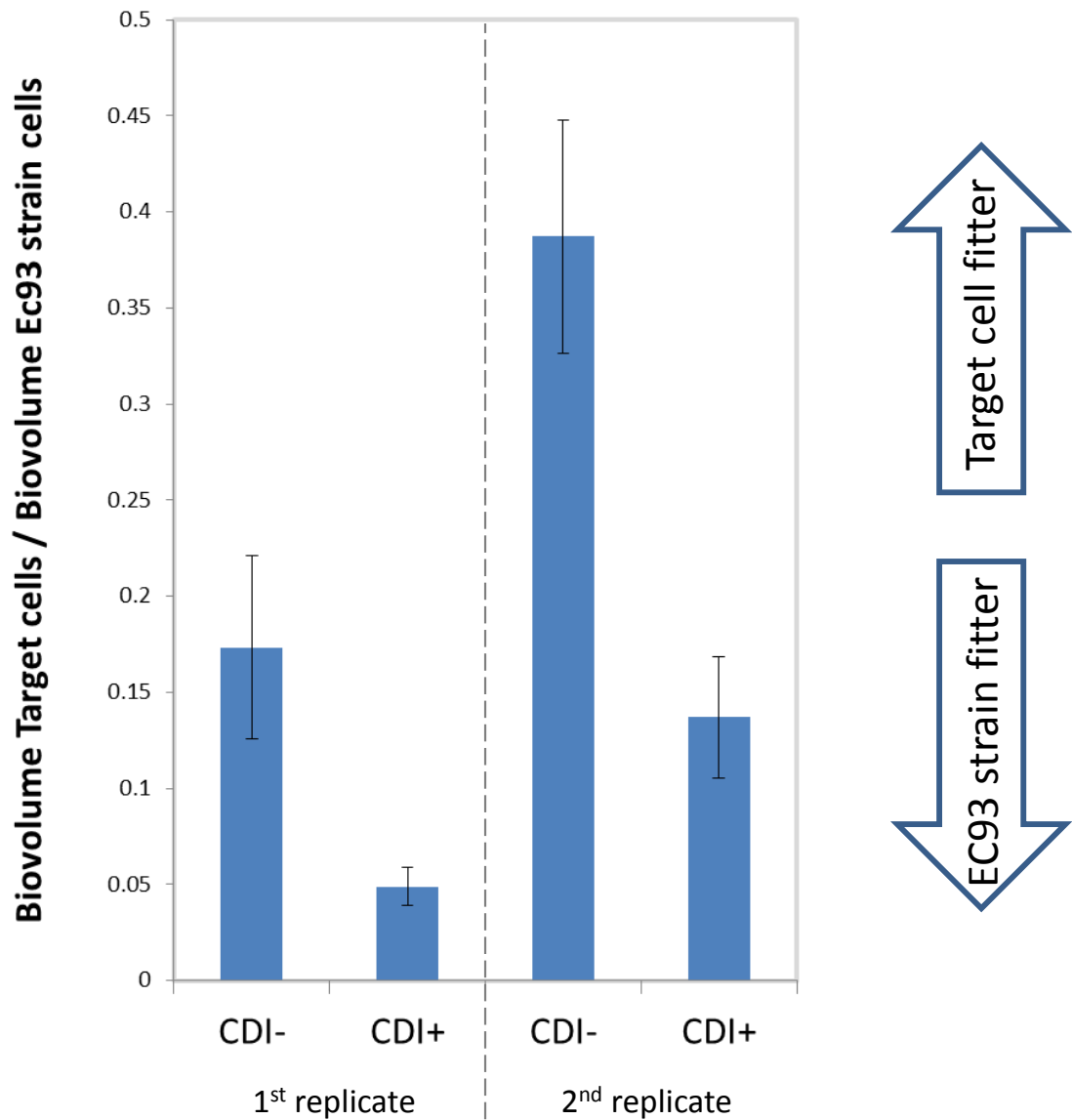
Figure 18: Ec93 CDI toxin effect on competition within a biofilm

Comparison of the competitive index of K12 F+ cells versus EC93 strains (seeding OD_{600} = 0.32) grown in flow-cell biofilms, n=5 fields, +/- 1 standard deviation for each replicate. EC93 strains used, EC93 wild type (CDI+) and EC93 CdiA C-terminal deletion.

to now be embedded in the bulk of the inhibitor cells and carried along with its continued growth. Which is what would be predicted given the growth arrest action of the EC93 system in planktonic systems but is the first demonstration of the continued integrity of cells in a biofilm environment.

5.4 Effect of EC93 CDI system on biofilm formation

In the course of looking at the effect of the EC93 CDI toxin on competition between biofilms it became apparent that there was an unexpected secondary effect of the system on how significant a biofilm EC93 strains were capable of forming. Occasionally parts of a CDI+ biofilm would appear to be covered in a thin layer of target cells suggestive of a directed interaction. More commonly it was noted as shown in Figure 20 that the nature of the cell to cell packing within a biofilm was different between the EC93 wild type and EC93 ΔCdiA strains. The wild type EC93 strain has a majority of cells closely opposed to each other such that the signal from the cytoplasmic fluorescent protein cannot be resolved between cells due to the limits of confocal microscopy. In contrast the Ec93 ΔcdiA strain images show cells that are well separated, presumably by being embedded in matrix material although this is not visualised using this experimental approach, such that individual cells are resolved. Taken together with the apparent trend for ΔcdiA cells to produce an overall less robust biofilm it was decided to study the effect of different deletion mutants (see Figure 14) to determine the molecular basis of this effect.

5.4.1 Deletion of CDI system leads to changes in biofilm robustness

In order to test what effect the presence or absence of a functional EC93 CDI system would have comparative experiments using the Ec93 wild type strain and the Ec93 ΔcdiA strain were performed. Unlike the experiments in the previous section this work was performed using single strains to isolate the effect of self-self interactions. Cells were seeded onto coverslips as previously described with the second injection just using media as a blank. This was performed so that the protocol followed would be identical to that used for the coseeding experiments to aid comparison of results. Flow cell growth was undertaken for 9 hours at 37°C before confocal image acquisition under static flow conditions.

Overlays of confocal z stacks from each strain, see Figure 21, show the wild type cells forming a well developed biofilm extending tens of μm away from the surface of the coverslip while the deletion mutant was only capable of forming a sparse biofilm that is largely a monolayer.

Quantitation of the total biovolume formed by each strain, see Figure 22, shows a 3-5 fold greater level of biofilm formation when the strain possesses a functional EC93 CDI system. This confirms that the effect that was seen in the coseeding experiments is due to the EC93
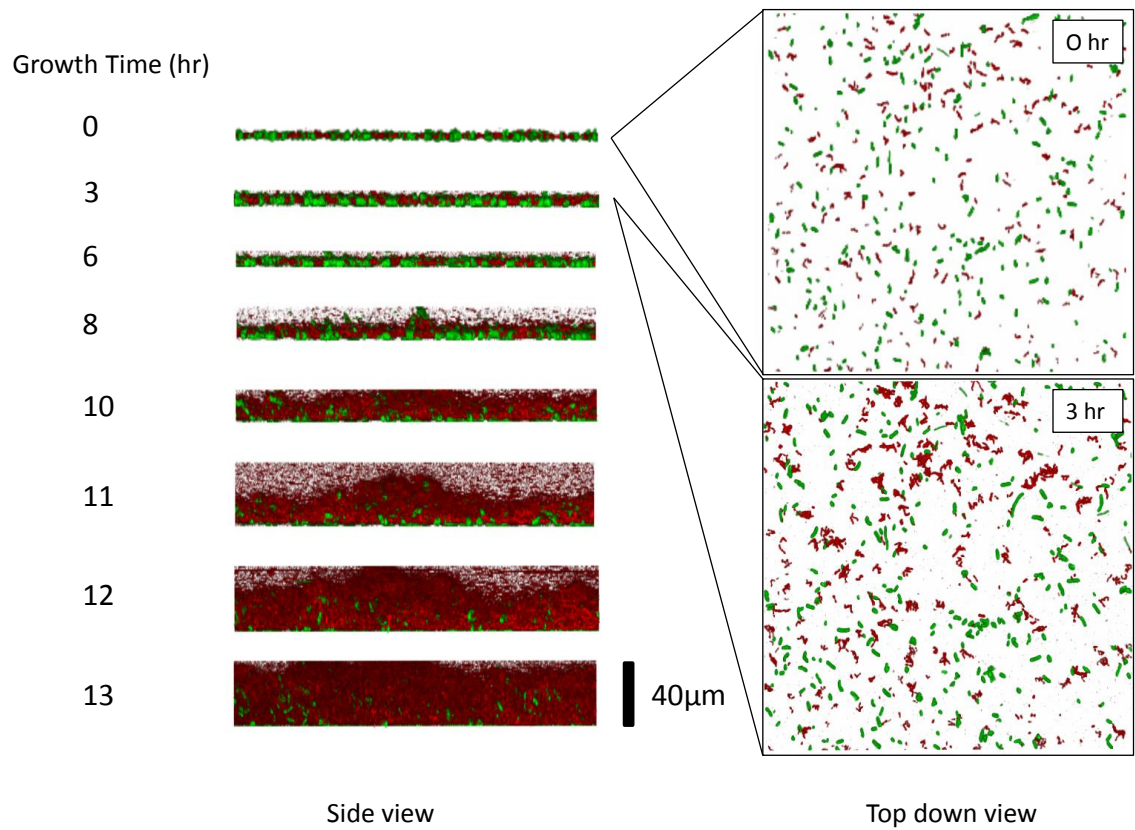
Figure 19: Confocal time lapse of EC93 wild type and K12 F+ cogrowth in a flowcell biofilm Growth of cells is shown at indicated time points as a maximum projection side view on the xz axis, K12 F+ (green), EC93 wild type (red). In addition for time = 0 and 3 hours the x,y view at the coverslip surface is shown to highlight initial coverage and microcolony growth.
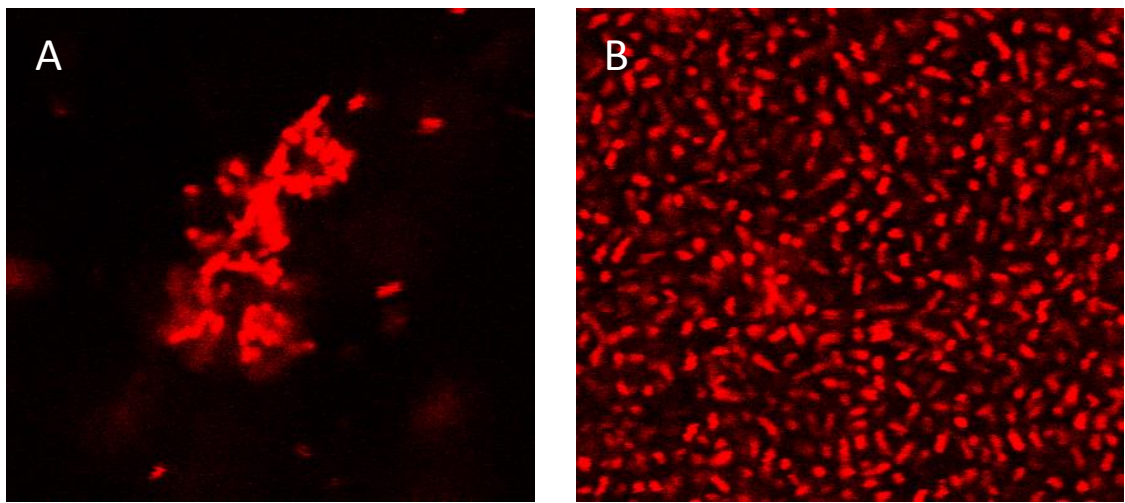
Figure 20: Packing density of bacterial cells is altered by CdiA expression

Confocal xy slices showing packing density of strains after 14 hours of growth : A) EC93 wild type close packing was predominantly seen in towers extending from substratum b) EC93 Δ cdiA cells were seen to be more widely separated.

CDI system and that it only requires EC93 cells to be present, not target strains (K12). Taken together with the cell-cell packing discussed previously this data supports a role for the EC93 CDI in cell-cell interactions within biofilms.

5.4.2 Hypermotiility modulation of biofilm formation in deletion mutants

After the work performed in the previous section had been completed it was learned (personnel communication, Zachary Ruhe) that during the generation of the ΔcdiA mutant, selection for hypermotility had also occurred. Hypermotile cells show an increase in flagella driven motility rates, as measured by movement of cells through low percentage agar, which can be due to a number of factors such as increases in flagellar rotational speed, increases in number of flagella and changes to rotational switch frequency (Donato et al., 1998).

This has the potential to skew the experimental interpretation of the results as the comparison being made was not a simple loss of the cdiA system but instead this and the addition of hypermotility. As two variables were changed at once it is not possible to say which has caused the effect and so additional experimental work was performed using a newly generated ΔcdiA mutant which was not hypermotile (supplied by Zachary Ruhe). This data is show in Figures 22 and 23 were it can be seen that the level of biofilm formation is significantly reduced for both ΔcdiA strains compared to the wild type strain. This shows that the key modulating factor is the presence or absence of cdiA molecules regardless of the cells state of hypermotility. Hypermotility itself leads to a small reduction in levels of biofilm formation which may reflect differences in levels of initial attachment. Thus it can be seen that there is no change to the conclusion reached in the previous section that the presence of the EC93 CdiA protein increases levels of biofilm formation.

5.4.3 Conserved CdiA region is sufficent to confer robust biofilm formation

In order to further dissect the molecular basis of CdiA's role in increasing biofilm formation a comparison was made of the single strain biofilm growth of EC93 wild type cells with an EC93 strain with a C-terminal only deletion of CdiA, see Figure 14. With this mutant the variable toxin tip region and cognate cdiI are not produced by the cells leaving only the much more highly conserved core region of cdiA. This region is presumed to contain the interaction site for BamA on the 'target' cell which was a possible site for mediating adhesion between cells. Single strain biofilms were grown as previously described with results as shown in Figure 24. It can be seen that maintaining only the conserved region of the CdiA molecule, EC93 CdiA C-terminal deletion strain, is sufficient for retention of wild type levels of biofilm formation. The C terminal deletion strain forms biofilms which extend 10's of μm from the substratum and shows the same close cell-cell packing phenotype reported above. The two most likely possibilities for an adhesive interaction, that of a homo dimer formation of cdiA between CDI

	Strain	Orthogonal projections	3D render side on

A

Ec93
wild
type

C

D

E

B

Ec93
delta
cdiA

40µm
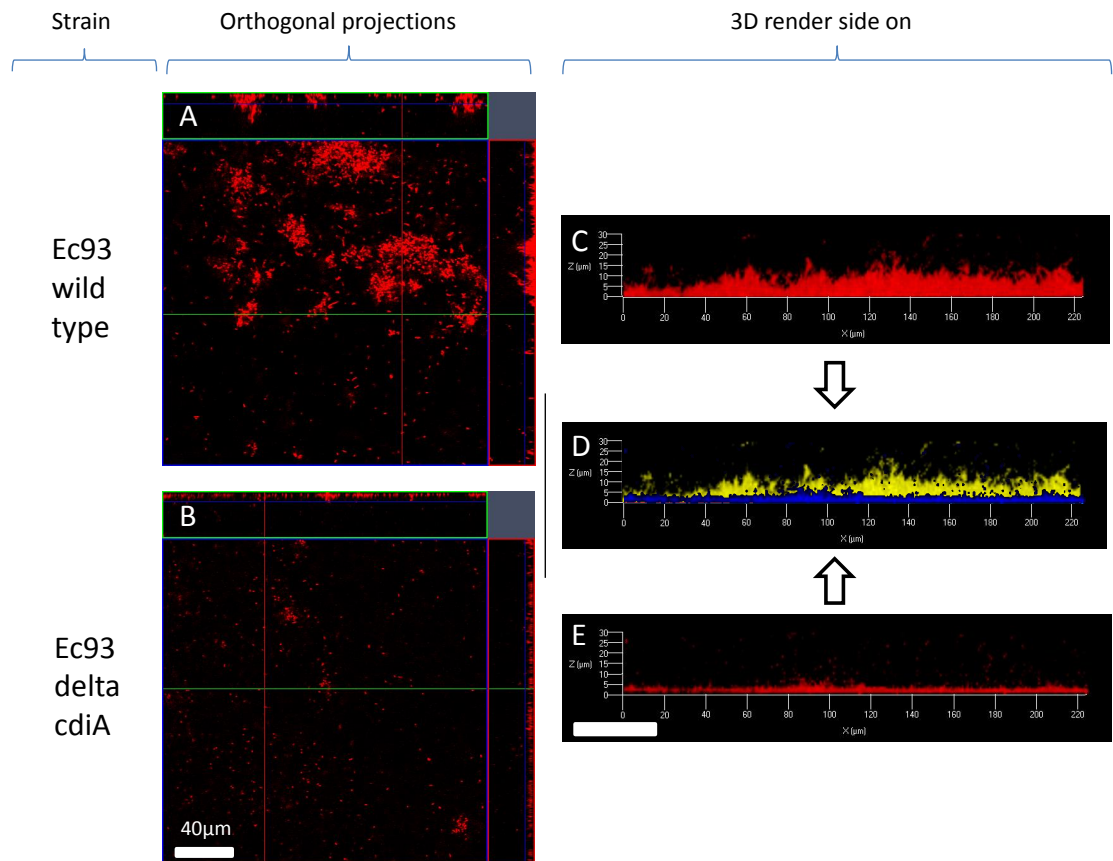
Figure 21: Expression of EC93 CdiA increase the level of single strain biofilm formation
Single strain flow cell biofilms were grown for 9 hours before confocal image acquisition. A,B :
Orthogonal projections of indicated strains, C,E Maximum intensity projection along xy axis,
D Overlay of C (yellow) and E (blue).
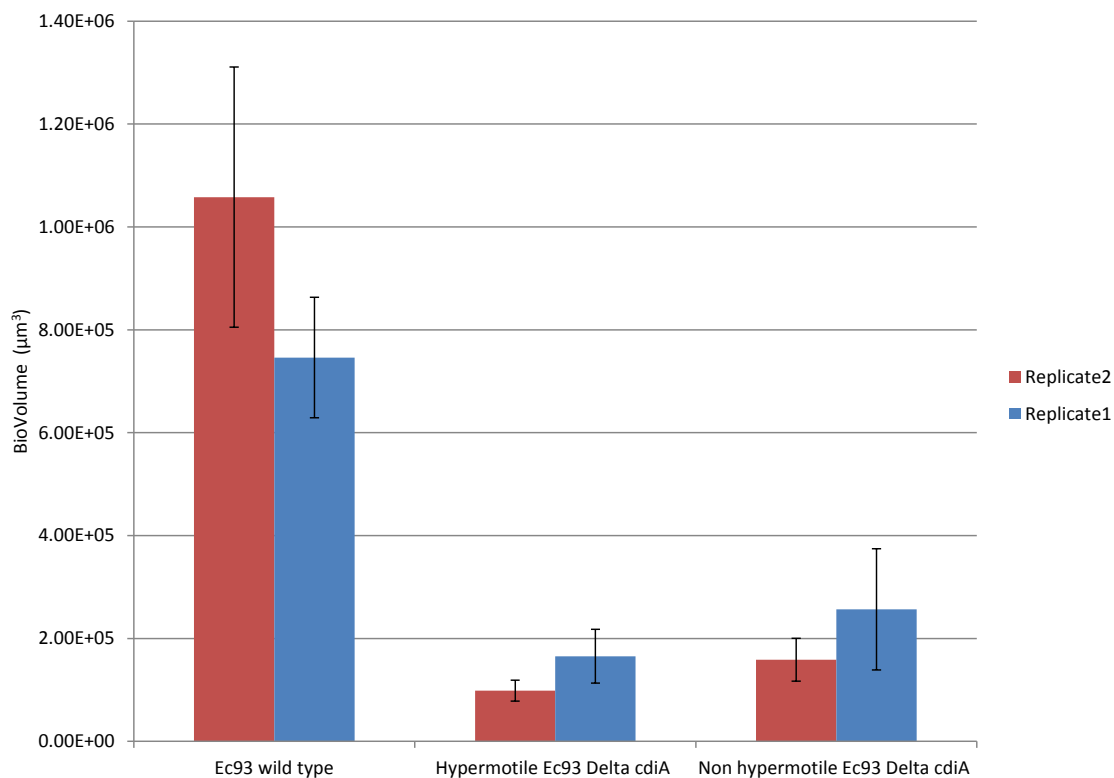
**Figure 22: Quantification of the effect of hypermotility on EC93 CdiA conserved region me-
diated biofilm formation**

Single strain biofilms grown for 9 hours in flow-cells. Biovolume was quantified from confocal
z stacks using Volocity software, n=5, +/- 1 std deviation for each replicate.
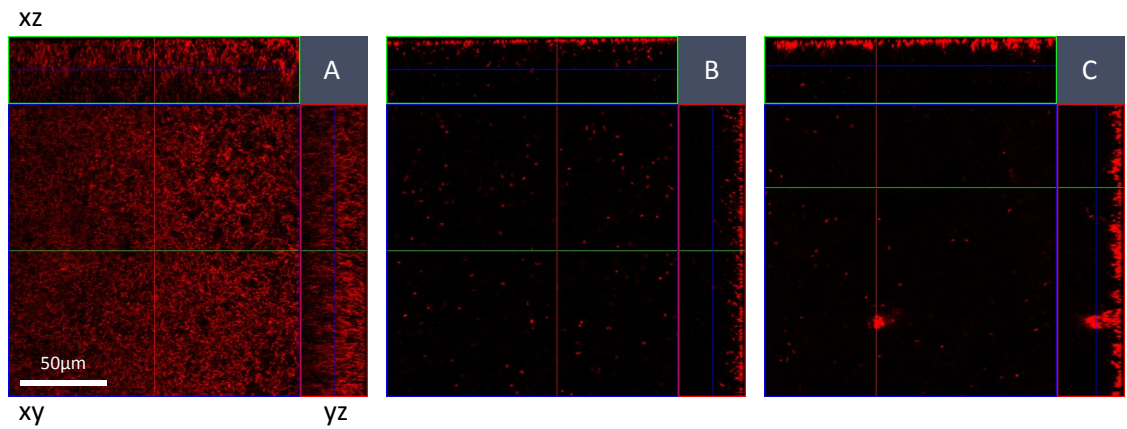
Figure 23: Effect of hypermotility on EC93 CdiA conserved region mediated biofilm formation

Confocal microscopy z stacks of flow-cell biofilms after 9 hours of growth of Ec93 wild type (A), Hypermotile Ec93 ΔcdiA (B) or Non hypermotile Ec93 ΔcdiA (C) strains showing the variation in biofilm formation levels.
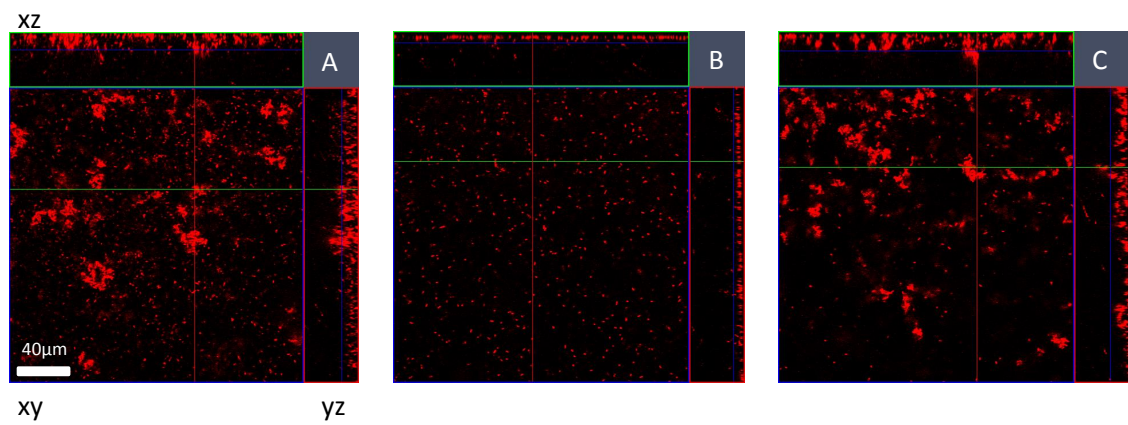
Figure 24: Conserved region of EC93 CdiA aids biofilm formation independent of CdiA CT toxin tip

Confocal microscopy z stacks of flow-cell biofilms after 9 hours of growth of Ec93 wild type (A), Ec93 ΔcdiA (B) or Ec93 cdiA terminal deletion (C) strains showing the variation in biofilm formation levels.

producing cells and a CdiA - BamA interaction cannot be distinguished in this data set. Data on the biofilm forming ability of an EC93 strain expressing a BamA variant not recognised by EC93 CdiA would be required to determine if BamA played a role in adhesion as well as toxin translocation. This data shows that the EC93 CDI toxin portion of the CdiA protein is not required for an increase in levels of biofilm formation.

5.4.4   EC93 effect on adhesion is not suffcent to allow cell capture

Bacteria growing in biofilms do not only experience growth in environments which have not been previously colonised but also are expected to encounter situations in which they are either carried too or actively move to new locations in which bacteria are already growing as biofilms. In order to assess whether the EC93 CDI toxin system could affect interactions between planktonic bacteria and cells in an existing biofilm an adaption of the previous flow cell protocol was made. An early stage biofilm of EC93 wild type cells was grown for 5 hours and then cells from different strains expressing a different fluorescent protein were flowed onto this biofilm, held with no flow for 10 minutes and then the flow resumed for a further 4 hours. Measurement of cell biovolume ratio at the end of the experiment then gives a measure of the ability of the cells that have been flowed on to interact with the preexisting biofilm. The strains used were hypothesised to be ones that would show a wide range of intracellular adhesiveness, from high (EC93 wild type) to low (EC93 ΔcdiA). As shown in Figure 25 and Figure 26 no evidence of EC93 CDI mediated adhesion was seen with similar levels of interaction seen whether or not CdiA was present on cell surfaces. The results from the EC93 strain with *S. enterica* derived from *BamA* would have been expected to be comparable to, or show less interaction than, those seen for the EC93 wild type strain on the basis of planktonic assays showing no role for BamA interactions in EC93 mediated cell-cell adhesion. In fact the EC93 strain expressing *S. enterica* BamA showed higher levels of interaction for reasons unknown but causes could include changes in the nature of interactions between planktonic and biofilm growth states and variability inherent in the assay set up. None of the confocal images obtained showed evidence of any 'coating' kind of interaction between cells.

5.5   Conclusion and Discussion

This work has demonstrated that the EC93 CDI toxin is capable of acting in the context of biofilm competition and that in addition the core conserved region of the cdiA molecule is capable of aiding biofilm formation.

Prior to this works it was not clear if CDI systems would be capable of functioning in the context of a biofilm due to two main factors found in the planktonic studies done to date:

1) Assays performed in liquid culture required inhibitor cells to be growing in log phase
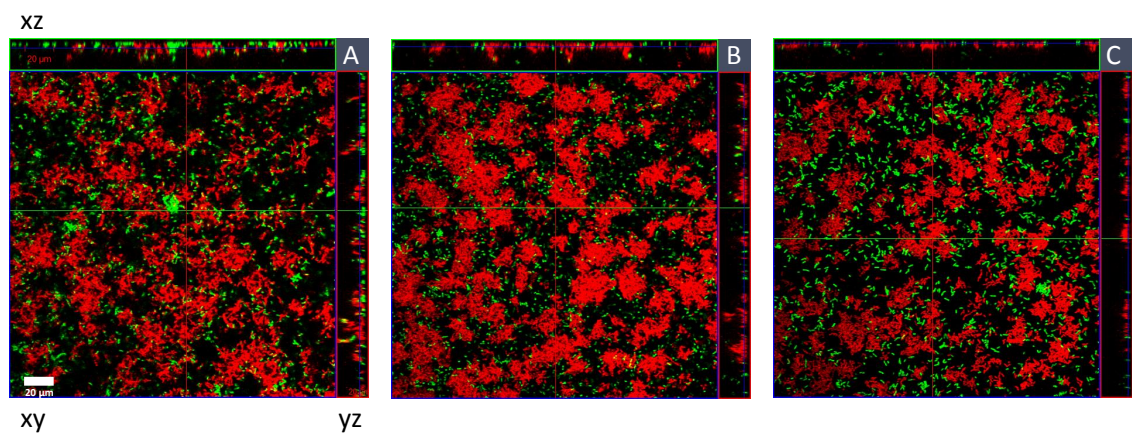
Figure 25: Effect of EC93 CDI and BamA expression on cell interactions with EC93 wild type biofilm

Confocal microscopy z stacks of flow-cell biofilms after 4 hours of initial growth of EC93 wild type strain (red, mCherry), followed by incubation for 10 minutes with one of the following strains expressing GFP Ec93 (*S. enterica bamA*) (A), Ec93 ΔcdiA (B), Ec93 wild type (C), and 4 hours further growth.
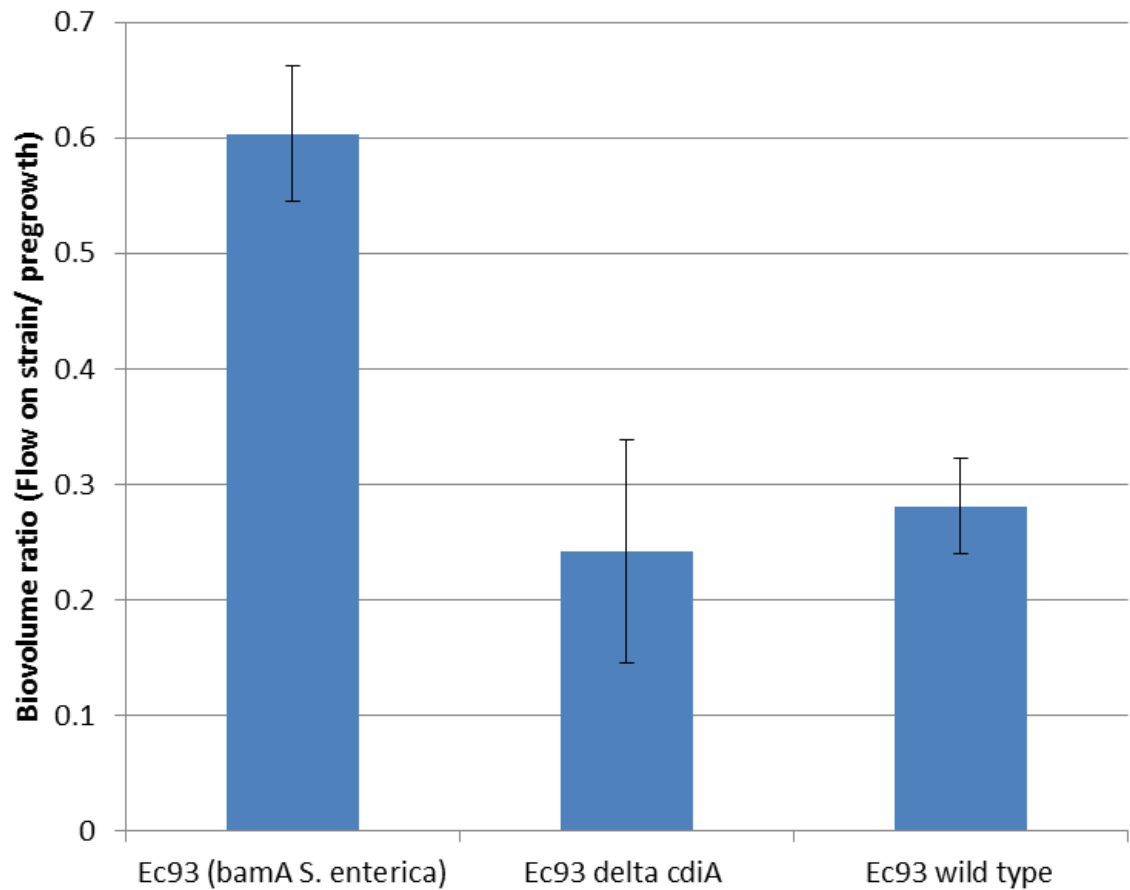
Figure 26: Quantification of the interaction of EC93 wild type strains with self and mutant strains

EC93 wildtype strain (expressing mCherry) was grown in flow-cells for 5 hours, strains expressing GFP were flowed on and held for 10 minutes. Flow was then continued for 4 hours. Biovolume was quantified for each fluorescent channel from confocal z stacks using Volocity software, n=5, +/- 1 std deviation for each replicate.

for the growth inhibitory effect of CDI to be seen. They also commonly used a large excess of inhibitor to target cells which would be consistent with many opportunities for toxin delivery which would not be available in the more structured environment of a biofilm.

2) It was already reported by Aoki et al (Aoki et al., 2005) that bacterial surface components such as pili could act to protect cells from the action of EC93 CDI toxin. Biofilms classically contain a significant matrix component surrounding and separating cells which could easily be envisaged to also act to block cells coming together or make such contacts infrequent enough to have a negligible effect on overall biofilm competition.

The results of the coseeding flow cell analysis show that at growth rates attainable in a biofilm, albeit one with constant fresh media flow at 37°C and hence likely to represent near maximal biofilm growth rates, the EC93 CDI system is effective. The presence of significant levels of matrix, as judged by the amount / spacing of immobilised cells did not stop the action of CDI. This is presumably due to the significant levels of cell mixing on biofilm growth, see Figure 19 that were seen using this protocol, which would give increased opportunities for inhibitor - target cell interactions. It would be interesting to see if the effect was as pronounced under different biofilm growth conditions, such as different flow rates (static), lower growth rate, or with strains which naturally have a more monoclonal growth pattern.

Based on the action of other bacterial toxin systems such as colicins (Chao et al., 1981; Kerr et al., 2002; Prado et al., 2008; Nahum et al., 2011) it had initially been thought that the action of EC93 CDI system could result in the generation of spatial structure in populations. Under the conditions tested it was however found that even though the toxin has an absolute contact requirement (see Chapter 4) a mixed population of cells resulted, with the action of the toxin resulting in CDI+ cells dominating the environment with growth halted K12 F+ target cells carried along in the bulk. This is likely in part to be due to the particular growth conditions used as variation in growth rates, cell shape (Rudge et al., 2013) and motility (Houry et al., 2012) can all impact on degrees of cell mixing even in the absence of toxin activity.

Recently published work by the Foster lab (Kim et al., 2014) highlights the role that factors other than toxin action can play in competition between strains in a biofilm, in that case positioning due to matrix production. It is interesting to compare this finding with the ability of the EC93 CDI system to not only be effective in biofilm competition by explicitly blocking growth of competitors but also by enabling more rapid self biofilm assembly. This ability to form a thicker biofilm than K12 cells at nine hours but not at 14 hours gives EC93 cells a second competitive advantage by enabling more rapid colonisation of new environmental niches in which biofilm formation is of benefit to the cells. It is possible that there may have been an evolutionary drive to link biofilm forming ability with toxin activity to block the growth of any 'non self' cells which were capable of interaction with a proto adhesion molecule. In this model the CDI system acts to both to build and recruit self cells to multicellular structures while

simultaneously stopping other closely related strains from growing in the same environmental niche. Tethering the toxin to the same point as that required for interaction can then be seen as a very efficient way to out compete non self cells.

The work shown in this chapter taken in conjunction with the planktonic results reported by Zachary Ruhe, show that the CdiA protein in the EC93 CDI system plays two roles, the expected delivery of a toxin moiety to target cells to block their growth and a previously unknown role in aiding biofilm formation. This is probably related to the data reported in (Ruhe et al., 2013b) showing a requirement for specific extracellular loop sequences for CdiA and BamA to interact a model of CdiA with not only a C terminal toxin region but also two, presumably independent regions, responsible for binding interactions. The precise molecular motifs within the protein responsible for the non toxin interactions remain to be identified.

While this work was being performed the Cotter group ((Garcia et al., 2013; Anderson et al., 2014)) identified a similar link between CDI systems and biofilm production for the *Burkholderia* CDI systems which are closely related to the rest of the CDI family but show a different operon organisation. For the Burkholderia CDI systems expression of CDI molecules in only a small subset of cells and the presence of extracellular DNA is required for increased biofilm formation indicating that there may be a significant difference in the mechanism of operation between the two types of CDI systems.

Chapter 6

Effect of EC869o11 toxin on target cells at the single cell level

6.1 Introduction

E. coli CDI toxins have been classified into at least 18 sequence types (Ruhe et al., 2013a; Beck et al., 2014b) only a few of which have been assigned a specific function (Aoki et al., 2010). In order to better understand if this variety of toxin classes is capable of changing the nature of CDI effects on target cells it is important to contrast the effects of different toxin types. Insight into this area may increase our understanding of the variety of possible roles that the CDI systems could play in bacterial ecology. As the previously examined EC93 toxin was shown to have a reversible action which only occurred after a delay post contact a toxin which was likely to show more dramatic effects was looked for in order to provide an informative contrast in effects. One class of those which has been given a defined function is the EC869o11 toxin which by sequence similarity and then experimental analysis was identified as a nuclease toxin capable of degrading double stranded DNA (Morse et al., 2012). It was hypothesised that this can be seen as a more aggressive mode of toxin action, that is degradation of genomic DNA, which would more quickly lead to growth inhibition which was irreversible. As this is a markedly different toxin activity compared to the effect of the EC93 toxin on metabolism it presents an interesting candidate for comparative examination of CDI toxins effects on the single cell level.

6.2 Analysis of the time course of inhibition

Toxin analysis was undertaken with the protocol developed in Chapter 3 and used successfully for analysis of the EC93 CDI toxin at the single cell level in Chapter 4. The EC869 strain from which the o11 toxin is derived is a sub strain of the O157:H7 EHEC *E. coli* strain which was identified as containing a CDI sequence (Eppinger et al., 2011) and in further studies (Nou

et al., 2013) was shown to contain 11 orphan toxin sequences in addition to the main *cdiA* gene. This parent strain was shown to be capable of inhibiting the growth of another O157:H7 strain (Nou et al., 2013) presumably due to the action of the main CdiA toxin molecule. This study also identified that a K12 strain expressing a chimeric EC869o11 CdiA protein from a cosmid was capable of inhibiting the growth of K12 strains but interestingly not the O157:H7 strain inhibited by the parent strain.

As EC869o11 is an orphan toxin in the strain background it was originally identified in and is hence not expressed / functional in that strain. Therefore in order to analyse the effect of the EC869o11 toxin a chimeric protein has been used in previously published work, (Morse et al., 2012; Nou et al., 2013). This protein is generated by fusing the conserved region of the EC93 *cdiA* gene with the sequence for the C terminal toxin portion of EC869o11, see Figure 27. This sequence allows a cell to generate a functional chimeric CdiA molecule which has the levels of expression and ability to display toxin on the cell surface of the EC93 CdiA molecule but which delivers the toxin activity of EC869o11 instead of its usual payload. This construct was used for the work described in this chapter, and was provided by Zachary Ruhe.

6.2.1 Effect of EC869o11 toxin on cell growth rate and morphology

Based on the previous work on general CDI toxins and analysis specifically of EC869o11 in planktonic assays (Morse et al., 2012) it was hypothesised that intoxication of target cells would lead to growth arrest in a manner broadly similar to the EC93 toxin. That is on contact with inhibitor cells, after an initial delay, target cell growth rate would decrease and eventually halt. However as can be seen in Figure 28 what was instead observed for target cells in contact with inhibitor cells (coloured blue) was a steady increase in growth rate, measured as increase in cell area per unit time, as intoxication continued see Figure 29.

Indeed if the data shown in Figure 29 is grouped in a similar manner as that used for the analysis of the EC93 toxin system then unlike the case for the EC93 toxin, extended contact with inhibitor cells leads to faster growth rates. Note that as cell division was not observed for cells affected by the EC869o11 toxin, the average time of the initial period from the EC93 analysis was used as the point at which to split the growth curve. As this increase in growth rate occurs when cells are longer, sufficiently long that their length extends outside the expected range for normal cell growth, consideration must be made as to how comparable the increase in gradient over time is between intoxicated cells and normal target cells. This is because as the cell volume increases, assuming comparable levels of cytoplasmic components such as ribosomes and mRNA, the biosynthetic capacity of the cell should also increase proportionally. Therefore while an apparently greater growth rate may be assigned to these cells this could be a normal growth rate for the given biovolume, that is simply being summed for a larger area/length. This was corrected for by dividing growth rate by the length of the cell to get a
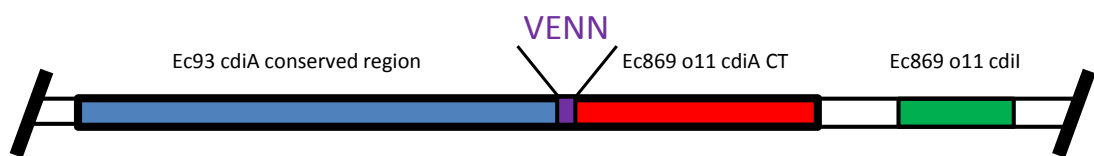
Figure 27: Schematic of EC869o11 / EC93 chimera

Components shown are conserved cdiA region (blue), VENN motif (purple), cdiA C terminal region (red) and cdiI inhibitor (green). Black slashes indicate transition to the cosmid backbone.
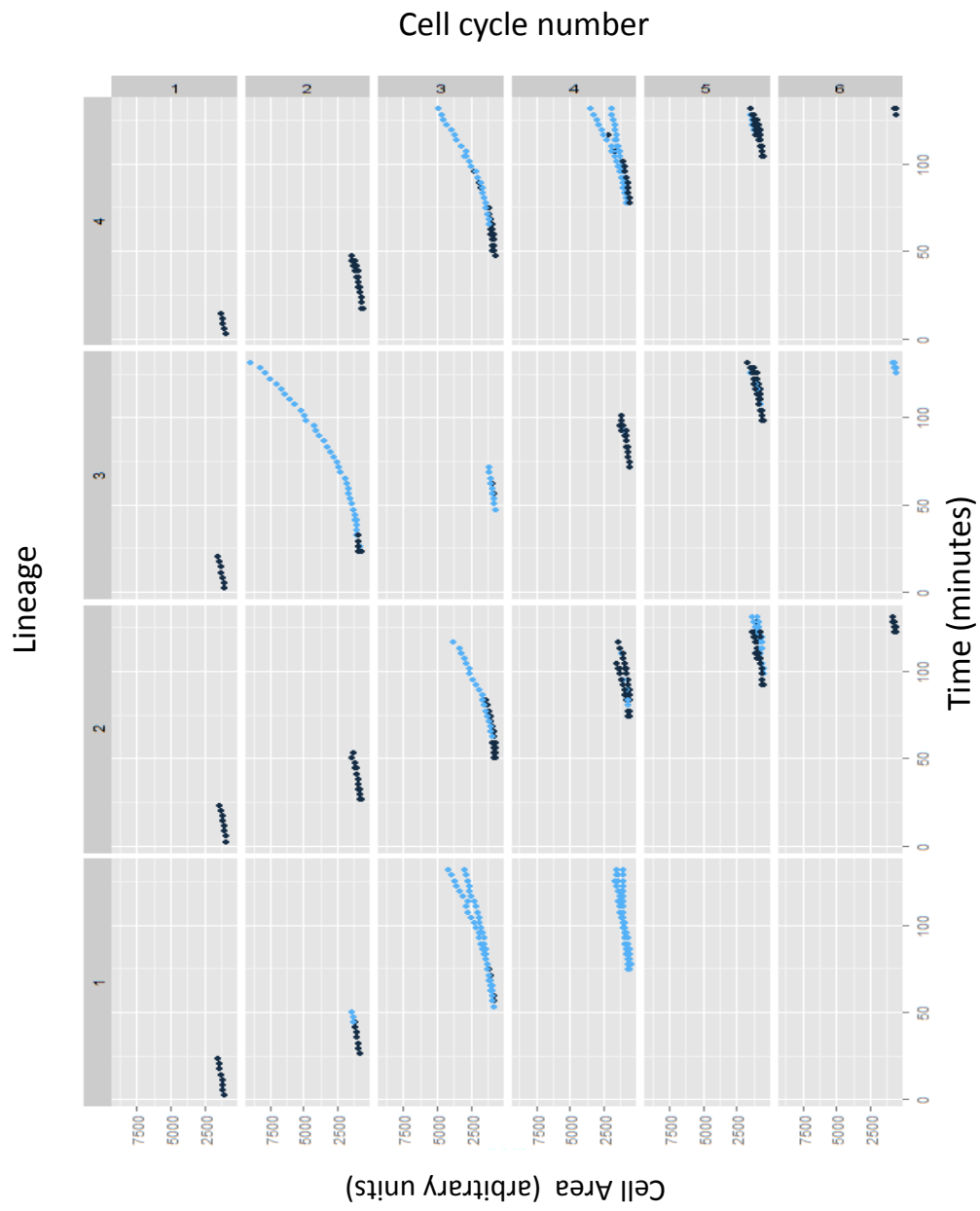
Figure 28: Comparison of K12 F+ single cell growth curves with and without contact with EC869o11 toxin

Growth cell curves derived from MicrobeTracker analysis of time-lapse data, see section 2.4.5, split as indicated on the axis, blue data points indicate K12 F+ cell is in contact with cell expressing EC869o11 CDI toxin.
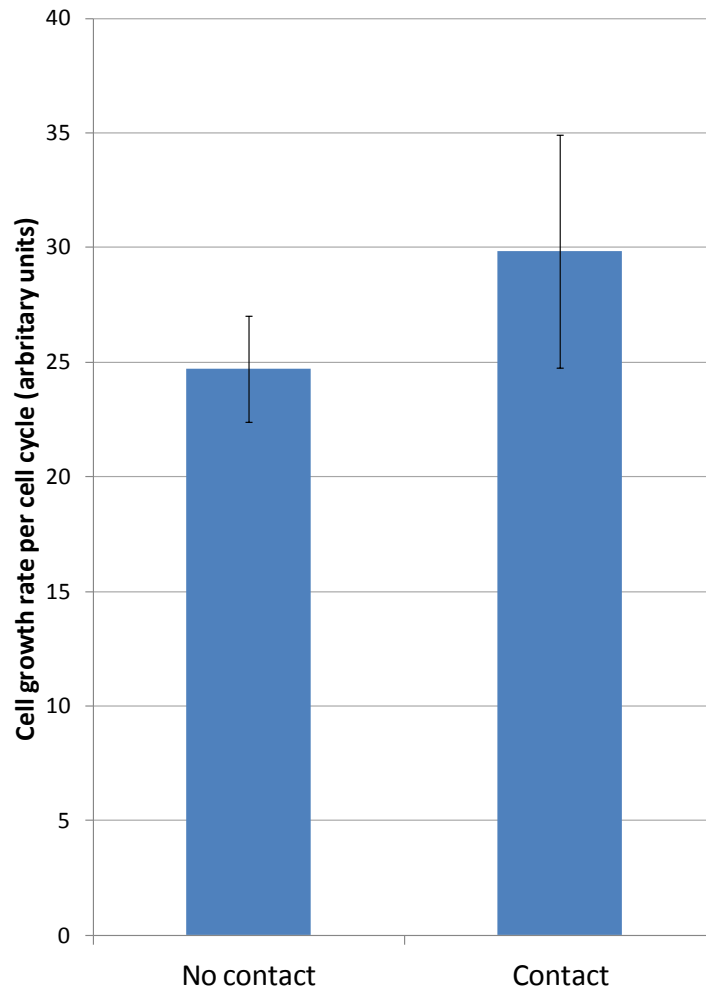
Figure 29: Effect of contact with cells expressing EC869o11 on K12 F+ *E. coli* growth rate
Growth rate per cell cycle of K12 F+ cells either in / out of contact with EC869o11 cells was
determined by MicrobeTracker analysis. Cell cycle numbers measured, contact n= 27, no con-
tact n= 41, +/- 2 s.e. with no significant difference between contact and no contact results.

standardised value, note this will be an approximation due to complicating factors such as no end caps needing to be produced and possibly (see section 6.3.3) less DNA production. This value was found to be comparable (data not shown) between uninhibited and intoxicated target cells indicating that the per cell growth rate increase is due to the cells being longer and hence possessing greater biosynthetic capabilities. An effect of cell length on growth rate can be detected for normal cells as a slight bias in plot points around the approximation of linear growth rate at normal cell sizes, but is not significant enough to affect the usefulness of the fit.

This was linked with a failure to septate at the expected cell size, as compared to target cells not in contact with CDI+ cells. The effect on septation was so pronounced that for all cells observed to become intoxicated, no further cell division was observed during the time course of the experiment leading to exceptionally long cells, >40μm in length compared to 5μm for normal cells, see Figure 30 Panels B,D. This morphology is different to the occasional lengthened cell that can be observed in standard cell cultures e.g. MG1655 strain, as in this case after a period of growth to a longer length prior to division the cell then rapidly septates off multiple cells that go on to grow normally. The latter behaviour presumably relates to the mechanisms behind UPEC *E. coli* filamentous stage of growth in cell invasion (Justice et al., 2006).

The effect of the EC869o11 toxin can be seen to be rapid as there is no division of cells post contact despite the time point in the cell cycle when contact is made with inhibitor cells being random. If there was any significant delay in toxin effect it would be predicted that those cells which where about to divide prior to contact with inhibitors would have sufficient time to complete that division cycle before the toxin could act. The absence of any such cell divisions therefore shows that the time for the initial effects of the toxin to act to block cell division must be less than the three minute gap between observations.

Target K12 cells are constitutively expressing GFP during the course of the experiment in order to allow strain types to be distinguished. As cells are growing during the experiment there will be a diluting effect on fluorescent protein levels unless cellular protein production keeps pace (Adiciptaningrum et al., 2009; Helaine et al., 2010). In addition the excitation light required for fluorescent imaging of cells, even when used infrequently as it was in this protocol, results in some level of bleaching of fluorescent proteins and hence loss of signal. Hence the ability of a cell to maintain it's level of functional GFP protein while growing can be taken as a measure of its ability to still synthesise significant levels of functional proteins.

As shown in Figure 30 Panels A,B, and Figure 33 Panel A levels of GFP in intoxicated cells are maintained at comparable levels to target cells not in contact with inhibitor cells. This shows that sufficient protein synthetic capacity must be present in the cell to allow synthesis of enough new GFP molecules to counteract the loss of fluorescence signal from the reasons detailed above. Indeed in some intoxicated cells, see Figure 30 Panel B, it can be seen that even
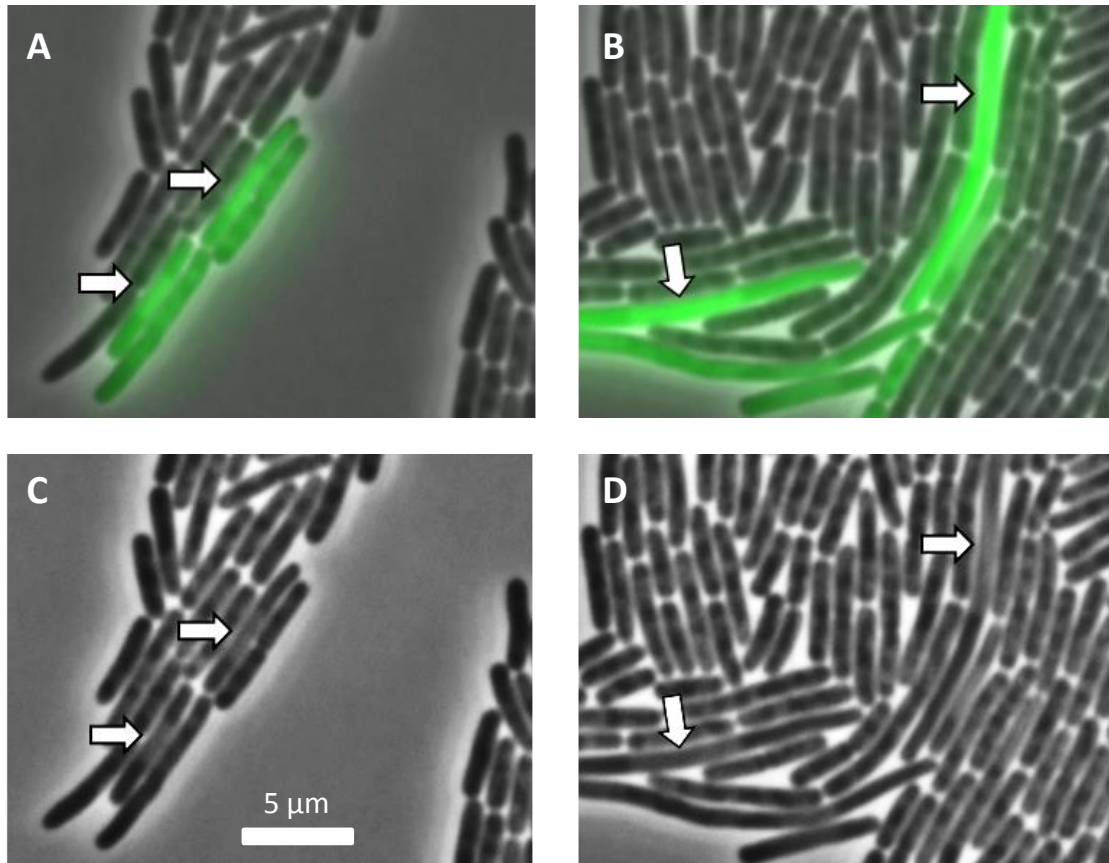
Figure 30: EC869 o11 toxin induced changes in phase contrast density of K12 F+ cells
Panels show the following time points, 18 min post contact, (A,C) and 87 min post contact (B,D). GFP fluorescence signal (Green = K12 F+ cell) overlayed on phase contrast image (A,B), phase contrast image only (C,D). White arrows indicate location of the same K12 F+ cells across the two frames.

higher levels of GFP production have occurred as the fluorescent signal from those cells has increased compared to uninhibited cells. As discussed above this is not due to a slower growth rate on intoxication as within the time course of the experiment growth rates are comparable. These higher rates of protein expression may be due to the failure of the normal regulation mechanisms present in *E. coli* cells due to DNA damage caused by the EC869o11 toxin.

6.2.2   Toxin action appears to be irreversible

For all of the cells that were observed in the two biological replicates on no occasion was a return to normal growth rates or septation of elongated cells of any kind either erroneously or to normal cell sizes seen. It should be noted that due to the rapid nature of inhibition and the growth of long cells with no division there were fewer occasions when cells broke contact than in the EC93 experiments. This is because as cells fail to divide some area of the cell membrane will remain in contact with inhibitor cells. In addition in the monolayer situation enforced in this experimental set up the very long cells act as a barrier preventing contact of inhibitor cells with the remaining cells of the microcolony behind it.

6.3   Effect of EC869o11 nuclease expression on nucleoid

During growth analysis of the EC869o11 toxin system it became apparent that the light / dark patterning of cells present in phase contrast images of *E. coli* monolayers, first noted in the EC93 experiments in Chapter 4, was different in intoxicated target cells. This was investigated further as the patterning correlated with cell growth in a manner suggesting it was related to genome replication, which was supported by it being perturbed by the action of a known nuclease toxin.

Patterning in microcolony phase images correlates with predicted nucleoid positions

During cell growth *E. coli* must replicate and segregate the nucleoid material of the mother and daughter cells. While prokaryotes do not have a nuclear envelope segregating their DNA from the cytoplasm the DNA is sufficently closely associated with itself for their to be a significant difference in density between the nucleoid and cytoplasm even in the absence of a defined physical barrier. This density difference has been exploited in the historic (Mason et al., 1956) and modern (Wang et al., 2005) literature to visualise nucleoid positions by embedding cells in a high percentage gelatin matrix. Using a media that more closely matches the cytoplasmic density allows more subtle changes in refractive index to be visualised. In the case of positive phase contrast microscopy this gives a cell image in which the higher density cytoplasm (Eltsov et al., 2006) is dark with the nucleoid visible as a lower density lighter, white region.

Whilst other techniques reliant on manipulating the density of the environment of single cells have been reported (Kellenberger et al., 1994; Valkenburg et al., 1984) an extensive literature search failed to find any mention of the phenomena described above in cell monolayers grown on standard media allowing full microcolony growth. As can be seen in Figure 31 individual cells are initially completely black as they grow (Panels A,B). As small microcolonies form the fact that cells are growing closely together starts to change the density gradient surrounding cells, and patterning starts to emerge (Panel C). As larger microcolonies form it can be seen that the majority of cells show patterning and that as they grow this patterning correlates with the position that is predicted for nucleoid positions at a given stage of bacterial cell division (Panels D,E and F). That is immediately after cell division there is a centrally located nucleiod that then grows as replication occurs, with the two genomes segregated to the proto mother and daughter regions of the cytoplasm prior to septation generating two separate cells.

6.3.1 Abnormal nucleoid morphology apparent in intoxicated cells in phase images

The regular patterning noted in the previous section was clearly altered when target cells came into contact with cells expressing the EC869o11 CdiA molecule. After initial contact had occurred between inhibitor and target cells the nucleoid remained in a central position as the cell grew showing no signs of separation of the two genomes, see Figure 32 Panel B. No K12 F+cells which came into contact with EC869o11 toxin were observed to divide or have a normal nuclear morphology with nucleoids adopting an unusual 'squared off' morphology and maintaining their central position within the cell, whilst increasing in size. In contrast a K12 F+ cell growing normally prior to division, see Figure 32A, can be seen to have two well separated nucleoids with a clear region of cytoplasm in between. Target cells affected by the EC93 toxin, either before or after growth arrest, did not show a significant difference in nucleoid morphology from that of unaffected target cells. Analysis in ImageJ of transects across targets cells growing normally and cells growing while intoxicated, see Figure 32 show that the phase image can be analysed to highlight nucleoid location.

6.3.2 Determination of suitable observation parameters for nucleoid visualisation by DAPI in live cells

While the phase images were strongly indicative of an effect on nucleoid morphology use of a DNA specific stain would provide conclusive proof that this was occurring. DAPI is a widely used nuclear stain for both prokaryotes and eukaryotes which shows a 20 fold increase in fluoresence on binding to double stranded DNA. It has been previously reported (Fishov et al., 1999; Bakshi et al., 2014) that in *E. coli* that viable cells will take up sufficient dye for imaging without any permeabilisation of cell membranes being required. As the dye had not been used
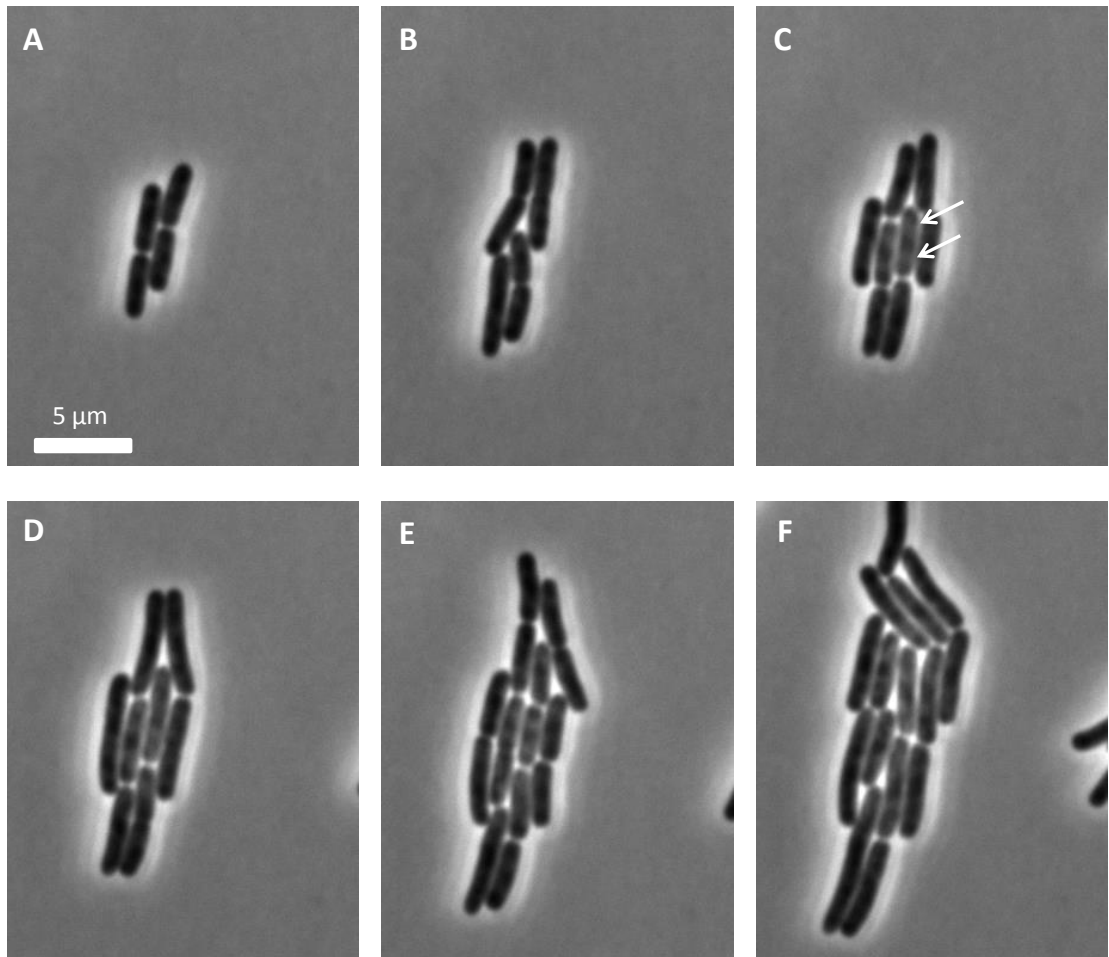
Figure 31: Phase contrast imaging of K12 F+ *E. coli* shows patterning inside cells as microcolony growth occurs

Panels show the growth of a single microcolony of K12 F+ *E. coli* cells over time, bacterial cells during initial growth periods (A, B), emergence of patterning indicated by white arrows (C), continuation of patterning of cells in interior of microcolony over time (D, E, F) .

A
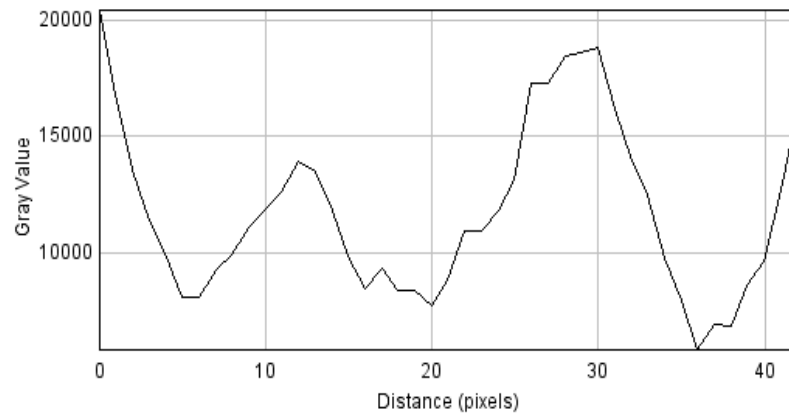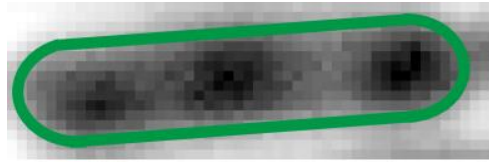
B
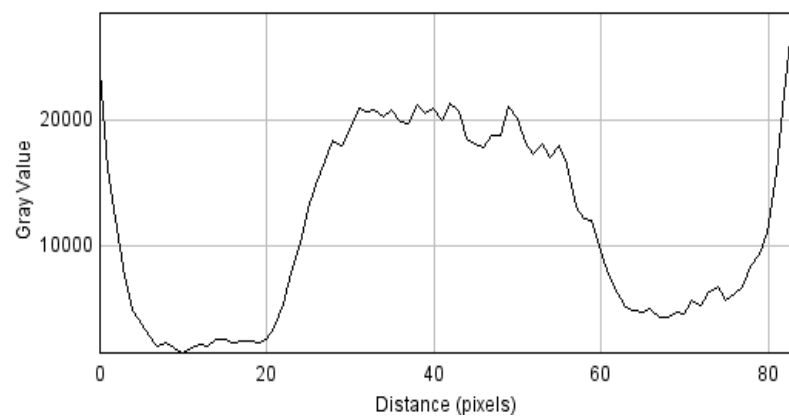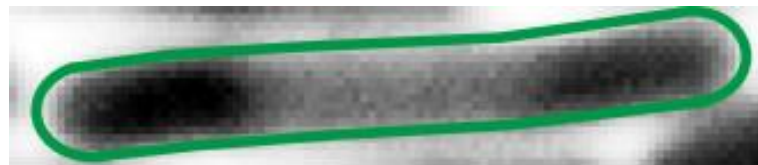
Figure 32: Identification of nucleoid position by plotting grayscale values

Comparison of phase contrast patterning of K12 F+ *E. coli* under the following conditions : A : K12 F+ no contact with EC869o11 expressing cells B : K12 F+ contact with EC869o11 expressing cells. Histograms show midline plot profile of grayscale image.

previously in this lab / protocol its cytotoxicity and photoxicity needed to be assessed.

Sufficiently high levels of DAPI have cytotoxic effects which can lead to a reduction or complete arrest of cell growth. At what concentration this cytotoxic effect occurs was assessed by growing bacteria on pads across a 20 fold range of concentrations, 0.1-2μg/μl, on agarose pads. Suitable concentrations were deemed to be those which cells grew at comparable rates to cells on media only pads. This work identified that the range 0.1-0.25μg/μl, was suitable with regards to its cytotoxic effects.

Phototoxic effects can occur during live cell fluoresence microscopy due to the excitation light required for visualisation of fluorophores. In the case of the DAPI fluorophore, excitation requires light in the region of 358nm which is sufficently high energy that it can readily reduce cell viability. A balance of sufficent illumination power to obtain sufficent image signal over background noise versus minimising potentially damaging light flux through the sample.

Technical advice from the Dept of Biology Technology Facility from experience working with eukaryotic organisms was that lower levels of illumination over longer periods of time are much better tolerated than the equivalent total light flux over shorter time periods. However with live cell imaging there can be a limit to the possible exposure time due to movement of cells during acquistion, leading to smearing in the resultant image, which results in a significant loss of resolution. In the case of *E. coli* growing under these conditions this time equates to 125mseconds based on previous fluorescent protein analysis before cell movement becomes too excessive.

This exposure time was then used as a basis for assessing the effects of different exctiation light levels on cells growing on pads which contained 0.1-0.25μg/μl DAPI concentrations which had been shown not to be cytotoxic. A suitable illumination protocol was defined as one which captured the natural state of the nucleiod and for which normal cell growth had occured up to that point. It was found that higher levels of DAPI lead to increased background signal without a significant increase in nucleoid specific signal so the lowest level of DAPI, 0.1μg/μl was used so as to minimise any possibly more subtle effects on cell physiology. During this process it was noted that even when using the lowest light levels spread over the longest practical time period there was a significant difference in DAPI signal from the nucleoid between the first 'naive' image and a second image taken immediately afterwards. Exposure to imaging light induces an apparent 'contraction' of the nucleoid DAPI signal with a highly patterned appearance resulting on subsequent exposures. Recovery of the nucleoid to a normal state was not observed in the time course followed, 15 minutes, and cell growth rate was drastically reduced / arrested even using minimal illumination levels. Higher illumination levels for shorter time periods where also trialled with similar effects on nucleoid state and cell growth being seen.

As using the gentlest possible imaging parameters for this experimental setup induced

significant changes in cell growth rate and nucleoid state it was decided to proceed with end point imaging using DAPI rather than following growth over time as a timelapse.

6.3.3   EC869o11 induced changes in phase images correlate with DNA location

Using the protocol defined in the previous section the interaction of target and inhibitor cells was followed in the presence of 0.1μg/μl DAPI. After incubation had continued for 3 hours, sufficient time for separate microcolonies of inhibitor and target cells to grow together and interact, DAPI imaging was performed as the end point of the experiment for the reasons discussed in the previous section.

As was previously observed in timelapse experiments elongated target cells in contact with inhibitor cells had formed with a central pale region visible in phase images, see Figure 33 Panel B. This shows that the presence of DAPI in the agarose pads has not affected the ability of the EC869o11 toxin to inhibit target cells. Examining the Ph/DAPI image, Panel A, it can be seen that no inhibitor cells had signs of unusual nucleoid morphology showing that this concentration of DAPI has not affected their growth. All target cells that have been in contact with inhibitor cells for a significant period of time show an enlarged nucleoid, as seen in DAPI channel, which increases in size the longer the intoxicated cell has grown.

That the DAPI signal corresponds to a high degree with the pale areas of the phase image, in particular for the higher contrast situation where target cells show abnormal nucleoid morphology, is confirmation that the phase patterning is indeed due to the position of the nucleiod and not other cellular factors / imaging artefacts.

6.4   Conclusion and Discussion

This work has shown that the EC869o11 system acts to disrupt the normal cellular division process leading to cells that are extremely elongated and incapable of nucleoid division. This disruption is presumably due to the inability of the normal cellular DNA repair processes to cope with the extent of DNA damage caused by the presence of constitutive DNAase activity in the cytoplasm. This would in turn lead to arrest of normal cellular processes related to growth and division by standard cellular checkpoints. That no segregation of nucleoids is seen in the extended cell indicates a failure of the normal seperation systems as might be expected with multiple double stranded breaks. It does however appear that DNA synthesis continues as the nucleoid region expands over time, although as the fluorescent signal is not linear this could be wholly or partly attributable to increased diffusion of the nucleoid over time. This can be also be seen with the lack of septation leading to anomalously long cells which would be predicted to be due to the action of SlnA blocking the initiation of septation due to the presence of the central nucleoid.
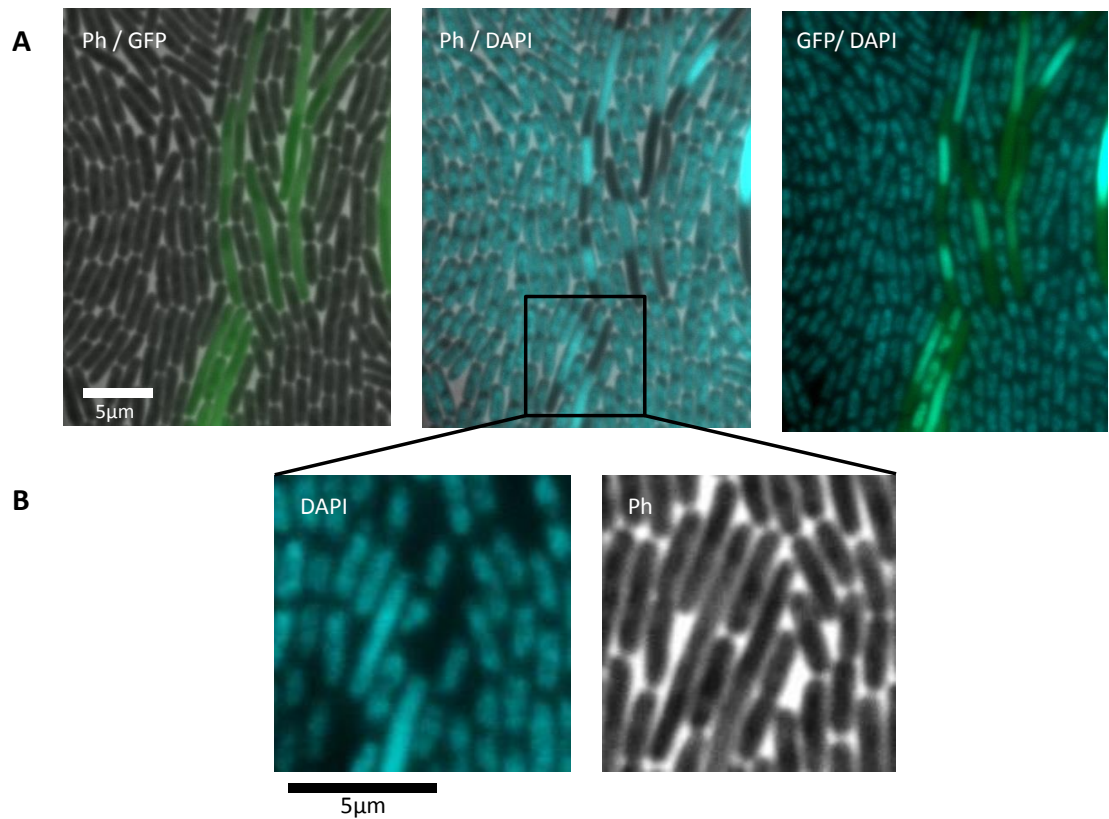
Figure 33: Comparison of phase contrast patterning of *E. coli* cells

Panels labeled to indicate imaging modalities used Ph = Phase contrast, GFP = Fluorescence signal from GFP, DAPI = Fluorescence signal from DAPI A : Comparison of same field of view with different pairings of imaging modalities, B : Zoomed view of indicated region to aid comparison of DAPI and phase contrast images K12 F+ cells shown in green (GFP), EC869o11 CDI toxin expressing cells only visible in phase contrast and DAPI views.

That cells are capable of growing, at least over the first several hours, in the presence of DNA damage indicates that the normal cellular machinery for biosynthesis (peptidoglycan, lipids etc.) and energy generation are broadly intact. This is confirmed by the ability of intoxicated cells to maintain levels of GFP expression that are at least a match for those seen in unaffected target cells.

Target cells exposed to EC869o11 toxin do not show a decrease in growth rate, at least within the time course of this experiment, a finding which is in apparent contradiction to the 'inhibition of growth' portion of the CDI systems definition. However while the intoxicated cells are not seen to stop growth within the time course of the experiment they are clearly destined to be non viable over longer time periods as the levels of DNA damage / abnormal nucleoid morphology are inconsistent with a cell capable of reproducing itself. Final growth halt will presumably occur when insufficient genetic material remains for essential cell components to be renewed and/or malformed / truncated cellular products are produced which 'poison' the cell. It should be noted that abnormally long *E. coli* cells can be viable under certain situations, (El-Hajj et al., 2015; Justice et al., 2004) , but in those cases at least part of the filamentous bacteria contains correctly segregated intact nucleoids.

This situation contrasts to the population level observations on growth rate made from planktonic studies were two factors are likely to result in a more pronounced effect. Firstly that multiple rapid contacts with inhibitor cells will be possible in this situation and secondly that in a freely mixed solution all target cells are available for contact with inhibitor cells. This should result in high levels of toxin delivered to all cells in the culture and hence a more pronounced effect. Images of target cells incubated for 6 hours planktonically shown in (Morse et al., 2012) show elongated cells which are either anucleate or show only a small DAPI signal compared to uninhibited cells. The measurement of growth in this case is the ability to form colonies rather than the growth of cells at the time of incubation.

It should also be noted that loss of nucleoids from cells due to the action of CDI toxin has been observed in contexts unrelated to the action of nucleases. It was shown for the EC93 CDI system that induction of toxin activity intracellularly lead to generation of a population of cells which were anucleate (Aoki et al., 2009). In this case the abnormal morphology is presumably due to the loss of Δpmf as a result of EC93 CDI activity, leading to errant septation which generates the anucleate cells.

Being able to probe anomalous nucleoid structure at the single cell level provides a very sensitive probe of EC869o11 CDI toxin effects. As the toxin has a rapid irreversible effect, see previous sections, it can be thought of as acting as a more sensitive probe for any non contact meditated effects of CDI. As an absolute contact dependence has now been demonstrated for two CDI toxins with different toxin activities it is likely that this characteristic will be present throughout the CDI family.

The ability to observe the EC869 toxin effects at the single level has enabled the time course of inhibition to be followed for the first time and shown that it has a much more rapid effect than that seen with the EC93 toxin and one which is not reversible. In this case the bulk scale growth inhibition is not linked to a straight forward arrest of cell growth due to lack of energy as seen for EC93 but to a diversion of cells into a non viable pathway where growth can continue for significant periods of time but without the capability for cellular division.

The cosmid based system used for this work is a good mimic for the natural system in that the cosmid is maintained as a single copy per cell with the chimeric CDI operon present in only a single copy as would be found when present in the genome. In addition the expression of the CDI proteins is driven from natural operators which taken together should lead to a level of CDI expression which is relevant to growth in the natural environment.

Chapter 7

Discussion

7.1 Introduction

This discussion will give an overview of the findings presented in this thesis and how the conclusions drawn from this work contribute to the model of our understanding of CDI. The results of the biofilm work and then the single cell level data will be set in the context of previous work. Implications for our understanding of the role of CDI in natural systems will then be discussed. Finally, conclusions on the state of our model of CDI toxin action in light of these results and suggestions for future work in this area will be made.

7.2 Effect of the EC93 CDI toxin system on growth within a biofilm

Initial expectations of the effect of the EC93 CDI system were that it might allow a strain expressing the system to out compete other strains due to the growth inhibition mediated by toxin expression. During the course of experimental work to test this hypothesis it became apparent that expression of the EC93 CDI system had a significant ability to increase the rate of biofilm formation. These two different aspects are discussed below.

7.2.1 Effect of toxin on biofilm competition

The work shown in Chapter 5 demonstrates that the presence of the EC93 CDI toxin when cells are grown co-seeded gives a significant competitive advantage to CDI inhibitor cells growing in the context of a biofilm. Such a strong impact of CDI on competitive fitness shows that sufficient contact must be occurring between K12 F+ cells and EC93 wild type cells so that an effective dose of toxin is delivered.

However it is known from planktonic studies that contact alone is not sufficient, the EC93 wild type cells must also be in log phase for growth inhibition to occur, although the factors driving this requirement are not understood. That inhibition occurs within biofilms, which are generally seen to be a nutrient limited environment supporting slower growth, indicates

that log phase growth may not be a requirement in this situation. It is possible that the state of growth of EC93 wild type cells in biofilms is such that, while the absolute growth rate is lower, sufficient cells in the biofilm are in an exponential, log like, growth phase for EC93 CDI toxin to be effective.

If a state analogous to planktonic log phase growth is not occurring in the biofilms then other factors inherent to biofilm growth are presumably compensating to allow efficient inhibition. One candidate difference would be the marked increase in exposure time to CDI toxin expressing cells due to the sessile nature of biofilm communities. An alternative explanation is that there could be a difference in the susceptibility to CDI toxin when K12 F+ cells are growing in a biofilm, although the ability of log phase EC93 wild type cells to inhibit K12 cells independent of their growth phase (Aoki et al., 2005) would argue that this was not a significant factor. However multiple additional changes to the way that bacterial cells are growing occur in biofilms, which mean that the situation is not exactly analogous to similar growth rates in planktonic culture and so a difference in susceptibility cannot be completely ruled out. This could be tested further by flow-cell experiments at lower temperatures / using less amenable C-sources , e.g. glycerol, to see if EC93 CDI toxin remained effective, this would also be informative as to which environmental niches CDI could be relevant in.

Due to the doubling increase in bacterial numbers as they grow by binary fission even a small impact on growth rate / growth halt for a subset of the population early in the colonisation process can be sufficient to lead to a significant growth advantage for the competing strain. Combined with the known competition / stratification effects of biofilm formation due to the generation of nutrient gradients which have been shown in model and experimental systems to be able to lead to domination of environments once a certain level of overgrowth has occurred (Lardon et al., 2011). It is also possible that initial shedding / tumbling behavior (Anderson et al., 2007) as the mixed strain biofilm is forming could lead to increased opportunities for inter-strain contacts. This could be further investigated by phase contrast video acquisition at earlier stages of biofilm formation, which was shown to be successful at observing shed cells free in solution / rolling cells interacting with the biofilm surface at the mature stage of biofilm formation. Such a mechanism of interactions might also be expected to lead to a gradient in competitive effectiveness across the length of the flow cell, as the nearer to the outlet the higher the level of tumbling cells would be expected to be from the greater area of cells available upstream, no such gradient was observed in this work. Which suggest that the effect is not significant or that rolling interactions are occurring only over relatively short distances.

On the basis that previous work has shown that target cell surface structures, pili (Aoki et al., 2005) and capsule (Aoki et al., 2008), are protective against the action of CDI it would not have been unexpected for the biofilm matrix to interfere with the action of CDI. That matrix ex-

pression has not inhibited CDI toxin action could be due to a number of factors, firstly that the expression of capsule components, shown previously to reduce CDI's effectiveness (Aoki et al., 2008) is down regulated within biofilms (Beloin et al., 2008). Due to its lack of cell attachment the biofilm matrix represents a more fluid barrier (Houry et al., 2012) between cells compared to the more closely tethered capsule components. There is also recent evidence to support phase separation of matrix and cells acting to drive cells to cluster preferentially (Ghosh et al., 2015). Finally there will also be a difference in the dynamics of interactions between cells free in solution that would not be able to generate significant forces against adjacent cells without sliding past. In contrast when growing in the more constrained environment of a biofilm a greater potential for forces between cells exists.

CDI molecules are large and potentially extend from the cell surface a sufficient distance to aid overcoming barriers of steric hindrance. Whilst the only structure available for CDI proteins (Morse et al., 2012; Beck et al., 2014a) are for the C-terminal toxin tip alone it is possible to make size estimates on the basis of structural homology. The structure of the homologous filamentous haemaglutin (FHA) protein has been determined with this 220kDa rod like protein having a length of 50nm. Given the known mass range 180-650kDa of CdiA molecules a length estimate of 40-150nm can be made based on the naive assumptions of a linear size length relationship and that the molecules behave as rigid rods projecting directly from the cell surface . These sizes are significantly smaller than the 1000nm length scales of pili and capsule, including Type I pili which does not affect EC93 CDI toxins effectiveness (Mulvey, 2002). Taken together these calculations / observations suggest both that CDI molecules are not long enough to 'reach past' / through blocking structures such as capsule and that steric interference isn't solely responsible for how these structures affect CDI effectiveness (Aoki et al., 2005).

Secondly the timing of interactions may occur before levels of matrix expression in the biofilm are significant enough to interfere with CDI have formed. The preliminary time-lapse confocal microscopy data indicates that this may explain part of the effect, with initial of target cell growth halted at the point of micro-colony interaction, with little evidence of cell growth at later dates. If shorter range rolling interactions are occurring they could act to increase the rate of potential interactions over those that would occur through microcolony growth alone. Given the potential reversibility of the EC93 toxin action it would be expected that continued inhibition and hence contact would be required to prevent regrowth. The lack of such escape indicates that even at later stages of biofilm growth with significant matrix levels contact between cells is still occurring.

7.2.2   EC93 CDI system aids the formation of biofilms

Constitutive expression of the EC93 CDI system led to an increase in the rate of biofilm formation but not in overall levels of biofilm formation compared to K12 F+ cells, as illustrated in Figure 34, even in the absence of the CDI toxin tip. This significant increase in the rate of biofilm formation confers a large competitive advantage independent of toxin activity

The increased ability to form biofilms has been shown to be dependent solely on the presence of the conserved region of the CdiA molecule by comparing the levels of biofilm growth between wild type and CdiA-CT deletion mutants. This region could either act as an auto-adhesin or bind to a different partner molecule on the partner cell. So expression of CDI could lead either to recruitment specifically of cells expressing CDI or a more general population of cells dependent on which option is correct. Work performed by Zachary Ruhe (personnel communication) has shown that adhesion is not dependent on the BamA molecule in planktonic systems but that does not rule out that an unidentified surface target for adhesion exists or that situation could be different in biofilms. Additional information on the nature of how the EC93 CDI system increases the rate of biofilm formation can be seen in differences in cell packing. Close packing of cells was noted more commonly in parts of the biofilm with cells expressing the conserved region of CdiA, compared to the less dense more uniform cell packing seen with *E. coli* K12 F+ Figure 20. Though in a few rare cases towers composed almost completely of inhibitor cells with a covering of target cells were seen this was the exception. In contrast FACS analysis of CDI cells has shown an association between target and inhibitor cells which would support an interaction between different molecules.

The finding that the EC93 toxin system was capable of acting to increase the rate of biofilm formation occurred in my work at the same time as the first published reports of a similar behavior in Burkholderia systems (Garcia et al., 2013). In contrast to my findings in *E. coli* it is reported that *Burkholderia* biofilms show a structural change in their biofilms when CDI systems are expressed, with an increase in clonal 'tower' formation being seen as well as a competitive advantage.

The differences that are seen between the two systems may relate to the level of CDI expression, with the *Burkholderia* systems being thought to be restricted to a subset of cells within a biofilm while the EC93 strain has constitutive expression throughout all the cells of the biofilm. Although given the systems are in different species the inherent differences in biofilm formation must be also be born in mind. In addition the data reported for the *Burkholderi*a systems to date is for colony 'biofilms' or static biofilms in contrast to the flow cell work reported in this thesis, meaning that the different nutrient / flow conditions could also account for differences.

Intercellular adhesion is a factor which could potentially alter the effectiveness of toxin delivery, by increasing the time cells are in contact, and was considered as a possible explanation for the discrepancy in effectiveness in planktonic culture between *E. coli* CDI and T6SS
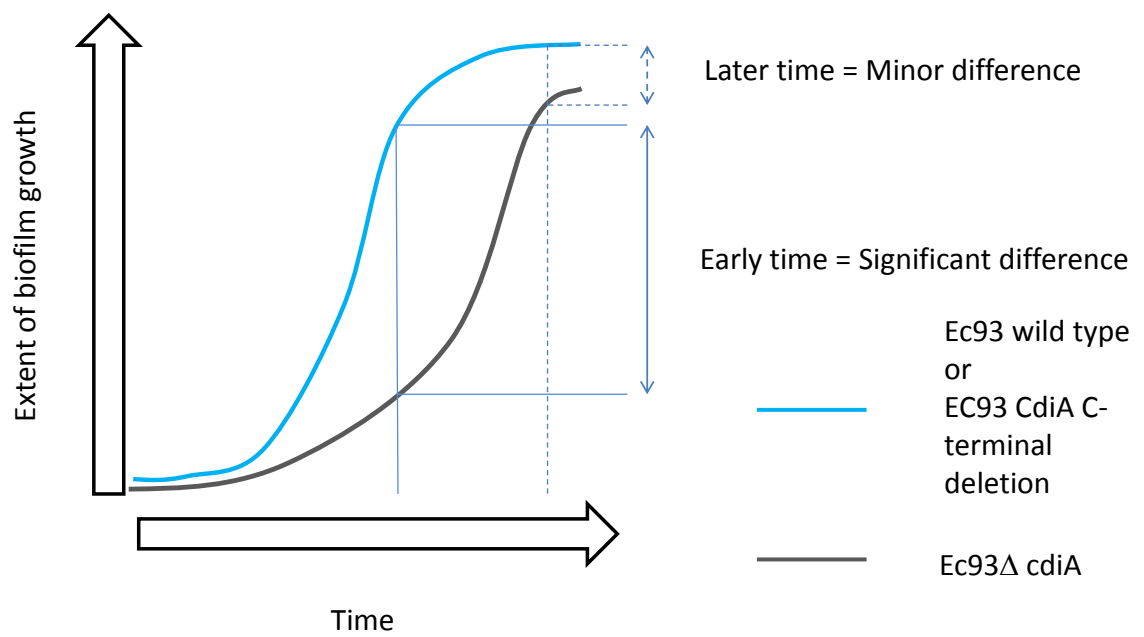
Figure 34: EC93 CDI system aids biofilm formation

Schematic illustrating the time dependent difference between levels of biofilm formation of EC93 wildtype / EC93 CdiA C-terminal deletion (blue) or EC93 ΔcdiA (black) single strain biofilms.

which are effective and inactive respectively. In this case the model would be that intercellular adhesion stabilised what would otherwise be transient interactions, in the freely mixed environment of planktonic culture, leading to more effective toxin interactions. However the fact that *Burkholderia* CDI systems show increased adhesion but are not effective in competition in planktonic culture argues against this interpretation.

7.3 Different toxin modes of action lead to a range of inhibition phenotypes at the single cell level

One of the key questions raised by the wide range of toxin types is how does this impact on their ability to affect target cells and if there are significant differences in action how would they impact on ecologically relevant situations such as competition during colonisation of new surfaces. In order to determine this detail studies at the single cell level are required as only then can the levels of toxin delivery be determined and the outcome of target inhibitor interactions be followed over time rather than being sampled as an end point result.

7.3.1 Time course of growth inhibition

There is a marked difference seen between the time course of effects on the EC93 and EC869o11 toxins over the period which can be studied by the techniques used in this study. The EC93 toxin has a significant delay in action before growth inhibition of the intoxicated cell occurs while in comparison the EC869o11 toxin induces an abnormal nucleoid morphology more rapidly but did not show growth arrest during the time course of the experiment. This is a novel observation as all previous work has been conducted using assays reporting at the population level and/or in experiments were the levels and timing of toxin delivery cannot be monitored.

7.3.2 Reversibility of toxin action

The action of toxins can be classified as irreversible, e.g. colicin, one hit one kill paradigm (Johnson et al., 2013), or reversible as indicated by the work of (Aoki et al., 2009) on the EC93 CDI toxin using inducible degradation of CdiI to study cytoplasmic self intoxication.

The work in this thesis demonstrates for the first time that the action of the EC93 toxin is reversible under natural conditions where toxin is delivered through the normal transport pathways and recovery occurs without the presence of cognate CdiI molecules being present in the affected cells cytoplasm. It also indicates that reversibility is not a characteristic of all CDI toxins as no recovery from inhibition was seen for the EC869o11 toxin. This difference is presumably due to the nature of the toxin action, DNA damage vs membrane potential. DNA damage where both strands have been destroyed by the action of a nuclease will be impossible to repair effectively as no template strand will exist, so even if the chromosome is ligated to

reform a circle information will be lost. In contrast reestablishment of pmf across the inner membrane is known to be possible.

The range of CDI toxin types could potentially effect a spectrum of phenotypes in target cells between, and possibly beyond, the extremes seen with the two tested at the single cell level to date. Differences in reversibility could lead to different outcomes when target cells are only transiently in contact with inhibitor cells for example when a low ratio of inhibitor cells are present in liquid culture or when expression of matrix leads to widely separated cells later in biofilm maturation.

It is interesting to note that the role of pmf in CDI toxin translocation as reported by Ruhe and colleagues (Ruhe et al., 2014) could presumably mean that the action of the EC93 toxin acts to block its own further import. As toxins partially imported and held in the periplasm appear competent for import, any return of the pmf could then act to continue inhibition. Alternatively as this role of pmf was tested using other toxin types and considering that AcrB is reported to only have a role in EC93 CDI import it may be that EC93 uses a pmf independent mechanism for import across the inner membrane than the other toxins and hence avoids interfering with its own import.

Further work on the nature of the EC93 toxin reversibility could look at the time over which recovery was possible by combining planktonic inhibition for various times with analysis at the single cell level on agarose pads to look at population levels of growth inhibition / recovery. This would allow target cells which have broken contact with inhibitor cells growth to be followed at the single cell level for longer time periods

7.3.3   Toxin induced changed in cell morphology

For both toxins it can be seen that the normal cellular processes that regulate cell size (Campos et al., 2014) are failing to operate. In the case of EC93 short, sometimes anucleate, cells are seen in autoinhibition planktonic culture (Aoki et al., 2009) with none of the highly elongated cells seen during agarose pads, which in turn did not show any sign of forming anucleate cells. Whilst for the EC869o11 toxin planktonic studies (Webb et al., 2013) showed that anucleate cells were generated, although interestingly not all of the population were so affected even though the level of growth inhibition was nearly total, whilst in the agarose pad assay gross changes in nucleoid morphology were induced but DNA levels in the cell were not significantly decreased as determined by DAPI signal and in fact showed some evidence of increasing.

In both cases the extent of disruption of cell morphology is different, generally less pronounced, than has been reported for cells inhibited planktonically. While the two dimensional experimental set up limits the number of potential contacts this is a quality that will carry over into interactions in the biofilm. This presumably represents the potential for a large number of interactions (particularly with the high inhibitor cell ratios used) between inhibitor and target

cells in free solution to deliver a higher dose of toxin molecules over a short time period, and additionally that any surface depletion of CdiA from one inhibitor cell is readily compensated for by interactions by other inhibitor cells in the culture.

This would tie in with the increased efficiency of intoxication when inhibitor cells lacking a cognate BamA molecule are used, which indicates that depletion of surface CdiA molecules can occur when expressed at natural levels. Hence the levels of toxin available for delivery and the amounts required to be effective in the target cell are not in excess / very low respectively and therefore modulations in these levels can be effective in altering outcomes of inhibition. Also in the case of the EC93 CDI toxin autoinhibition assay there is the potential effects from internal toxin expression.

A simple view of toxin action would suggest that the faster a toxin acts the more effective it would be in competition. However in environments with constrained spatial interactions it is possible that the kinetics of toxin action could act in non-intuitive ways were by a rapidly acting toxin induces a barrier of inhibited cells that block any further contact between inhibitor and target cells. An aspect of this behavior can be seen when contrasting the number of cells affected between the EC93 and EC869o11 single cell data, the rapid intoxication of target cells by EC869o11 inhibitors which go on to form very elongated cells means that there is less mixing than in the case of the slower acting EC869o11 cells. Modeling work to examine the range of effects would most probably require a 3D model due to the particular pattern formation inherent in a 2D constrained system (Rudge et al., 2012).

7.3.4 Comparison of single cell and planktonic analysis

Previous work in the literature has concentrated on planktonic assays with a read out of cfu/ml for cells recoverable after dilution plating out on agar plates. In addition the ratio of cells used is markedly different with a 10 fold or higher excess of inhibitor cells over target cells being used to obtain the quoted growth inhibition levels. This compares to the interactions studied at the single cell level where equal seeding levels were used, although it should be noted that as interactions occur on the level of single cells of adjoining microcolonies the macro cell ratio would not be expected to impact the initial hours of interaction prior to cell overgrowth.

The observation that complete inhibition of growth at the population level (as seen for e.g. with zones of clearance by colicins on lawns of susceptible cells) has not been reported for any CDI toxin to date indicates that some aspect of CDI's operation in this environment has not been fully characterised. This is in contrast to the observation that all cells in contact with inhibitor cells for a sufficient time, dependent on toxin type, go onto stop growth / become non viable.

It is difficult to envisage how such escape could occur in a well mixed environment as each cell would be exposed to multiple contacts, which FACS analysis suggests are relatively long

lived interactions. However it is possible that the assumption of a fully mixed environment is not true if some element of aggregation occurs, as is known for example with Ag43 (Woude, 2006). In this case aggregates of sufficient size would provide a 3D analogue to the border protective effect seen in the monolayer studies, whereby inhibited cells on the outside of the micro-colony block the ability of inhibitor cells to contact target cells on the inside which can therefore continue to grow. It would be interesting to study the impact of adhesin expression in planktonic cultures on susceptibility to CDI toxins.

Another explanation would be that escape from inhibition has occurred through chance lack of contact of a very few cells. In the case of EC93 this may be plausible but it does not account for the similar situation seen for the EC869o11 toxin which shows no sign of having a reversible action.

7.4 Role for CDI toxins in nature

From the first published report on CDI showing that showed commonly expressed surface structures could lead to marked reductions in the efficiency of CDI systems on target cells the question of how relevant such systems could be in nature was raised. The demonstration of the effectiveness of the EC93 CDI system in the context of biofilm growth extends the range of situations in which CDI systems could be relevant. Coupled with the evidence for markedly different outcomes of inhibition on surfaces dependent on the CDI toxin type expressed and it is possible to hypothesise that the different toxins could fulfill different ecological roles.

In the natural environment a range of competitive outcomes may be the most beneficial response for CDI expressing bacteria varying from complete domination of an environment to maintaining a 'wall' blocking overgrowth by neighboring cells. Having different options would allow the possibility for stable cooperation with neighbouring cells or avoiding lysis of competitors which would alert host immune systems during infections.

Three different hypothetical competition scenarios are shown in Figure 35, with the impact of different toxin types on outcomes illustrated. It is possible that more 'aggressive' CDI toxins such as EC869o11 which act more rapidly and are irreversible could allow expressing strains to act in the manner of the fast acting inhibitor cells (red, Panels A,B,C) while toxins such as Ec93 which are slower acting and reversible could act more akin to the slow acting inhibitor cells (yellow, Panels D,E,F). The absolute contact dependence of CDI systems is potentially an asset in engineering some of these situations in comparison to freely diffusible toxin systems. In either case the ratio of inhibitor to target cells, environmental conditions and spatial constraints are likely to also have a significant impact on outcomes.

The ability of bacteria to express a range of CdiI toxins combined with both the evidence for recombination of toxin tips in vivo and the effectiveness of artificially constructed chimeric

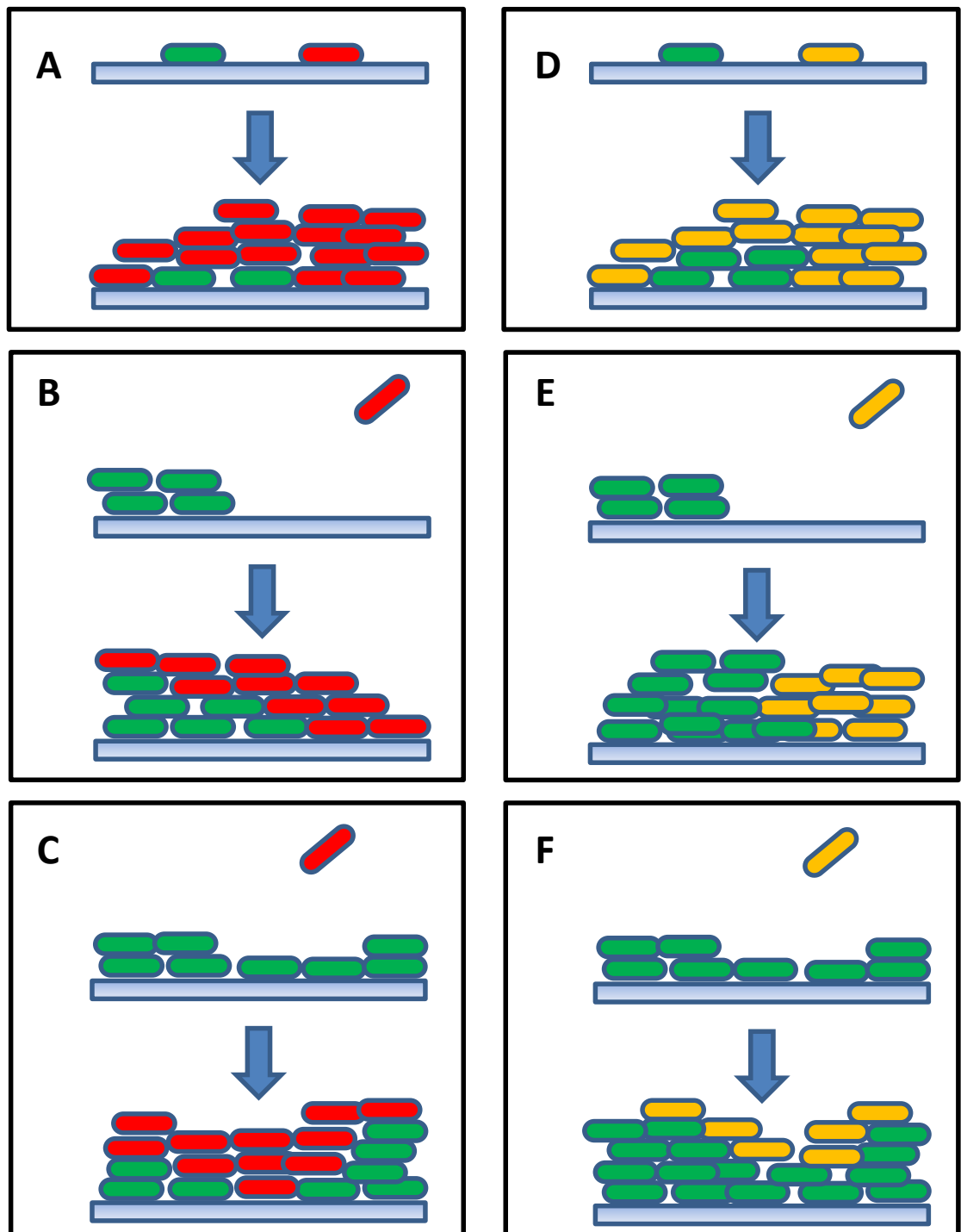**Figure 35: Scenarios illustrating different outcomes of competition caused by toxins acting at different rates**

Three different starting scenarios are shown: Coseeded strains (A,D), Invasion by inhibitor strain at microcolony growth stage (B,E) or biofilm growth stage (C,F). Target strains shown in green, fast acting inhibitor strains shown in red (A,B,C), slow acting inhibitor strains shown in orange (D,E,F).

CdiA molecules indicates that the competitive situation in nature may be quite complex with some strains being resistant to multiple toxins while also having the capability to generate additional diversity.

The situation in nature is likely to be even more complex as not only can strains express the CDI variants discussed above but the T6SS are another recent example of contact dependent toxins capable of affecting inter-bacterial competition.

CDI systems can be thought of as acting to demonstrate both kin and kind discrimination in a manner reminiscent of the so called 'green beard' genes (Strassmann et al., 2011; Ruhe et al., 2013b). The linking of toxin activity with aggregation provides a means for cells to screen recruitment of cells to a biofilm in two ways firstly the interaction between cells expressing CdiA which is a way to discriminate 'kind', similar but not necessarily directly related, while the toxin element allows discrimination again on the basis of 'kind' but on a much more restricted level with only those cells expressing the relevant cognate CdiI molecule. In both cases of selection, as the CDI allele is sufficient to confer 'recognition', kinship is not being recognised but practically in the environment the bulk of cells interacting in this way are likely to be the clonal kin mates of the interacting cell. As described previously this competitive environment will necessarily be limited to cells expressing

7.4.1 Alternate roles other than competition

It is possible that for some CDI systems, as has been proposed in some cases for antibiotics (Yim et al., 2007; Boehm et al., 2009), that rather than effecting domination of a niche they act in a subtler way to modulate other cells behavior. In particular the requirement of the UPEC536 toxin for the target cell to express the protein CysK (Diner et al., 2012) is hard to reconcile with an effective toxin action as escape of a population of cells could presumably be readily achieved by down regulating / losing the non essential protein.

As switching of toxin tips appears to occur in nature a situation reminiscent of that proposed for toxin-antitoxin systems induction of persistence could occur within an initially clonal population. In this scenario a cell undergoes a CDI toxin tip switching event that leaves it able to inhibit its surrounding clonemates as it is expressing a toxin which they are not immune too. In this way heterogeneity in cell state could be achieved in an initially uniform population.

7.5 Future work

In order to further investigate the hypothesis that the mode of action of CDI toxins leads to different outcomes in competition between bacteria the effect of EC869o11 toxin expression on competition within a biofilm could be studied. As this would allow comparison of both

single cell and biofilm population level data for two toxin types, thus enabling any impact of the different effects seen in mono-layers of cells on biofilm competition to be measured.

The effectiveness of the other classes of toxin for which functions are known could be analysed at the single cell level for representative examples of the rRNAase (ECL (Beck et al., 2014a)) and tRNAase (UPEC536 (Aoki et al., 2010)) classes of CDI toxin. Having a knowledge of the dynamics of a wider range of toxin types would aid in understanding the breadth of possible effects of CDI systems.

Use of computational modeling of bacterial interactions may aid better understanding of the implications of the variability of CDI toxins effects as experimental approaches are necessarily limited in the range of parameters that can be assessed in a practical manner.

It is interesting to note that the phenotype of EC869o11 inhibition visible in microscope images with DAPI staining is comparable to the action of DNA replication inhibitors such as Daunorubicin as seen in (Nonejuie et al., 2013). This suggests that it may be possible to apply the principal component analysis (PCA) of image approach outlined in the Nonejuie paper to broadly classify the effects of the many CDI toxin tips which do not show sequence homology to known proteins. In this way it maybe be possible to assign mechanisms of toxin action purely on single cell level image phenotypes.

7.6   Conclusion

This work has shown that the archetypal CDI toxin system of *E. coli* strain EC93 is effective when bacteria are growing in a biofilm and that the conserved portion of the EC93 CdiA molecule increases the rate of biofilm formation. The linkage of CDI toxin activity with an increased ability to form biofilms ensures that only closely related bacteria are able to benefit from growth within the biofilm. Single cell level analysis of the EC93 and EC869o11 CDI toxins has shown that different toxin mechanisms induce different inhibition phenoypes in suscep-tible cells. The time course of action and the degree to which the toxin action was reversible were both shown to be affected by the class of toxin. The discovery of this difference suggests that the class of CDI toxin could affect competition outcomes. Taken together these two main findings support a model in which CDI toxin systems could play a variety of different roles in interbacterial competition within biofilms.

Appendix A

Table of *E. coli* Strains used in this study

See Appendix B for further information on plasmids used in this study.

Name	Strain background	Plasmid	Source
DH5α	F$^-$ ϕ80*lac*ΔM15 Δ(*lac*ZYA-*arg*F)U169 *rec*A1 *end*A1 *hsd*R17(r$_k^-$,m$_k^+$) *pho*A *supE44 thi*-1 *gyr*A96 *rel*A1 λ^-		Invitrogen
MV487	XL-1 Blue	pMG32a	Lab stock
MV540	DL537	pMG35	Lab stock
MV784	MG1655		Lab stock
MV1008	MG1655		Lab stock
MV1085	PIR2		Lab stock
MV1213	K12 *attB*: *kan gfp*		(Da Re et al., 2007)
MV1219	K12 F+		(Da Re et al., 2007)
MV1257	MV1219	pZE21-gfp	(Lakins et al., 2009)
MV1393	MV1219	pmV356	(King, 2010)
MV1394	DL3852 EC93 wild type		(Aoki et al., 2005)
MV1395	DL5115 EC93 ΔcdiA (found to be hyper-motile)		(Aoki et al., 2005)
MV1396	DL6105 EC93 ΔcdiA-CT ΔcdiI		(Aoki et al., 2005)
MV1397	DL6173 EC93 ΔcdiA-CT$_{orphan}$ ΔcdiI$_{orphan}$		(Aoki et al., 2005)
MV1398	DL6174 EC93 ΔcdiA-CT ΔcdiI ΔcdiA-CT$_{orphan}$ ΔcdiI$_{orphan}$		(Aoki et al., 2005)
MV1406	MV1394	pZE21-gfp	This study

Name	Strain background	Plasmid	Source
MV1407	MV1396	pZE21-gfp	This study
MV1408	MV1397	pMV356	This study
MV1409	MV1397	pZE21-gfp	This study
MV1410	MV1398	pZE21-gfp	This study
MV1411	MV1085	pMV350	This study
MV1427	MV1394	pMV356	This study
MV1428	MV1395	pMV356	This study
MV1429	MV1395	pZE21-gfp	This study
MV1430	MV1394	pINT-ts	This study
MV1458	MV784	pKD46	This study
MV1459	MV1008	pKD46	This study
MV1460	MV1219	pKD46	This study
MV1461	MV1394	pKD46	This study
MV1462	MV1395	pKD46	This study
MV1463	MV784 *attB*: *kan gfp*		This study
MV1464	MV1219 *attB*: *kan gfp*		This study
MV1465	MV1395 *attB*: *kan gfp*		This study
MV1472	MV784	pMV370	This study
MV1474	DL5209 MG1655		Sanna Koskiniemi (unpublished)
MV1480	MV784 *attB*: *kan tdtomato*		This study
MV1481	MV784 *attB*: *kan tdtomato*		This study
MV1482	MV540 restreaked and new frozen stock layed down	pMG35	
MV1483	MV487 restreaked and new frozen stock layed down	pMG32a	This study
MV1484	MV1008	pmCherry	This study
MV1485	MV784	pMV371	This study
MV1486	MV784	pMV372	This study
MV1487	MV784	pMV373	This study
MV1488	MV784 *attB*: *kan mcherry*		This study
MV1489	MV784 *attB*: *kan cfp*		This study
MV1490	MV 784 *attB*: *kan yfp*		This study
MV1582	MV1219	pMV371	This study

Name	Strain background	Plasmid	Source
MV1583	MV1219	pMV372	This study
MV1584	MV1219	pMV373	This study
MV1585	MV1394	pZE21-gfp	This study
MV1586	MV1394	pMV371	This study
MV1587	MV1394	pMV372	This study
MV1588	MV1394	pMV373	This study
MV1589	MV1395	pZE21-gfp	This study
MV1590	MV1395	pMV371	This study
MV1591	MV1395	pMV372	This study
MV1592	MV1395	pMV373	This study
MV1594	M1398	pmCherry	This study
MV1595	MV1474	pCH9305	This study
MV1598	MV1474	pCH9305	This study
MV1599	MV1474	pCH10165	This study
MV1600	DH5α	pCH9305	This study
MV1601	DH5α	pCH10165	This study
MV1611	CH10094 EC93 ΔcdiA (not hypermotile)		Zachary Ruhe (unpublished)
MV1612	CH10060 Ec93 bamA (*S. enterica*)		Zachary Ruhe
MV1613	CH10024 Ec93 ΔcdiA-CT		Zachary Ruhe
MV1614	ZR60 Ec93 bamA (*S. enterica*) ΔcdiA		Zachary Ruhe
MV1617	MV784	pZE21-gfp	This study
MV1618	MV784	pMV371	This study
MV1619	MV1611	pZE21-gfp	This study
MV1620	MV1611	pMV371	This study
MV1621	MV1612	pZE21-gfp	This study
MV1622	MV1612	pMV371	This study
MV1623	MV1613	pZE21-gfp	This study
MV1624	Mv1613	pMV371	This study
MV1625	MV1614	pZE21-gfp	This study
MV1626	MV1614	pMV371	This study

Appendix B

Table of Plasmids used in this study

Antibiotic resistance confered by the plasmid is indicated in the AB^R column, were relevant primers used in the construction of the plasmid are indicated.

Name	AB^R	Parent plasmid	Description	Source
pZE21-gfp	Kan		Constitutive expression of GFP	(Da Re et al., 2007)
pInt-ts	Amp		CRIM helper plasmid λ - integrase, temperature sensitive	Hasan et al., 1994
pKD46	Amp		Helper plasmid λ-red, temperature sensitive	(Datsenko et al., 2000)
pMG35	Amp		Transcriptional fusion of *cfp* to *ompF*	(Batchelor et al., 2003)
pMG32a	Amp		Derived from pGFPmut3.1 (Clontech) with *yfp* replacing *gfp*	Mark Goulian (unpublished)
pmCherry	Amp		Constitutive mCherry expression	Clontech
pCH9305	Amp		EC93-EC869o11 chimera cosmid	(Morse et al., 2012)
pCH10165	Cm		EC93-EC869o11 D198A chimera cosmid	(Morse et al., 2012)
pMV285	Cm		Crim vector *gfp*	Sarah Broadbent
pMV350	Cm	pMV285	pMV285 with ptac promoter	MSc (King, 2010)
pMV356	Kan	pZE21-gfp	Constitutive expression of td-Tomato	MSc (King, 2010)

Name	AB^R	Parent plasmid	Description	Source
pMV370	Kan	pMV356	Constitutive expression of td-Tomato	This study
pMV371	Kan	pMV370	Constitutive expression of mCherry	This study
pMV372	Kan	pMV370	Constitutive expression of Cfp	This study
pMV373	Kan	pMV370	Constitutive expression of Yfp	This study

Appendix C

Table of Oligonucleotides used in this study

The direction of primers is indicated in the F/R column by the designation F - Forward or R - Reverse. Primers which were designed by other members of the van der Woude lab are shown with the lab members name.

Name	Sequence	F/R	Description
oMV393	CATCACCTTCACCCTCTCC	R	Sequence upstream of *gfp* (Goulian et al., 2006)
oMV429	GGCATCACGGCAATATAC		Screen CRIM integration, sequencing (Sarah Broadbent)
oMV430	ACTTAACGGCTGACATGG		Screen CRIM integration (Sarah Broadbent)
oMV432	TCTGGTCTGGTAGCAATG		Screen CRIM integration, sequencing (Sarah Broadbent)
oMV656	CTTGCGCTAATGCTCTGTTACAGG		Screen CRIM integration (Sarah Broadbent)
oMV931	ACGGATCCTCCCTATCAGTGATAGAGAT	F	Clone promoter and *gfp* from pZE21-gfp
oMV932	AGATGCATTTATTTGTATAGTTCATCCA	R	Clone promoter and *gfp* from pZE21-gfp
oMV933	ACGGATCCTCCCTATCAGTGATAGAGAT	F	Clone promoter and *td-tomato* from pMV356

Name	Sequence	F/R	Description
oMV934	AGATGCATTTACTTGTACAGCTCGTCCA	R	Clone promoter and *td-tomato* from pMV357
oMV935	TGTTCACAGGTTGCTCCGGG	F	Ampify *gfp* and pr promoter cassette from MV1213
oMV936	CGCAATGCCATCTGGTATCA	R	Amplify *gfp* and pr promoter cassette from MV1213
oMV939	TTGCTCCGGGCTATGAAATAGAAAAATGAATC CGTTGAAGACTAGTGCTTGGATTCTCACCA	F	Amplify cassette for λ red system from pZE21-gfp
oMV940	ATTAAAAACAACTTTTTGTCTTTTTACCTTCCC GTTTCGCCCTAGGTCTAGGGCGGCG GATTTGT	R	Amplify cassette for λ red system from pZE21-gfp
oMV941	ATAGGATCCCTTCCCAACCTTACCAGAGG	F	Clone promoter and *gfp* from MV1213 genome
oMV942	ACGATGCATGCTTATTTGTATAGTTCATCC	R	Clone promoter and *gfp* from MV1213 genome
oMV943	TGCGCTGACAGCCGGAACAC	F	Sequencing pZE21-gp plasmid
oMV944	TCTTTGATGACCTCCTCGCC		Sequencing upstream of *tdtomato*
oMV945	AAGGTACCGCATGGTGAGCAAGGGCGA	F	Amplify *mcherry* from pmcherry
oMV946	CAAAGCTTCTACTTGTACAGCTCGTC	R	Amplify *mcherry* from pmcherry
oMV947	AAGGTACCGCATGCGTAAAGGAGAAGAA	F	Amplify *yfp* from pMG32a / Amplify *cfp* from pMG35
oMV948	CAAAGCTTATTTGTATAGTTCATCCATGCC	R	Amplify *yfp* from pMG32a / Amplify *cfp* from pMG36

Appendix D

Final flow cell design

Final flowcell design for biofilm microscopy, designed in collaboration with Mark Bentley, diagram and fabrication by Mark Bentley.
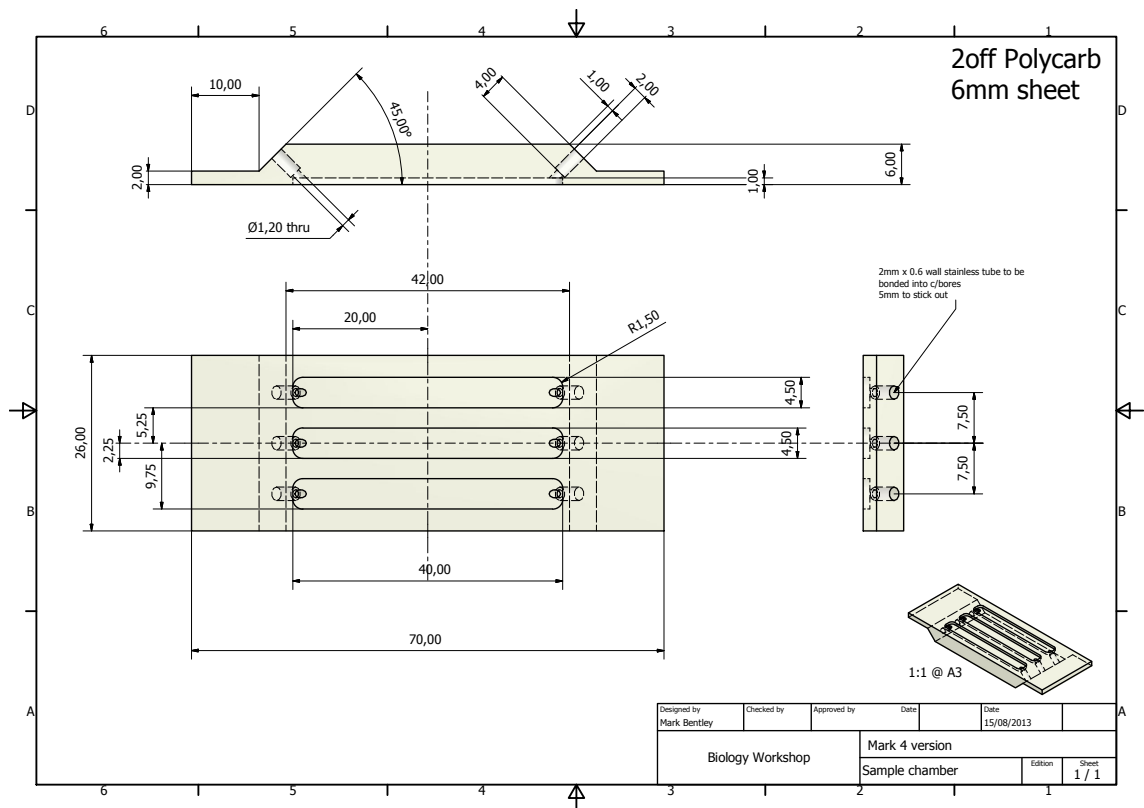
Abbreviations

A_{600}	Absorbance at 600nm
Amp	Ampicillin
CCD	Charge coupled device
CDI	Contact dependent inhibition of growth
CDI+	Strain expressing functional CDI toxin system
CDI-	Strain without functional CDI toxin system
cfu	Colony forming units
CFP	Cyan fluorescent protein
CLSM	Confocal scanning laser microscopy
Cm	Chloramphenicol
CRIM	Conditional-replication, integration and modular plasmid system
CT	C terminal
DAPI	4',6-Diamidino-2-Phenylindole
dH_2O	Deionised water
EB	Elution buffer
EHEC	Enterohemorrhagic *E. coli*
EPS	Extracellular polymeric substances
F+	Strain containing the F' plasmid
FACS	Fluorescent activated cell sorting
FHA	Filamentous haemaglutin protein
FISH	Fluorescent in sity hybridisation
GFP	Green fluorescent protein
GUI	Graphical user interface
H-NS	Histone-like nucleoid-structuring protein
Kan	Kanamycin
LAF	Laminar air flow
mCherry	Monomeric Cherry red fluorescent protein
OD_{600}	Optical density at 600nm
PCA	Principal component analysis
PCR	Polymerase chain reaction
Ph	Phase microscopy
pmf	Proton motive force
RT-PCR	Reverse transcriptase polymerase chain reaction
SIP	Sanitisation in place

T3SS	Type III secretion system
T4SS	Type IV secretion system
T5SS	Type V secretion system
T6SS	Type VI secretion system
tdTomato	Tandem dimer Tomato red fluorescent protein
TPS	Two partner secretion system
UHQ H$_2$O	Ultra high quality water
UPEC	Uropathogenic *E. coli*
UTI	Urinary tract infection
YFP	Yellow fluorescent protein

References

Adiciptaningrum, Aileen M, Ian C Blomfield, Sander J Tans (2009), Direct observation of type 1 fimbrial switching. *EMBO reports*, 10, 527–32.

Ali, Sabrina S, Bin Xia, Jun Liu, William Wiley Navarre (2012), Silencing of foreign DNA in bacteria, *Current Opinion in Microbiology*, 15, 175–181.

Alteri, Christopher J., Stephanie D. Himpsl, Shannon R. Pickens, Jonathon R. Lindner, Jonathan S. Zora, Jessa E. Miller, Peter D. Arno, Samuel W. Straight, Harry L. T. Mobley (2013), Multicellular Bacteria Deploy the Type VI Secretion System to Preemptively Strike Neighboring Cells, *PLoS Pathog*, 9, e1003608.

Anderson, Brett N, Albert M Ding, Lina M Nilsson, Kaoru Kusuma, Veronika Tchesnokova, Viola Vogel, Evgeni V Sokurenko, Wendy E Thomas (2007), Weak rolling adhesion enhances bacterial surface colonization. *Journal of bacteriology*, 189, 1794–802.

Anderson, Melissa S, Erin C Garcia, Peggy A Cotter (2012), The *Burkholderia bcpAIOB* Genes Define Unique Classes of Two-Partner Secretion and Contact Dependent Growth Inhibition Systems. *PLoS genetics*, 8, e1002877.

Anderson, Melissa S., Erin C. Garcia, Peggy A. Cotter (2014), Kind Discrimination and Competitive Exclusion Mediated by Contact-Dependent Growth Inhibition Systems Shape Biofilm Community Structure, *PLoS Pathog*, 10, e1004076.

Aoki, S K, J S Webb, B A Braaten, D A Low (2009), Contact-dependent growth inhibition causes reversible metabolic downregulation in *Escherichia coli*, *Journal of Bacteriology*, 191, 1777–86.

Aoki, Stephanie K, Rupinderjit Pamma, Aaron D Hernday, Jessica E Bickham, Bruce a Braaten, David a Low (2005), Contact-dependent inhibition of growth in *Escherichia coli. Science*, 309, 1245–8.

Aoki, Stephanie K, Juliana C Malinverni, Kyle Jacoby, Benjamin Thomas, Rupinderjit Pamma, Brooke N Trinh, Susan Remers, Julia Webb, Bruce A Braaten, Thomas J Silhavy, David A Low (2008), Contact-dependent growth inhibition requires the essential outer membrane protein BamA (YaeT) as the receptor and the inner membrane transport protein AcrB, *Molecular Microbiology*, 70, 323–340.

Aoki, Stephanie K, Elie J. Diner, Claire T'Kint de Roodenbeke, Brandt R. Burgess, Stephen J. Poole, Bruce A. Braaten, Allison M. Jones, Julia S. Webb, Christopher S. Hayes, Peggy A. Cotter, David A. Low (2010), A widespread family of polymorphic contact-dependent toxin delivery systems in bacteria, *Nature*, 468, 439–442.

Bakshi, Somenath, Heejun Choi, Nambirajan Rangarajan, Kenneth J. Barns, Benjamin P. Bratton, James C. Weisshaar (2014), Nonperturbative Imaging of Nucleoid Morphology in Live Bacterial Cells during an Antimicrobial Peptide Attack, *Applied and Environmental Microbiology*, 80, 4977–4986.

Batchelor, Eric, Mark Goulian (2003), Robustness and the cycle of phosphorylation and dephosphorylation in a two-component regulatory system. *Proceedings of the National Academy of Sciences of the United States of America*, 100, 691–6.

— (2006), Imaging OmpR localization in *Escherichia coli. Molecular microbiology*, 59, 1767–78.

Bates, Douglas, Martin Maechler, Ben Bolker, Steven Walker (2013), *lme4: Linear mixed-effects models using Eigen and S4.*

Beck, Christina M, Robert P Morse, David A Cunningham, Angelina Iniguez, David A Low, Celia W Goulding, Christopher S Hayes (2014a), CdiA from *Enterobacter cloacae* Delivers a Toxic Ribosomal RNase into Target Bacteria, *Structure (London, England: 1993)*, 22, 707–718.

Beck, Christina M., Elie J. Diner, Jeff J. Kim, David A. Low, Christopher S. Hayes (2014b), The F pilus mediates a novel pathway of CDI toxin import, *Molecular Microbiology*, 276–290.

Beloin, C, J Valle, P. Latour-Lambert, P Faure, M Kzreminski, D Balestrino, J.A.J. Haagensen, S. Molin, G. Prensier, B. Arbeille, Others (2004), Global impact of mature biofilm lifestyle on *Escherichia coli* K-12 gene expression, *Molecular microbiology*, 51, 659–674.

Beloin, C, A Roux, J Ghigo (2008), "*Escherichia coli* Biofilms", in: *Bacterial Biofilms, Microbiology and Immunology 322*, ed. by T. Romeo, Springer-Verlag Berlin Heidelberg, pp. 249–289.

Beloin, Christophe, Jean-Marc Ghigo (2005), Finding gene-expression patterns in bacterial biofilms. *Trends in microbiology*, 13, 16–9.

Beloin, Christophe, Kai Michaelis, Karin Lindner, Paolo Landini, Jörg Hacker, Jean-Marc Ghigo, Ulrich Dobrindt (2006), The Transcriptional Antiterminator RfaH Represses Biofilm Formation in *Escherichia coli*, *Journal of Bacteriology*, 188, 1316–1331.

Berg, H C, L Turner (1993), Torque generated by the flagellar motor of *Escherichia* coli. *Biophysical Journal*, 65, 2201–2216.

Boehm, Alex, Samuel Steiner, Franziska Zaehringer, Alain Casanova, Fabienne Hamburger, Daniel Ritz, Wolfgang Keck, Martin Ackermann, Tilman Schirmer, Urs Jenal (2009), Second messenger signalling governs *Escherichia coli* biofilm induction upon ribosomal stress. *Molecular microbiology*, 72, 1500–16.

Braun, Volkmar, Silke I Patzer, Klaus Hantke (2002), Ton-dependent colicins and microcins: modular design and evolution, *Biochimie*, 84, 365–380.

Braun, Volkmar, Silke I. Patzer (2013), Intercellular communication by related bacterial protein toxins: colicins, contact-dependent inhibitors, and proteins exported by the type VI secretion system, *FEMS Microbiology Letters*, 345, 13–21.

Campos, Manuel, Ivan Surovtsev, Setsu Kato, Ahmad Paintdakhi, Bruno Beltran, Sarah Ebmeier, Christine Jacobs-Wagner (2014), A Constant Size Extension Drives Bacterial Cell Size Homeostasis, *Cell*, 159, 1433–1446.

Cao, Bin, Paul D. Majors, Bulbul Ahmed, Ryan S. Renslow, Crystal P. Silvia, Liang Shi, Staffan Kjelleberg, Jim K. Fredrickson, Haluk Beyenal (2012), Biofilm shows spatially stratified metabolic responses to contaminant exposure, *Environmental Microbiology*, no–no.

Cascales, Eric, Susan K Buchanan, Denis Duché, Colin Kleanthous, Roland Lloubès, Kathleen Postle, Margaret Riley, Stephen Slatin, Danièle Cavard (2007), Colicin biology. *Microbiology and molecular biology reviews : MMBR*, 71, 158–229.

Ceri, H, M E Olson, C Stremick, R R Read, D W Morck, A G Buret (1999), The Calgary Biofilm Device: new technology for rapid determination of antibiotic susceptibilities in bacterial biofilms, *J. Clin. Microbiol.* 37, 1771–1776.

Chao, L., Bruce R Levin (1981), Structured Habitats and the Evolution of Anticompetitor Toxins in Bacteria, *Proceedings of the National Academy of Sciences*, 78, 6324–6328.

Chavez-Dozal, Alba, Clayton Gorman, Martina Erken, Peter D Steinberg, Diane McDougald, Michele K Nishiguchi (2013), Predation Response of *Vibrio fischeri* Biofilms to Bacterivorus Protists. *Applied and environmental microbiology*, 79, 553–8.

Choi, Heejun, Zhilin Yang, James C. Weisshaar (2015), Single-cell, real-time detection of oxidative stress induced in *Escherichia coli* by the antimicrobial peptide CM15, *Proceedings of the National Academy of Sciences*, 112, E303–E310.

Chung, C T, S L Niemela, R H Miller (1989), One-step preparation of competent *Escherichia coli*: transformation and storage of bacterial cells in the same solution. *Proceedings of the National Academy of Sciences of the United States of America*, 86, 2172–5.

Ciofu, Oana, Lotte F Mandsberg, Henzuang Wang, Niels Hø iby (2012), Phenotypes selected during chronic lung infection in cystic fibrosis patients: implications for the treatment of *Pseudomonas aeruginosa* biofilm infections. *FEMS immunology and medical microbiology*, 65, 215–25.

Claessen, Dennis, Daniel E. Rozen, Oscar P. Kuipers, Lotte Søgaard-Andersen, Gilles P. van Wezel (2014), Bacterial solutions to multicellularity: a tale of biofilms, filaments and fruiting bodies, *Nature Reviews Microbiology*, 12, 115–124.

Conibear, Tim C R, Samuel L Collins, Jeremy S Webb (2009), Role of mutation in *Pseudomonas aeruginosa* biofilm development. *PloS one*, 4, ed. by Angus Buckling, e6289.

Cormack, B P, R H Valdivia, S Falkow (1996), FACS-optimized mutants of the green fluorescent protein (GFP). *Gene*, 173, 33–8.

Costerton, J. W. (1999), Bacterial Biofilms: A Common Cause of Persistent Infections, *Science*, 284, 1318–1322.

Costerton, J W, Z Lewandowski, D E Caldwell, D R Korber, H M Lappin-Scott (1995), Microbial biofilms. *Annual review of microbiology*, 49, 711–45.

Costerton JW, Geesey GG, Cheng K-J (1978), How bacteria stick, *Scientific American*, 238, 86–95.

Cowan, T (2011), Biofilms and their management: from concept to clinical reality. *Journal of wound care*, 20, 220–30.

Croxen, Matthew A, B Brett Finlay (2010), Molecular mechanisms of *Escherichia coli* pathogenicity. *Nature reviews. Microbiology*, 8, 26–38.

Crusz, Shanika A, Roman Popat, Morten Theil Rybtke, Miguel Cámara, Michael Givskov, Tim Tolker-Nielsen, Stephen P Diggle, Paul Williams (2012), Bursting the bubble on bacterial biofilms: a flow cell methodology. *Biofouling*, 28, 835–42.

Da Re, Sandra, Jean-Marc Ghigo (2006), A CsgD-independent pathway for cellulose production and biofilm formation in *Escherichia* coli, *Journal of Bacteriology*, 188, 3073–3087.

Da Re, Sandra, Benjamin Le Quéré, Jean-Marc Ghigo, Christophe Beloin (2007), Tight modulation of *Escherichia coli* bacterial biofilm formation through controlled expression of adhesion factors. *Applied and Environmental Microbiology*, 73, 3391–403.

Danese, P N, L a Pratt, S L Dove, R Kolter (2000), The outer membrane protein, antigen 43, mediates cell-to-cell interactions within *Escherichia coli* biofilms. *Molecular microbiology*, 37, 424–32.

Datsenko, K A, B L Wanner (2000), One-step inactivation of chromosomal genes in *Escherichia coli* K-12 using PCR products. *Proceedings of the National Academy of Sciences of the United States of America*, 97, 6640–5.

Davies, D. G., M. R. Parsek, J. P. Pearson, B. H. Iglewski, J. W. Costerton, E P Greenberg (1998), The Involvement of Cell-to-Cell Signals in the Development of a Bacterial Biofilm, *Science*, 280, 295–298.

Dean, Paul (2011), Functional domains and motifs of bacterial type III effector proteins and their roles in infection, *FEMS microbiology reviews*, 35, 1100–1125.

Denkhaus, Evelin, Stefan Meisen, Ursula Telgheder, Jost Wingender (2006), Chemical and physical methods for characterisation of biofilms, *Microchimica Acta*, 158, 1–27.

Diner, Elie J, Christina M Beck, Julia S Webb, David A Low, Christopher S Hayes (2012), Identification of a target cell permissive factor required for contact-dependent growth inhibition (CDI). *Genes & development*, 26, 515–25.

Donato, Gina M., Thomas H. Kawula (1998), Enhanced Binding of Altered H-NS Protein to Flagellar Rotor Protein FliG Causes Increased Flagellar Rotational Speed and Hypermotility in *Escherichia coli*, *Journal of Biological Chemistry*, 273, 24030–24036.

Ecker, David J, Rangarajan Sampath, Christian Massire, Lawrence B Blyn, Thomas A Hall, Mark W Eshoo, Steven A Hofstadler (2008), Ibis T5000: a universal biosensor approach for microbiology. *Nature reviews. Microbiology*, 6, 553–8.

El-Hajj, Ziad W., Elaine B. Newman (2015), An *Escherichia* coli Mutant That Makes Exceptionally Long Cells, *Journal of Bacteriology*, 197, 1507–1514.

Eltsov, Mikhail, Benoît Zuber (2006), Transmission electron microscopy of the bacterial nucleoid, *Journal of Structural Biology*, 156, 246–254.

Eppinger, Mark, Mark K Mammel, Joseph E Leclerc, Jacques Ravel, Thomas A Cebula (2011), Genome Signatures of *Escherichia coli* O157:H7 Isolates from the Bovine Host Reservoir. *Applied and environmental microbiology*, 77, 2916–25.

Fishov, I, C L Woldringh (1999), Visualization of membrane domains in *Escherichia coli. Molecular microbiology*, 32, 1166–72.

Flemming, Hans-Curt, Thomas R Neu, Daniel J Wozniak (2007), The EPS matrix: the "house of biofilm cells". *Journal of bacteriology*, 189, 7945–7.

Foulston, Lucy, Alexander K. W. Elsholz, Alicia S. DeFrancesco, Richard Losick (2014), The Extracellular Matrix of *Staphylococcus aureus* Biofilms Comprises Cytoplasmic Proteins That Associate with the Cell Surface in Response to Decreasing pH, *mBio*, 5, e01667–14.

Fux, C a, J W Costerton, P S Stewart, P Stoodley (2005), Survival strategies of infectious biofilms. *Trends in microbiology*, 13, 34–40.

Garcia, Erin C., Melissa S. Anderson, Jon A. Hagar, Peggy A. Cotter (2013), *Burkholderiae* BcpA mediates biofilm formation independently of interbacterial contact-dependent growth inhibition, *Molecular Microbiology*, 89, 1213–1225.

Gbejuade, Herbert O., Andrew M. Lovering, Jason C. Webb (2014), The role of microbial biofilms in prosthetic joint infections, *Acta Orthopaedica*, 86, 147–158.

Genevaux, P, S Muller, P Bauda (1996), A rapid screening procedure to identify mini-Tn10 insertion mutants of Escherichia coli K-12 with altered adhesion properties. *FEMS microbiology letters*, 142, 27–30.

Ghigo, J (2003), Are there biofilm-specific physiological pathways beyond a reasonable doubt?, *Research in Microbiology*, 154, 1–8.

Ghigo, J M (2001), Natural conjugative plasmids induce bacterial biofilm development. *Nature*, 412, 442–5.

Ghosh, Pushpita, Jagannath Mondal, Eshel Ben-Jacob, Herbert Levine (2015), Mechanically-driven phase separation in a growing bacterial colony, *Proceedings of the National Academy of Sciences*, 201504948.

González Barrios, Andrés F, Rongjun Zuo, Yoshifumi Hashimoto, Li Yang, William E Bentley, Thomas K Wood (2006), Autoinducer 2 controls biofilm formation in Escherichia coli through a novel motility quorum-sensing regulator (MqsR, B3022). *Journal of bacteriology*, 188, 305–16.

Gottrup, Finn, Jan Apelqvist, Thomas Bjarnsholt, Rose Cooper, Zena Moore, Edgar J. G. Peters, Sebastian Probst (2014), Antimicrobials and Non-Healing Wounds. Evidence, controversies and suggestions-key messages, *Journal of Wound Care*, 23, 477–482.

Goulian, Mark, Marjan van der Woude (2006), A simple system for converting lacZ to gfp reporter fusions in diverse bacteria. *Gene*, 372, 219–26.

Haldimann, Andreas, Barry L Wanner (2001), Conditional-Replication , Integration , Excision , and Retrieval Plasmid-Host Systems for Gene Structure-Function Studies of Bacteria, *Journal of Bacteriology*, 183, 6384–6393.

Hamilton, W. D. (1964), The genetical evolution of social behaviour. I, *Journal of Theoretical Biology*, 7, 1–16.

Hardie, Kim Rachael, Karin Heurlier (2008), Establishing bacterial communities by 'word of mouth': LuxS and autoinducer 2 in biofilm development. *Nature reviews. Microbiology*, 6, 635–43.

Hasan, N., M. Koob, W. Szybalski (1994), *Escherichia coli* genome targeting, I. Cre-lox-mediated in vitro generation of ori- plasmids and their in vivo chromosomal integration and retrieval, *Gene*, 150, 51–56.

Hayes, Christopher S, Stephanie K Aoki, David a Low (2010), Bacterial contact-dependent delivery systems. *Annual review of genetics*, 44, 71–90.

Hayes, Christopher S., Sanna Koskiniemi, Zachary C. Ruhe, Stephen J. Poole, David A. Low (2014), Mechanisms and Biological Roles of Contact-Dependent Growth Inhibition Systems, *Cold Spring Harbor Perspectives in Medicine*, 4, a010025.

Helaine, Sophie, Jessica A. Thompson, Kathryn G. Watson, Mei Liu, Cliona Boyle, David W. Holden (2010), Dynamics of intracellular bacterial replication at the single cell level, *Proceedings of the National Academy of Sciences*, 107, 3746–3751.

Hernández-Jiménez, Enrique, Rosa Del Campo, Victor Toledano, Maria Teresa Vallejo-Cremades, Aurora Muñoz, Carlota Largo, Francisco Arnalich, Francisco García-Rio, Carolina Cubillos-Zapata, Eduardo López-Collazo (2013), Biofilm vs. planktonic bacterial mode of growth: which do human macrophages prefer?, *Biochemical and biophysical research communications*, 441, 947–952.

Herzberg, Moshe, Ian K Kaye, Wolfgang Peti, Thomas K Wood (2006), YdgG (TqsA) controls biofilm formation in Escherichia coli K-12 through autoinducer 2 transport. *Journal of bacteriology*, 188, 587–98.

Heydorn, A, A T Nielsen, M Hentzer, C Sternberg, M Givskov, B K Ersbøll, S Molin (2000), Quantification of biofilm structures by the novel computer program COMSTAT. *Microbiology (Reading, England)*, 146 (Pt 1, 2395–407.

Hirschfeld, Josefine (2014), Dynamic interactions of neutrophils and biofilms, *Journal of Oral Microbiology*, 6, 26102.

Hood, Rachel D, Pragya Singh, Fosheng Hsu, Tüzün Güvener, Mike a Carl, Rex R S Trinidad, Julie M Silverman, Brooks B Ohlson, Kevin G Hicks, Rachael L Plemel, Mo Li, Sandra Schwarz, Wenzhuo Y Wang, Alexey J Merz, David R Goodlett, Joseph D Mougous (2010), A type VI secretion system of *Pseudomonas aeruginosa* targets a toxin to bacteria. *Cell host & microbe*, 7, 25–37.

Houry, A., M. Gohar, J. Deschamps, E. Tischenko, S. Aymerich, A. Gruss, R. Briandet (2012), Bacterial swimmers that infiltrate and take over the biofilm matrix, *Proceedings of the National Academy of Sciences*, 109, 13088–93.

Hung, Chia, Yizhou Zhou, Jerome S Pinkner, Karen W Dodson, Jan R Crowley, John Heuser, Matthew R Chapman, Maria Hadjifrangiskou, Jeffrey P Henderson, Scott J Hultgren (2013), *Escherichia coli* biofilms have an organized and complex extracellular matrix structure, *mBio*, 4, e00645–00613.

Johnson, Christopher L., Helen Ridley, Robert J. Pengelly, Mohd Zulkifli Salleh, Jeremy H. Lakey (2013), The unstructured domain of colicin N kills *Escherichia coli*, *Molecular Microbiology*, 89, 84–95.

Justice, Sheryl S, Chia Hung, Julie a Theriot, Daniel a Fletcher, Gregory G Anderson, Matthew J Footer, Scott J Hultgren (2004), Differentiation and developmental pathways of uropathogenic *Escherichia coli* in urinary tract pathogenesis. *Proceedings of the National Academy of Sciences of the United States of America*, 101, 1333–8.

Justice, Sheryl S, David a Hunstad, Patrick C Seed, Scott J Hultgren (2006), Filamentation by *Escherichia coli* subverts innate defenses during urinary tract infection. *Proceedings of the National Academy of Sciences of the United States of America*, 103, 19884–9.

Kaper, James B, James P Nataro, Harry L Mobley (2004), Pathogenic *Escherichia coli*. *Nature reviews. Microbiology*, 2, 123–40.

Kapitein, Nicole, Axel Mogk (2013), Deadly syringes: type VI secretion system activities in pathogenicity and interbacterial competition, *Current Opinion in Microbiology*, 16, 52–58.

Kellenberger, E, C Kellenberger-Van der Kamp (1994), Unstained and in vivo fluorescently stained bacterial nucleoids and plasmolysis observed by a new specimen preparation method for high-power light microscopy of metabolically active cells, *Journal of microscopy*, 176, 132–142.

Kerfeld, Cheryl A, Sabine Heinhorst, Gordon C Cannon (2010), Bacterial microcompartments. *Annual review of microbiology*, 64, 391–408.

Kerr, Benjamin, Margaret a Riley, Marcus W Feldman, Brendan J M Bohannan (2002), Local dispersal promotes biodiversity in a real-life game of rock-paper-scissors. *Nature*, 418, 171–4.

Kim, Wook, Fernando Racimo, Jonas Schluter, Stuart B. Levy, Kevin R. Foster (2014), Importance of positioning for microbial evolution, *Proceedings of the National Academy of Sciences*, 111, E1639–E1647.

King, Andrew (2010), "Advantages and limitations of the use of fluorescent protein expression systems in microscopy based studies of bacterial biofilms at the single cell level", Unpublished MSc report, University of York.

Kjaergaard, K, M a Schembri, C Ramos, S Molin, P Klemm (2000), Antigen 43 facilitates formation of multispecies biofilms. *Environmental microbiology*, 2, 695–702.

Kolenbrander, Paul E, Robert J Palmer, Saravanan Periasamy, Nicholas S Jakubovics (2010), Oral multispecies biofilm development and the key role of cell-cell distance. *Nature reviews. Microbiology*, 8, 471–80.

Koskiniemi, Sanna, James G. Lamoureux, Kiel C. Nikolakakis, Claire t'Kint de Roodenbeke, Michael D. Kaplan, David A. Low, Christopher S. Hayes (2013), Rhs proteins from diverse bacteria mediate intercellular competition, *Proceedings of the National Academy of Sciences*, 110, 7032–7037.

Koskiniemi, Sanna, Fernando Garza-Sánchez, Linus Sandegren, Julia S. Webb, Bruce A. Braaten, Stephen J. Poole, Dan I. Andersson, Christopher S. Hayes, David A. Low (2014), Selection of Orphan Rhs Toxin Expression in Evolved Salmonella enterica Serovar Typhimurium, *PLoS Genet*, 10, e1004255.

Koskiniemi, Sanna, Fernando Garza-Sánchez, Natasha Edman, Swarnava Chaudhuri, Stephen J. Poole, Colin Manoil, Christopher S. Hayes, David A. Low (2015), Genetic Analysis of the CDI Pathway from *Burkholderia pseudomallei* 1026b, *PLoS ONE*, 10, e0120265.

Kostakioti, Maria, Maria Hadjifrangiskou, Scott J Hultgren (2013), Bacterial biofilms: development, dispersal, and therapeutic strategies in the dawn of the postantibiotic era, *Cold Spring Harbor perspectives in medicine*, 3, a010306.

Lakins, M A, J L Marrison, P J O'Toole, M W van Der Woude (2009), Exploiting advances in imaging technology to study biofilms by applying multiphoton laser scanning microscopy as an imaging and manipulation tool. *Journal of Microscopy*, 235, 128–37.

Lanni, Eric J., Rachel N. Masyuko, Callan M. Driscoll, Jordan T. Aerts, Joshua D. Shrout, Paul W. Bohn, Jonathan V. Sweedler (2014), MALDI-guided SIMS: Multiscale Imaging of Metabolites in Bacterial Biofilms, *Analytical Chemistry*.

Lardon, Laurent A, Brian V Merkey, Sónia Martins, Andreas Dötsch, Cristian Picioreanu, Jan-Ulrich Kreft, Barth F Smets (2011), iDynoMiCS: next-generation individual-based modelling of biofilms. *Environmental microbiology*, 13, 2416–2434.

Leaper, David J, Gregory Schultz, Keryln Carville, Jacqueline Fletcher, Theresa Swanson, Rebecca Drake (2012), Extending the TIME concept: what have we learned in the past 10 years?, *International wound journal*, 9 Suppl 2, 1–19.

Lebeaux, David, Jean-Marc Ghigo, Christophe Beloin (2014), Biofilm-Related Infections: Bridging the Gap between Clinical Management and Fundamental Aspects of Recalcitrance toward Antibiotics, *Microbiology and Molecular Biology Reviews*, 78, 510–543.

Lee, Jin-Hyung, Yong-Guy Kim, Moo Hwan Cho, Thomas K. Wood, Jintae Lee (2011), Transcriptomic analysis for genetic mechanisms of the factors related to biofilm formation in *Escherichia* coli O157:H7, *Current Microbiology*, 62, 1321–1330.

Leroux, Michele, Justin A De Leon, Nathan J Kuwada, Alistair B Russell, Delia Pinto-Santini, Rachel D Hood, Danielle M Agnello, Stephen M Robertson, Paul A Wiggins, Joseph D Mougous (2012), Quantitative single-cell characterization of bacterial interactions reveals type VI secretion is a double-edged sword. *Proceedings of the National Academy of Sciences of the United States of America*, 109, 19804–19809.

Locke, James C W, Michael B Elowitz (2009), Using movies to analyse gene circuit dynamics in single cells. *Nature reviews. Microbiology*, 7, 383–92.

Lossi, Nadine S., Eleni Manoli, Pete Simpson, Cerith Jones, Kailyn Hui, Rana Dajani, Sarah J. Coulthurst, Paul Freemont, Alain Filloux (2012), The archetype Pseudomonas aeruginosa proteins TssB and TagJ form a novel subcomplex in the bacterial type VI secretion system, *Molecular Microbiology*, 86, 437–456.

Lu, Guoqing, Etsuko N. Moriyama (2004), Vector NTI, a balanced all-in-one sequence analysis suite, *Briefings in Bioinformatics*, 5, 378–388.

Lucchini, Sacha, Gary Rowley, Martin D Goldberg, Douglas Hurd, Marcus Harrison, Jay C D Hinton (2006), H-NS mediates the silencing of laterally acquired genes in bacteria. *PLoS pathogens*, 2, e81.

Ma, Luyan, Matthew Conover, Haiping Lu, Matthew R Parsek, Kenneth Bayles, Daniel J Wozniak (2009), Assembly and development of the *Pseudomonas aeruginosa* biofilm matrix. *PLoS pathogens*, 5, e1000354.

Männik, Jaan, Fabai Wu, Felix J. H. Hol, Paola Bisicchia, David J. Sherratt, Juan E. Keymer, Cees Dekker (2012), Robustness and accuracy of cell division in *Escherichia coli* in diverse cell shapes, *Proceedings of the National Academy of Sciences*, 109, 6957–6962.

Mason, D J, D M Powelson (1956), Nuclear division as observed in live bacteria by a new technique. *Journal of Bacteriology*, 71, 474–9.

Matz, Carsten, Staffan Kjelleberg (2005), Off the hook - how bacteria survive protozoan grazing, *Trends in Microbiology*, 13, 302–307.

Mayfield, C I, W E Inniss (1977), A rapid, simple method for staining bacterial flagella. *Canadian journal of microbiology*, 23, 1311–3.

McDougald, Diane, Scott A Rice, Nicolas Barraud, Peter D Steinberg, Staffan Kjelleberg (2011), Should we stay or should we go: mechanisms and ecological consequences for biofilm dispersal. *Nat. Rev. Microbiol.* 10, 39–50.

Morse, Robert P, Kiel C Nikolakakis, Julia L E Willett, Elias Gerrick, David A Low, Christopher S Hayes, Celia W Goulding (2012), Structural basis of toxicity and immunity in contact-dependent growth inhibition (CDI) systems. *Proceedings of the National Academy of Sciences of the United States of America*, 109, 21480–21485.

Mulcahy, Lawrence R, Jane L Burns, Stephen Lory, Kim Lewis (2010), Emergence of *Pseudomonas aeruginosa* strains producing high levels of persister cells in patients with cystic fibrosis. *Journal of bacteriology*, 192, 6191–9.

Mulvey, Matthew A. (2002), Adhesion and entry of uropathogenic *Escherichia coli*, *Cellular Microbiology*, 4, 257–271.

Murphy, K C (1998), Use of bacteriophage lambda recombination functions to promote gene replacement in *Escherichia coli. Journal of bacteriology*, 180, 2063–71.

Murphy, Kenan C, Kenneth G Campellone (2003), Lambda Red-mediated recombinogenic engineering of enterohemorrhagic and enteropathogenic *E. coli. BMC molecular biology*, 4, 11.

Nadell, Carey D., Knut Drescher, Ned S. Wingreen, Bonnie L. Bassler (2015), Extracellular matrix structure governs invasion resistance in bacterial biofilms, *The ISME journal*, ismej.2014.246.

Nahum, J. R., B. N. Harding, B. Kerr (2011), Evolution of restraint in a structured rock-paper-scissors community, *Proceedings of the National Academy of Sciences*, 108, 10831–10838.

Navarre, William Wiley, Michael McClelland, Stephen J. Libby, Ferric C. Fang (2007), Silencing of xenogeneic DNA by H-NS-facilitation of lateral gene transfer in bacteria by a defense system that recognizes foreign DNA, *Genes & Development*, 21, 1456–1471.

Neidhardt, F C, P L Bloch, D F Smith (1974), Culture medium for enterobacteria. *Journal of bacteriology*, 119, 736–47.

Nikolakakis, Kiel, Saba Amber, J Scott Wilbur, Elie J Diner, Stephanie K Aoki, Stephen J Poole, Apichai Tuanyok, Paul S Keim, Sharon Peacock, Christopher S Hayes, David A Low (2012), The toxin/immunity network of *Burkholderia pseudomallei* contact-dependent growth inhibition (CDI) systems. *Molecular microbiology*, 84, 516–529.

Nonejuie, Poochit, Michael Burkart, Kit Pogliano, Joe Pogliano (2013), Bacterial cytological profiling rapidly identifies the cellular pathways targeted by antibacterial molecules, *Proceedings of the National Academy of Sciences*, 110, 16169–16174.

Nou, Xiangwu, Jonathan Jones, Christopher Hayes, David Low (2013), "Contact dependent growth inhibition of *E. coli* O157:H7 by EC869 CDI system", in: *Environmental Microbial*

and Food Safety Laboratory Meeting Abstract 2013, retrieved from iapreview.ars.usda.gov on 06OCT2014.

Ogasawara, Hiroshi, Kaneyoshi Yamamoto, Akira Ishihama (2011), Role of the Biofilm Master Regulator CsgD in Cross-Regulation between Biofilm Formation and Flagellar Synthesis, *Journal of Bacteriology*, 193, 2587–97.

Oliver, James D (2005), The viable but nonculturable state in bacteria. *Journal of microbiology (Seoul, Korea)*, 43 Spec No, 93–100.

Pamp, Sünje Johanna, Claus Sternberg, Tim Tolker-Nielsen (2009), Insight into the microbial multicellular lifestyle via flow-cell technology and confocal microscopy. *Cytometry. Part A : the journal of the International Society for Analytical Cytology*, 75, 90–103.

Parsek, Matthew R, Pradeep K Singh (2003), Bacterial biofilms: an emerging link to disease pathogenesis. *Annual review of microbiology*, 57, 677–701.

Periasamy, Saravanan, Hwang-Soo Joo, Anthony C Duong, Thanh-Huy L Bach, Vee Y Tan, Som S Chatterjee, Gordon Y C Cheung, Michael Otto (2012), How *Staphylococcus aureus* biofilms develop their characteristic structure. *Proceedings of the National Academy of Sciences of the United States of America*, 109, 1281–6.

Poole, Stephen J, Elie J Diner, Stephanie K Aoki, Bruce A Braaten, Claire T'kint de Roodenbeke, David A Low, Christopher S Hayes (2011), Identification of Functional Toxin/Immunity Genes Linked to Contact-Dependent Growth Inhibition (CDI) and Rearrangement Hotspot (Rhs) Systems. *PLoS genetics*, 7, e1002217.

Prado, Federico, Benjamin Kerr (2008), The evolution of restraint in bacterial biofilms under nontransitive competition. *Evolution; international journal of organic evolution*, 62, 538–48.

R Core Team (2013), *R: A Language and Environment for Statistical Computing*, R Foundation for Statistical Computing, Vienna, Austria.

Rani, Suriani Abdul, Betsey Pitts, Haluk Beyenal, Raaja Angathevar Veluchamy, Zbigniew Lewandowski, William M Davison, Kelli Buckingham-Meyer, Philip S Stewart (2007), Spatial patterns of DNA replication, protein synthesis, and oxygen concentration within bacterial biofilms reveal diverse physiological states. *Journal of Bacteriology*, 189, 4223–33.

Reisner, Andreas, Mario Maierl, Michael Jörger, Robert Krause, Daniela Berger, Andrea Haid, Dijana Tesic, Ellen L Zechner (2014), Type 1 fimbriae contribute to catheter-associated urinary tract infections caused by *Escherichia coli*, *Journal of bacteriology*, 196, 931–939.

Ren, Dawei, Jonas Stenløkke Madsen, Claudia I de la Cruz-Perera, Lasse Bergmark, Søren J Sørensen, Mette Burmølle (2013), High-Throughput Screening of Multispecies Biofilm Formation and Quantitative PCR-Based Assessment of Individual Species Proportions, Useful for Exploring Interspecific Bacterial Interactions, *Microbial ecology*.

Römling, Ute, Michael Y. Galperin, Mark Gomelsky (2013), Cyclic di-GMP: the First 25 Years of a Universal Bacterial Second Messenger, *Microbiology and Molecular Biology Reviews*, 77, 1–52.

RStudio (2014), *RStudio*, RStudio, RStudio.

Rudge, Timothy J., Paul J. Steiner, Andrew Phillips, Jim Haseloff (2012), Computational Modeling of Synthetic Microbial Biofilms, *ACS Synthetic Biology*, 1, 345–352.

Rudge, Timothy J., Fernán Federici, Paul J. Steiner, Anton Kan, Jim Haseloff (2013), Cell Polarity-Driven Instability Generates Self-Organized, Fractal Patterning of Cell Layers, *ACS Synthetic Biology*, 2, 705–714.

Ruhe, Zachary C, David A Low, Christopher S Hayes (2013a), Bacterial contact-dependent growth inhibition, *Trends in microbiology*, 21, 230–237.

Ruhe, Zachary C, Adam B Wallace, David A Low, Christopher S Hayes (2013b), Receptor polymorphism restricts contact-dependent growth inhibition to members of the same species, *mBio*, 4, e00480–13.

Ruhe, Zachary C., Josephine Y. Nguyen, Christina M. Beck, David A. Low, Christopher S. Hayes (2014), The proton-motive force is required for translocation of CDI toxins across the inner membrane of target bacteria, *Molecular Microbiology*, 94, 466–481.

Russell, Alistair B., S. Brook Peterson, Joseph D. Mougous (2014), Type VI secretion system effectors: poisons with a purpose, *Nature Reviews Microbiology*, 12, 137–148.

Sawitzke, James A., Lynn C. Thomason, Nina Costantino, Mikhail Bubunenko, Simanti Datta, Donald L. Court (2007), "Recombineering: In Vivo Genetic Engineering in *E. coli*, *S. enterica*, and Beyond", in: *Methods in Enzymology*, ed. by Kelly T. Hughes and Stanley R. Maloy, vol. Volume 421, Advanced Bacterial Genetics: Use of Transposons and Phage for Genomic Engineering, Academic Press, pp. 171–199.

Schembri, Mark A., Dorte Dalsgaard, Per Klemm (2004), Capsule Shields the Function of Short Bacterial Adhesins, *Journal of Bacteriology*, 186, 1249–1257.

Schneider, Caroline A, Wayne S Rasband, Kevin W Eliceiri (2012), NIH Image to ImageJ: 25 years of image analysis, *Nature Methods*, 9, 671–675.

Schwarz, Sandra, T Eoin West, Frédéric Boyer, Wen-Chi Chiang, Mike A Carl, Rachel D Hood, Laurence Rohmer, Tim Tolker-Nielsen, Shawn J Skerrett, Joseph D Mougous (2010), *Burkholderia* type VI secretion systems have distinct roles in eukaryotic and bacterial cell interactions. *PLoS pathogens*, 6, e1001068.

Shaner, Nathan C, Robert E Campbell, Paul A Steinbach, Ben N G Giepmans, Amy E Palmer, Roger Y Tsien (2004), Improved monomeric red, orange and yellow fluorescent proteins derived from *Discosoma* sp. red fluorescent protein. *Nature biotechnology*, 22, 1567–72.

Shaner, Nathan C, Paul A Steinbach, Roger Y Tsien (2005), A guide to choosing fluorescent proteins, *Nature Methods*, 2, 905–909.

Shapiro, J a, C Hsu (1989), *Escherichia coli* K-12 cell-cell interactions seen by time-lapse video. *Journal of bacteriology*, 171, 5963–74.

Shapiro, J.A. (1988), Bacterua as multicellular organisms, *Scientific American*, 256, 82–89.

Shin, Minsang, Arvin Cesar Lagda, Jae Woong Lee, Abhay Bhat, Joon Haeng Rhee, Jeong-Sun Kim, Kunio Takeyasu, Hyon E. Choy (2012), Gene silencing by H-NS from distal DNA site, *Molecular Microbiology*, 86, 707–719.

Sliusarenko, Oleksii, Jennifer Heinritz, Thierry Emonet, Christine Jacobs-Wagner (2011), High-throughput, subpixel precision analysis of bacterial morphogenesis and intracellular spatio-temporal dynamics. *Molecular Microbiology*, 80, 612–27.

Sochacki, Kem A, Kenneth J Barns, Robert Bucki, James C Weisshaar (2011), Real-time attack on single *Escherichia coli* cells by the human antimicrobial peptide LL-37. *Proceedings of the National Academy of Sciences of the United States of America*, 108, E77–81.

Solano, Cristina, Maite Echeverz, Iñgo Lasa (2014), Biofilm dispersion and quorum sensing, *Current Opinion in Microbiology*, Cell regulation, 18, 96–104.

Strahl, H., L. W. Hamoen (2010), Membrane potential is important for bacterial cell division, *Proceedings of the National Academy of Sciences*, 107, 12281–12286.

Strassmann, Joan E., Owen M. Gilbert, David C. Queller (2011), Kin Discrimination and Cooperation in Microbes, *Annual Review of Microbiology*, 65, 349–367.

Thormann, Kai M., Renée M. Saville, Soni Shukla, Alfred M. Spormann (2005), Induction of Rapid Detachment in *Shewanella oneidensis* MR-1 Biofilms, *Journal of Bacteriology*, 187, 1014–1021.

Tikhonova, Elena B., Helen I. Zgurskaya (2004), AcrA, AcrB, and TolC of *Escherichia coli* Form a Stable Intermembrane Multidrug Efflux Complex, *The Journal of Biological Chemistry*, 279, 32116–32124.

Valkenburg, J A, C L Woldringh (1984), Phase separation between nucleoid and cytoplasm in *Escherichia coli* as defined by immersive refractometry. *Journal of Bacteriology*, 160, 1151–1157.

Volkmer, Benjamin, Matthias Heinemann (2011), Condition-Dependent Cell Volume and Concentration of *Escherichia coli* to Facilitate Data Conversion for Systems Biology Modeling, *PLoS ONE*, 6, e23126.

Vorregaard, Martin (2008), "Comstat2 - a modern 3D image analysis environment for biofilms", MSc, Informatics and Mathematical Modelling, Technical University of Denmark, DTU.

Walker, Daniel, Lorna Lancaster, Richard James, Colin Kleanthous (2004), Identification of the catalytic motif of the microbial ribosome inactivating cytotoxin colicin E3, *Protein Science : A Publication of the Protein Society*, 13, 1603–1611.

Walters, Marshall C., Frank Roe, Amandine Bugnicourt, Michael J. Franklin, Philip S. Stewart (2003), Contributions of antibiotic penetration, oxygen limitation, and low metabolic ac-

tivity to tolerance of *Pseudomonas aeruginosa* biofilms to ciprofloxacin and tobramycin, *Antimicrobial Agents and Chemotherapy*, 47, 317–323.

Wang, Ping, Lydia Robert, James Pelletier, Wei Lien Dang, Francois Taddei, Andrew Wright, Suckjoon Jun (2010), Robust Growth of *Escherichia coli, Current Biology*, 20, 1099–1103.

Wang, Xindan, Christophe Possoz, David J Sherratt (2005), Dancing around the divisome: asymmetric chromosome segregation in *Escherichia coli. Genes & development*, 19, 2367–77.

Warren, David J (2011), Preparation of highly efficient electrocompetent *Escherichia coli* using glycerol/mannitol density step centrifugation. *Analytical biochemistry*, 413, 206–7.

Webb, Julia S., Kiel C. Nikolakakis, Julia L. E. Willett, Stephanie K. Aoki, Christopher S. Hayes, David A. Low (2013), Delivery of CdiA Nuclease Toxins into Target Cells during Contact-Dependent Growth Inhibition, *PLoS ONE*, 8, e57609.

West, Stuart A., Andy Gardner (2010), Altruism, Spite, and Greenbeards, *Science*, 327, 1341–1344.

Wickham, Hadley (2007), *Reshaping Data with the reshape Package*, 12, pp. 1–20.

— (2009), *ggplot2: elegant graphics for data analysis*, Springer New York.

— (2011), *The Split-Apply-Combine Strategy for Data Analysis*, 1, pp. 1–29.

— (2012), *scales: Scale functions for graphics*.

Wickham, Hadley, Winston Chang (2013), *devtools: Tools to make developing R code easier*.

Wilson, Kate (2001), "Preparation of Genomic DNA from Bacteria", in: *Current Protocols in Molecular Biology*, John Wiley & Sons, Inc.

Wolfaardt, GM, JR Lawrence, RD Robarts, SJ Caldwell, DE Caldwell (1994), Multicellular organization in a degradative biofilm community, *Applied and environmental microbiology*, 60, 434.

Woude, Marjan W van der (2006), Re-examining the role and random nature of phase variation. *FEMS microbiology letters*, 254, 190–7.

Woude, Marjan W. van der, Ian R. Henderson (2008), Regulation and Function of Ag43 (Flu), *Annual Review of Microbiology*, 62, 153–169.

Yao, Zhizhong, Rut Carballido-López (2014), Fluorescence Imaging for Bacterial Cell Biology: From Localization to Dynamics, From Ensembles to Single Molecules, *Annual Review of Microbiology*, 68, 459–476.

Yawata, Yutaka, Kensuke Toda, Erika Setoyama, Junji Fukuda, Hiroaki Suzuki, Hiroo Uchiyam, Nobuhiko Nomura (2010), Monitoring biofilm development in a microfluidic device using modified confocal reflection microscopy. *Journal of bioscience and bioengineering*, 110, 377–80.

Yim, Grace, Helena Huimi Wang, Julian Davies Frs (2007), Antibiotics as signalling molecules, *Philosophical Transactions of the Royal Society of London B: Biological Sciences*, 362, 1195–1200.

Young, Jonathan W, James C W Locke, Alphan Altinok, Nitzan Rosenfeld, Tigran Bacarian, Peter S Swain, Eric Mjolsness, Michael B Elowitz (2012), Measuring single-cell gene expression dynamics in bacteria using fluorescence time-lapse microscopy. *Nature protocols*, 7, 80–8.

Zhang, Bo, Robert Powers (2012a), Analysis of bacterial biofilms using NMR-based metabolomics. *Future medicinal chemistry*, 4, 1273–306.

Zhang, Dapeng, Lakshminarayan M Iyer, L Aravind (2011), A novel immunity system for bacterial nucleic acid degrading toxins and its recruitment in various eukaryotic and DNA viral systems. *Nucleic acids research*, 39, 4532–4552.

Zhang, Dapeng, Robson F de Souza, Vivek Anantharaman, Lakshminarayan M Iyer, L Aravind (2012b), Polymorphic toxin systems: comprehensive characterization of trafficking modes, processing, mechanisms of action, immunity and ecology using comparative genomics. *Biology direct*, 7, 18.

Zobell, C E, E C Allen (1935), The Significance of Marine Bacteria in the Fouling of Submerged Surfaces. *Journal of bacteriology*, 29, 239–51.

Zobell, E, D Quentin, La Jolla (1936), Observations on the multiplication of bacteria in different volumes of stored seawater and the influence of oxygen tension and solid surfaces, *Biological Bulletin Woods Hole*, 71, 324–342.